TURKISH REPUBLIC
ERCIYES UNIVERSITY
GRADUATE SCHOOL OF NATURAL AND APPLIED SCIENCES
DEPARTMENT OF MECHANICAL ENGINEERING

EVALUATION OF IN-PLANE AND THROUGH THICKNESS HYBRIDIZATION OF CARBON-BASALT/EPOXY COMPOSITES ON IMPACT AND TENSILE BEHAVIOR

Prepared By
Hafız Muhammad Numan ZAFAR

Supervisor
Assoc. Prof. Dr. Fehmi NAİR

MSc Thesis

May, 2017
KAYSERİ

TURKISH REPUBLIC
ERCIYES UNIVERSITY
GRADUATE SCHOOL OF NATURAL AND APPLIED SCIENCES
DEPARTMENT OF MECHANICAL ENGINEERING

EVALUATION OF IN-PLANE AND THROUGH THICKNESS HYBRIDIZATION OF CARBON-BASALT/EPOXY COMPOSITES ON IMPACT AND TENSILE BEHAVIOR

Prepared By
Hafız Muhammad Numan ZAFAR

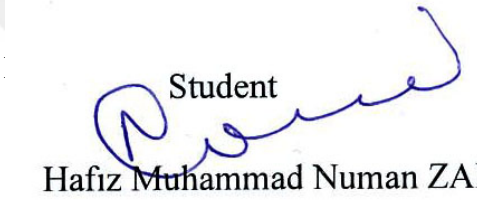
Supervisor
Assoc. Prof. Dr. Fehmi NAİR

MSc Thesis

May, 2017
KAYSERİ

SCIENTIFIC ETHICS SUITABILITY

I declare that all information in this work was obtained in accordance with academic and ethical rules. All results and material that not been at the essence of this work are also transferred and expressed by giving proper references as required by these rules and behavior.



SUITABILITY FOR GUIDE

The MS thesis entitled **'*Evaluation of In-Plane and Through Thickness Hybridization of Carbon-basalt / Epoxy Composites on Impact and Tensile Behaviour*'** has been prepared in accordance with Erciyes University Graduate Education and Teaching Institute Thesis Preparation and Writing Guide.

Student
Hafız Muhammad Numan ZAFAR

Supervisor
Assoc. Prof. Dr. Fehmi NAİR

Head of the Department
Mechanical Engineering

Prof. Dr. Necdet ALTUNTOP
Makine Mühendisliği
Bölüm Başkanı

ACCEPTANCE AND APPROVAL PAGE

This study entitled ***'Evaluation of In-Plane and Through Thickness Hybridization of Carbon-basalt / Epoxy Composites on Impact and Tensile Behaviour'*** prepared by Hafız Muhammad Numan ZAFAR under the supervision of Assoc. Prof. Dr. Fehmi NAİR was accepted by the jury as MSc. Thesis in Biology department.

24/05/2017

JURY:

Supervisor: Assoc. Prof. Dr. Fehmi NAİR .....

Juror: Prof. Dr. Sedat ÖZDEN .....

Juror: Assoc. Prof. Dr. Kemal YILDIZLI .....

APPROVAL

That the acceptance of this thesis has been approved by the decision of the Institute's Board of Directors with the 06-06-2017 date and 2017/25-24 numbered decision.

09 / 06 / 2017

Prof. Dr. Mehmet AKKURT

Director of the In

..... / ..... /

PREFACE / AKNOWLEDGEMENT

I am extremely thankful to my supervisor Doç. Dr. Fehmi NAİR for the time, help, interest and guidance throughout period of the preparation and writing of this study. I am also thankful to my family for helping me till this stage during my educational career. I am thankful to the Erciyes University management for providing the best available environment ensuring the completion of my education since my admission here. I would like to extend my thanks to research assistant Mr. Umut ÇALIŞKAN and Assoc. Prof. Dr. Recep GÜNEŞ for their assistance in carrying out the experiments related to this study in the laboratory. I am thankful to my brother Mr. Mashhood ZAFAR for providing moral and psychological support for the completion of this study.

Hafız Muhammad Numan ZAFAR

Kayseri, Mart, 2017

DÜZLEM İÇİ VE KALINLIK DOĞRULTUSUNDA HİBRİTLEMENİN KARBON-BAZALT/EPOKSİ KOMPOZİTLERİNİN DARBE VE ÇEKME DAVRANIŞLARIN İNCELENMESİ

Hafız Muhammad Numan ZAFAR

Erciyes Üniversitesi, Fen Bilimleri Enstitüsü
Yüksek Lisans Tezi, Mayıs-2017
Danışman: Doç. Dr. Fehmi NAİR

ÖZET

Kompozit malzemeleri metallere göre hafif, güçlü, esnek ve korozyona karşı yüksek dirence sahip olduğundan son senelerde mühendislerin dikkatini çekmeye başarmıştır. Özellikle Karbon fiberleri modern kompozitlerin en çok araştırılan fiberlerinden bir tanesidir. Bazalt fiberleri ise karbon fiberlerine göre daha esnek ve düşük Young Modülüne sahiptir ve üretimi daha basit olduğundan dolayı fiyatları daha uygundur. Hibrit Kompozitler birden fazla fiberlerin güçlendirici faz olarak bir matrisin içinde kullanıldığı yapılara denir. Akademik çalışmaların çoğu hibrit kompozitlerinde bulunan fiber tabakaların diziliş şeklini değiştirerek elde edilen yapıların mekanik özelliklerinin incelenmesine odaklanmıştır. Bu çalışma polimer matrisi olan bazalt ve karbon fiberlerin iki farklı tür hibrit kompozitlerin üretimine ve üretilen bu iki türlü hibritlerin darbe ve çekme davranışların incelenmesine odaklanmaktadır. Hibrit kompozit malzemelerinin içinde tamamen bazalt fiberlerinden, tamamen karbon fiberlerinden ve atkısı bazalt ama çözgüsü karbon olan örülmüş katmanlar kullanılmıştır. Birinci tür hibritlenme kalınlık doğrultusunda olmak üzere tamamen karbon ve tamamen bazalt fiberlerinden yapılmış katmanların dizilişinden meydana gelir. Birinci tür hibrit kompozitlerinde karbon ve bazalt katmanlarından oluşan üç farklı dizilişe sahip yapılar üretilmiştir. İkinci tür hibritlenme ise düzlem-içinde hibrit olmak üzere atkısı bazalt ve çözgüsü karbon olan örülmüş katmanların üst üste yerleştirilmesinden meydana gelir. Düzlem-içi hibrit kompozit ve kalınlık doğrultusunda hibrit olan kompozit VARTM (Vakum yardımıyla reçine enfüzyonu) tekniğiyle hazırlanmıştır. Her iki tür hibritlenmenin bu malzemelerin darbe ve çekme davranışlarını nasıl etkilediğini incelemek için çekme ve düşük hız darbe deneyi uygulanmıştır. Yapılan deneylerin sonuçları hem hangi diziliş şeklinin istenen mekanik özelliğine uygun olduğunu gösterir hem de hibritlenme türünün çekme ve darbe deneyinde nasıl davrandığını gösterir. Sonuçlara göre; çekme ve bastırma yüzeyinde bulunan katmanın türü (karbon veya

bazalt) ve sayısı malzemenin enerji soğurma kapasitesini ve de esnekliğini etkilemektedir. Kalınlık doğrultusundaki hibrit kompozitlerin çekirdeği karbon katmanlarından oluşur ve bunların sayısı ise malzemenin çekme mukavemetini etkiler. Düzlem-içi hibrit kompozitleri çekme deneyinde kırılmadan önce en yüksek gerilme değeri gösterdi. Karbon fiberlerinden yapılmış olan kompozitlerine bazalt fiberlerin eklenmesi, malzemenin genel düktilitesini ve darbe dayanaklığını arttırır ve bu artış miktarı bazalt fiberlerinin malzemedeki konumuna göre değişir.

Anahtar Kelimeler: Polimer Matris Kompozit, Hibrit Kompozit, VARTM (Vakum yardımıyla reçine enfüzyonu), Düşük Hız Darbe Deneyi, Çekme Deneyi.

EVALUATION OF IN-PLANE AND THROUGH THICKNESS HYBRIDIZATION OF CARBON-BASALT / EPOXY COMPOSITES ON IMPACT AND TENSILE BEHAVIOUR

Hafız Muhammad Numan ZAFAR

Erciyes University, Graduate School of Natural and Applied Sciences
M.Sc. Thesis, March, 2017
Supervisor: Assoc. Prof. Dr. Fehmi NAİR

ABSTRACT

The composite materials have succeeded in catching the attention of engineers in the recent years because of their superior properties such as flexibility, strength, lightweight and resistance to corrosion as compared to metals. Specially the carbon fibers are one of the most researched modern composites. Basalt fibers possess lower Young's Modulus and are cheaper due to their easier less complicated manufacturing process as compared carbon fibers. Hybrid composites are the materials with multiple fibers as reinforcement in a single matrix. A number of academic studies have focused on changing the stacking sequence of the hybrid composites to investigate its effect on the mechanical properties of the new material. This study addresses the fabrication of two types of polymer matrix hybrid composites made by carbon and basalt fibers and their tensile and impact behavior. Fabrics totally made by carbon fibers, basalt fibers and woven fabrics of carbon fibers as wrap and basalt fibers as weft are used in the fabrication of the hybrid composites. First type of hybrid composites is made by total carbon and basalt fabrics and called hybrid through thickness. A total of three different stacking sequences of the laminates are used in the first type of hybridization. Second type of hybridization is made by combining in-plane hybrid fabrics having wrap as carbon fibers and weft as basalt fibers and called in-plane hybridization. Bothe, hybrid through thickness and hybrid in plane are manufactured using VARTM (Vacuum Assisted Resin Transfer Molding) technique. In order to see the effect of such hybridizations on impact and tensile behavior, low speed drop weight impact test and tensile test are applied. The results lead to the appropriate stacking sequence for needed mechanical properties as well as shows how both types of hybridization behave under tensile loading and impact tests. According to results; the number and type of the fabric layers (Carbon, Basalt or In-plane hybrid fabric) on the compression and tension sides affects the damage absorption capacities and the flexure modulus of the laminates. The core hybrid through

thickness hybrid composites is made of carbon fabrics and their number affects the tensile strength. The introduction of basalt fibers in the composites made by carbon increases the ductility and the damage resistance of the overall product which depends on the location and quantity of the basalt fibers in the material.

Keywords: Polymer Composite Materials, Hybrid Laminates, VARTM (vacuum assisted resin infusion), Low Speed Drop Weight Impact Test, Tensile Test.

TABLE OF CONTENTS

EVALUATION OF IN-PLANE AND THROUGH THICKNESS HYBRIDIZATION OF CARBON-BASALT / EPOXY COMPOSITES ON IMPACT AND TENSILE BEHAVIOUR

SCIENTIFIC ETHICS SUITABILITY i
SUITABILITY FOR GUIDE ii
ACCEPTANCE AND APPROVAL PAGE iii
PREFACE / AKNOWLEDGEMENT iv
ÖZET v
ABSTRACT vii
TABLE OF CONTENTS viii
LIST OF THE FIGURES xiii
LIST OF THE TABLES xiv
INTRODUCTION 1

CHAPTER 1

LITERATURE SURVEY

1.1 BACKGROUND 5
1.2 BASALT FIBERS 9
1.2.1 Origin, Constituent, and History of Basalt Fibers 9
1.2.2 Manufacturing of Basalt fibers 9
1.2.4 Advantages of Basalt over Glass 11
1.2.5 Mechanical Properties of Basalt 13
1.2.6 Applications of Basalt Fibers 13
1.3 CARBON FIBERS 14
1.3.1 History of Carbon Fibers 14
1.3.2 Manufacturing of Carbon fibers 15
1.3.2.1 PAN Based Carbon Fibers 16
1.3.2.2 Pitch Based Carbon Fibers 16
1.3.3 Carbon Fibers' Mechanical Properties 17

1.3.4 Advantages-Disadvantages of Carbon Fibers 17

1.3.4.1 High Strength to Weight 17

1.3.4.2 Rigidity 18

1.3.4.3 Electrically Conductivity 18

1.3.4.4 Fatigue Resistance 18

1.3.4.5 Tensile Strength 18

1.3.4.6 Thermal Conductivity 18

1.3.4.7 Non Poisonous, Biologically Inert, X-Ray Permeable 19

1.3.4.8 Carbon Fiber Price 19

1.3.4.9 Brittleness 19

CHAPTER 2

MATERIALS AND METHODS

2.1 MANUFACTURING MATERIALS 20

2.1.1 Fabrics 20

2.1.2 Carbon Weave Fabrics 20

2.1.3 Basalt Weave Fabrics 22

2.1.4 Basalt-Carbon In-Plane Weave Fabrics 23

2.1.5 Adhesive Resin and Hardener 24

2.1.5.1 Effect of Hardener on Thermosetting. 24

2.1.5.2 Effect of Temperature on Thermosetting 25

2.2 VARTM (Vacuum Assisted Resin Infusion) Machine 26

2.2.1 Work Bench 26

2.2.2 Rotary Pump 27

2.2.3 Resin Trap 28

2.2.4 Temperature/Vacuum Control Panel 28

2.3 LABORATORY EQUIPMENT 29

2.4 MANUFACTURING METHODS 30

2.4.1 Preparation of the Fabrics 31

2.4.2 Stacking Sequences 31

2.4.2.1 1B1C Arrangement 32

2.4.2.2 2B2C Arrangement 33

2.4.2.3 3B3C Arrangement 35

2.4.2.4 Carbon-Basalt In-Plane Hybrid Laminate 36

2.2.3 Preparation of Epoxy Resin 37

2.2.4 Equipment Arrangement 38

2.2.5 Curing of the fabrics 41

2.5 DROP WEIGHT IMPACT TEST 44

2.5.1 Test Preparation 44

2.5.2 Naming of the Samples 44

2.5.3 Drop Test Machine Fractovis Plus 45

2.6 TENSILE TEST 48

2.6.1 Naming of the Samples 48

2.6.2 Dimensions of the Samples 49

2.6.3 Tensile Testing Machine 49

CHAPTER 3

RESULTS AND DISCUSSION

3.1 IMPACT TEST RESULTS 51

3.1.1 Force-Time Plots 51

3.1.2 Force-Displacement Plots 51

3.1.3 Energy-Time Plots 51

3.1.4 Two Samples' Tests 52

3.1.5 Results for Each Laminate 54

3.1.5.1 Plots for 1B1C 55

3.1.5.1.1 Force-Displacement Plot for 1B1C 55

3.1.5.1.2 Force-Time Plot for 1B1C 56

3.1.5.1.3 Energy-Time Plot for 1B1C 56

3.1.5.2 Plots for 2B2C 57

3.1.5.2.1 F-d Plot for 2B2C 58

3.1.5.2.2 Force-Time Plot for 2B2C 58

3.1.5.2.3 Energy-Time Plot for 2B2C 59

3.1.5.3 Plots for 3B3C 60

3.1.5.3.1 F-d Plot for 3B3C 60

3.1.5.3.2 Force-Time Plot for 3B3C 61

3.1.5.3.3 Energy-Time Plot for 3B3C 61

3.1.5.4 Plots for HYB 62

3.1.5.4.1 F-d Plot for Hybrid Composite 62

3.1.5.4.2 Force-Time Plot for Hybrid Composite 63

3.1.5.4.3 Energy-Time Plot for Hybrid Composite 64

3.1.6 Results for Each Impact Speed 65

3.1.6.1 Plots for 4 m/s 66

3.1.6.1.1 Force-Displacement Plot for 4 m/s 66

3.1.6.1.2 Force-Time Plot for 4m/s 67

3.1.6.1.3 Energy-Time Plot for 4m/s 67

3.1.6.2 Plots for 6 m/s 68

3.1.6.2.1 Force-Displacement Plot for 6 m/s 68

3.1.6.2.3 Energy-Time Plot for 6 $^{m/s}$ 70

3.1.6.3 Plots for 8 m/s 70

3.1.6.3.1 Force-Displacement Plot for 8 $^{m/s}$ 70

3.1.6.3.2 Force-Time Plot for 8 $^{m/s}$ 71

3.1.6.3.3 Energy-Time Plot for 8 $^{m/s}$ 71

3.1.7 Macroscopic View Results 72

3.1.7.1 OBSERVATIONS 72

3.2 TENSILE TEST RESULTS 75

3.2.1 Results Gained from the Tensile Test 75

3.4 EVALUATION OF RESULTS 76

3.4.1 Results of Impact Test 76

3.4.1.1 FORCE-DISPLACEMENT PLOTS 76

3.4.1.1.1 Observations on the F-d Plots 77

Area under the F-d curve and Maximum Displacement 78

3.4.1.2 FORCE-TIME PLOTICAL OUTPUTS 79

3.4.1.2.1 Force-Time Plots Observations 79

Symmetry of the Force-Time Plot 79

Ductility Index 80

3.4.1.3 Energy-Time Plots 83

3.4.1.3.1 Force-Time Plots Observations 83

Damage Degrees: 83

3.4.2 Discussion of Impact Test Results 85

3.4.3 Results of Tensile Test 89

3.4.3.1 Discussion of Low Speed Drop Weight Impact Test Results 89

CHAPTER 4

CONCLUSION AND SUGGESTIONS

4.1 Flexibility 92

4.2 Tensile Strength 93

4.3 Damage Absorption 93

4.4 Suggestions 93

REFERENCES 96

CURRICULUM VITAE 101

LIST OF THE FIGURES

Fig-1.1 Basalt fiberization processing line. 10
Fig-1.2 Mass loss of glass and basalt fibers..... 12
Fig-1.3 Stress-Strain diagram for Basalt Continuous/Short and glass fibers..... 12
Fig-1.3 Stress-Strain diagram for Basalt Continuous/Short and glass fibers..... 12
Fig-1.4 Different origin based carbon fibers and there tensile modulus ranges 14
Fig-2.1(a) Plain weave arrangement of yarns in a fabric..... 19
Fig-2.1(b) Arrangement of yarns in 100% Carbon Fabrics 20
Fig-2.2 Arrangement of yarns in Basalt Fabrics..... 21
Fig-2.3 Arrangement of Yarns in Hybrid Carbon-Basalt Fabrics..... 22
Fig-2.4 Temperature vs Time of curing for different Hardeners 24
Fig-2.5 VARTM Machine 25
Fig-2.6 Rotary Pump..... 26
Fig-2.7 Resin Trap 27
Fig-2.8 Electric Control Panel 28
Fig-2.9 Cut Pipe..... 29
Fig-2.10 Normal Flow Pipes..... 29
Fig-2.11 Flow Matrix..... 29
Fig-2.11(a) 100% Basalt Fabrics 30
Fig-2.11(b) 100% Carbon Fabrics 30
Fig-2.11(c) In-plane Carbon/Basalt Hybrid Fabrics 30
Fig-2.12(a) Carbon Fabric……. 31
Fig-2.12(b) Basalt Fabric..... 31
Fig-2.12(b) Basalt Fabric..... 31
Fig-2.13(a) 1B1C Composite Laminate..... 31
Fig-2.14(a) 2B2C Composite Laminate..... 33
Fig-2.14(b) Side View of 2B2C Composite Laminate 33
Fig-2.15(a) 3B3C Composite Laminate..... 34
Fig-2.15(b) Side View of 3B3C Composite Laminate 34
Fig-2.16(a) Carbon-Basalt Hybrid Fabric..... 35

Fig-2.16(b) Hybrid Composite Laminate 35
Fig-2.17 Mixing of resin and hardener with 40-60 % ratio 37
Fig-2.18 Stacking of the Fabrics 37
Fig-2.19(a) Green Flow Matrix 38
Fig-2.19(b) Pasting of Flow Pipe 38
Fig-2.20(a) Real view of arrangement of and flow of resin and fabrics 38
Fig-2.20(b) Schematic view of arrangement of the flow of resin and fabrics 39
Fig-2.21(a) Schematic view of the whole VARTM process and machine parts. 39
Fig-2.21(b) Process of infusion of the resin into layers 40
Fig-2.22 Fabrics after complete curing 40
Fig-2.23 D24000S by DEWALT cutting machine 41
Fig-2.24 Ready to cut laminates 42
Fig-2.25 Cutting of the Laminates 42
Fig-2.26 Ready for the tensile and impact test samples 42
Fig-2.27 Naming the Composite Laminates 44
Fig-2.28 Drop Test Machine 45
Fig-2.29(a) Clamping of the laminate 46
Fig-2.29(b) Clamping of the laminate 46
Fig-2.30 Naming of the samples before the tensile test. 47
Fig-2.31 AGS-X Shimadzu Tensile Strength Machine 48
Fig-2.32 Tensile Test of the hybrid composite laminates 49
Fig-3.1(a) Overlaying Force-Time Plot for two samples 51
Fig-3.1(b) Overlaying Force-Time Plot for two samples 42
Fig-3.1(c) Results Based on Each Composite Laminate 53
Fig-3.2(a) Force-Displacement Plot for 1B1C 54
Fig-3.2(b) Force-Time Plot for 1B1C 55
Fig-3.2(c) Energy-Time Plot for 1B1C 56
Fig-3.3(a) Force-Displacement Plot for 2B2C 57
Fig-3.3(b) Force-Time Plot for 2B2C 58
Fig-3.3(c) Energy-Time Plot for 2B2C 58

Fig-3.4(a) Force-Displacement Plot for 3B3C 59
Fig-3.4(b) Force-Time Plot for 3B3C 60
Fig-3.4(c) Force-Time Plot for 3B3C 61
Fig-3.5(a) Force-Displacement Plot for HYB 62
Fig-3.5(b) Force-Time Plot for HYB 63
Fig-3.5(b) Energy-Time Plot for HYB 63
Fig-3.5(d) Results Based on Each Composite Laminate 64
Fig-3.6(a) Force-Displacement Plot for 4 m/s 65
Fig-3.6(b) Force-Time Plot for 4 m/s 66
Fig-3.6(c) Energy-Displacement Graph for 4 m/s 66
Fig-3.7(a) Force-Displacement Plot for 6 m/s 67
Fig-3.7(b) Force-Time Plot for 6 m/s 68
Fig-3.7(c) Energy-Time Plot for 6 m/s 68
Fig-3.8(a) Force-Displacement Plot for 8 m/s 69
Fig-3.8(b) Force-Time Plot for 8 m/s 70
Fig-3.8(c) Energy-Time Plot for 8 m/s 71
Fig-3.9 Back face of the Hybrid Laminate at 6 m/s 72
Fig-3.10 Front and back side of the impacted samples for 4 m/s, 6 m/s and 8 m/s 73
Fig-3.11 Tensile Test results and the Stress-Percent Elongation of all laminates 76
Fig-3.12 Peak Values for all laminates for 6 m/s and 8 m/s 79
Fig-3.13 the symmetric layers of carbon fabrics in the middle of the Laminates 81
Fig-3.14 (a) Area under Curve before Peak Load for Force-Time Plot for 4 m/s 80
Fig-3.14 (b) Area under Curve after Peak Load for Force-Time Plot for 4 m/s 80
Fig-3.15 Values of the Ductility index calculated from Force-Time plots 81
Fig-3.16 Damage Degree for 4 m/s, 6 m/s and 8 m/s 84
Fig-3.17 Alternating layers of 1B1C (left) and 3B3C (right) 85
Fig-3.18 Interlaminar shear stress values for basalt and carbon fabrics 87
Fig-3.19 Failures of The Laminates Under Tensile Test 89
Fig-3.20 Failure pattern of the 3B3C 89

LIST OF THE TABLES

Table-1.1 Comparison of the basalt and glass fiberss....13
Table-1.2 Properties of the carbon and the basalt fibers....19
Table-2.1 Properties of 100 % Carbon Fabrics....21
Table-2.3 Properties of the basalt fabrics....22
Table-2.4 Properties of Basalt Fibers....22
Table-2.5 The properties of Carbon Fabrics....23
Table-2.6 Laminating resin L 285 Properties....24
Table-2.7 Properties of the H260S Hardener....24
Table-2.8 Rotary Pump Properties....27
Table-2.9 Properties of the D24000S Cutting Machine....42
Table-3.1(a) Force-Deformation Graph Values for 1B1C....55
Table-3.1(b) Energy-Time Plot Values for 2B2C....57
Table-3.2(a) Force-Deformation Graph Values for 2B2C....58
Table-3.2(b) Energy-Time Plot Values for 2B2C....60
Table-3.3(a) Energy-Time Plot Values for 3B3C....61
Table-3.3(b) Energy-Time Plot Values for 3B3C....62
Table-3.4(a) Energy-Time Plot Values for HYB....63
Table-3.4(b) Energy-Time Plot Values for in-plane Hybrid Composite....64
Table-3.5(a) Peak Force, Maximum Displacement and Area under Curve for 4 m/s....66
Table-3.5(b) Impact energy and absorbed energy for 4 m/s....68
Table-3.6(a) Peak Force for 6 m/s....69
Table-3.6(b) Impact energy and absorbed energy for 6 m/s....70
Table-3.7(a) Peak Force for 8 m/s....71
Table-3.7(b) Impact energy and absorbed energy for 6 m/s....72
Table-3.8(a) Numerical values of Maximum Stress....75
Table-3.8(b) Values of Peak Force, Max Displacement and the area under the curve....77
Table-3.9 Ductility index for all laminates at different impact speeds....83
Table-3.10 Impact, absorbed energy and damage degree....84

INTRODUCTION

A composite material is a material system composed of two or more macro constituents that have different types and chemical composition. They are insoluble in each other due to their different chemical properties. People have been making composites for many thousand years with the example of mud and bricks in which mud is dried out into a brick shape to give a building material. Concrete is another ancient composite which is mixture of small stones and sand. Ancient generations found that medal rods or wires in the concrete can increase the bending quality, tensile strength in modern scientific term. The modern example of the composite materials is the fiberglass which is widely used today for boat hulls, sports equipment, building panels and many car bodies. Some advanced composites are now made using carbon fibers instead of glass. These materials are lighter and stronger than fiberglass but more expensive to produce. They are used in aircraft structures and expensive sports equipment such as golf clubs. Carbon nanotubes have also been used successfully to make new composites. These are even lighter and stronger than composites made with ordinary carbon fibers but they are still extremely expensive but offer possibilities for making lighter cars and aircrafts. The new Airbus A380, the world's largest passenger airliner, makes use of modern composites in design.

The incorporation of several different types of fibers into a single matrix has led to the development of hybrid composites. Also, using a hybrid composite that contains two or more types of fiber, the advantages of one type of fiber could complement with what are lacking in the other. As a consequence, a balance in cost and performance can be achieved through proper material design. The properties of a hybrid composite mainly depend upon the fiber content, length of individual fibers, orientation, extent of intermingling of fibers, fiber to matrix bonding and arrangement of both the fibers. The strength of the hybrid composite is also dependent on the failure strain of individual fibers. There are several types of hybrid composites characterized as:

(1) interplay or tow-by-tow, in which tows of the two or more constituent types of fiber are mixed in a regular or random manner;

(2) sandwich hybrids, also known as core-shell, in which one material is sandwiched between two layers of another;

(3) laminated, where alternate layers of the two (or more) materials are stacked in a regular manner;

(4) intimately mixed hybrids, where the constituent fibers are made to mix as randomly as possible so that no over-concentration of any one type is present in the material;

(5) other kinds, such as those reinforced with ribs, pultruded wires, thin veils of fiber or combinations of the above.

In this study, sandwich hybrids with the different configurations which are discussed in chapter 3 are used. There are two types of fibers used to make the hybrid composites named as Carbon and Basalt. Basalt is a type of igneous rock formed by the rapid cooling of lava at the surface of a planet. It is the most common rock in the Earth's crust. Basalt rock characteristics vary from the source of lava, cooling rate, and historical exposure to the elements. High quality fibers are made from basalt deposits with uniform chemical makeup. Basalt fibers have a cheaper processing price, similar processing methods to the glass fibers and possesses mechanical properties between glass and carbon fibers. Ductile in nature, longer load to elongation lengths (compared to carbon) and lower young's modulus (compared to carbon fibers) are the main properties of the basalt. They are chemically stable and can operate at high temperatures. Carbon fibers are made with a higher cost but have higher operating temperatures, higher young's modulus and better mechanical properties. Is brittle in nature and is stiffer than glass and basalt. Its manufacturing started quite earlier than that of basalt and a lot of research on its properties and its hybrid composites. Basalt fibers, on the other hand, are relatively new in the industry and most of the research is carried on its replacement to the glass and sometimes to carbon fibers. This is because basalt fibers have similar properties to glass and carbon fibers. Carbon Fiber is made of carbon crystals aligned in a long axis. These honeycomb shaped crystals organize themselves in long flattened ribbons. This crystal alignment makes the ribbon strong in the long axis. The fiber shape is the original shape of the material (its precursor) used to produce the Carbon Fiber. These fibers (containing flat ribbons of carbon crystals) in turn are bundled by the manufacturer in thicker fibers and are woven into carbon cloth, made into felt, twisted or bundled without twisting. This is referred to as Roving. In order to modify the characteristics of the layup, other materials are sometimes added such as glass fibers, Kevlar, Aluminum or basalt. In boat building we usually think of

epoxy or polyester resins, but carbon fiber is also used as reinforcement for thermoplastics, concrete or ceramics.

In this study, the fabrics made of carbon, basalt and in-plane carbon-basalt hybrid are used to create the laminates of 4 types. The 3 laminates are made by using the fabrics made of 100% carbon and 100% basalt fabrics arranged in three different stacking sequences. The forth laminate is made by the fabric which is hybrid in-plane. It means the in-plane hybrid fabric which has yarns from basalt and carbon perpendicular to each other. 12 layers of 100% carbon and 12 layers of 100% basalt fabrics are used to produce the 3 laminates which have carbon fibers in the core, which are called the sandwich type hybrid composites. The in-plane hybrid laminates are used and 24 layers of these fabrics are used to create the in-plane hybrid composite laminates. It means in totally 4 laminates are prepared, 3 of them made by carbon and basalt fabrics stacked in different sequences and the 4^{th} laminate is made by using the in-plane hybrid fabrics.

Composite Materials have many mechanical characteristic behaviors that are different from those of more conventional engineering materials and some of characteristics are merely modifications for conventional behavior and some are totally new which require new analytical and experimental procedures. Tailoring of the composite materials for a required mechanical property is the most significant advantage of the composite materials because with a little effort the composite material which is produced serve the predetermined mechanical properties with change of the amount or the nature of the matrix or the reinforcing materials. Isotropic materials, which have symmetry of properties from the point of application, are easily tested to understand their mechanical properties by using the standards prescribed by the international testing standards. For isotropic materials application of the stress causes extension or contraction in accordance with the direction of the applied stress but no shearing deformation. The application of the shear stress causes only shearing deformation but no extension or contraction in any other direction. This, by definition is the property of the isotropic materials. For orthotropic materials the case is different because the extension or the contractions in the material under the load in particular direction is different from the other directions because due to the definition of the orthotropic materials they have different properties in three mutually perpendicular directions. The composite materials are normally inhomogeneous and this is the reason typical dog-bone tensile specimen cannot be used to determine their mechanical properties. New modified composite materials' tests are presented to examine the properties of the composite materials.

The hybrid composite materials which are hybrid in plane (one laminate) and hybrid through thickness (three laminates with different stacking sequences) are tested with the low speed drop weight impact test. The samples used for the impact test has a dimension of 100x100 mm^2. The speed of the impactor for the test is 4 m/s, 6 m/s and 8 m/s. The effect of the impact test on the different configurations of the stacking sequence for hybrid through thickness and effect of the impact test on the hybrid in-plane laminates are examined. In order to check the tensile strength of the laminates, hybrid through thickness and hybrid in-plane laminates are tested with the tensile test.

The results gained from these two tests which are tensile test and drop weight impact test are evaluated to understand the effect of two different types of hybridization on the mechanical properties of the composites. The mechanical properties is a broad term which includes a number of properties and not much tests can be applied on the single product because most of these mechanical properties determining tests require peculiar modification of the samples. That's why only two types of the mechanical tests were carried out to have an idea about the tensile and impact behavior of the composite laminates. Tensile strength, ductility index, damage degree and visual inspection are examined in the review. In the beginning of the thesis, introduction of the composite materials, hybrid composite materials, difference between in-plane and through thickness composites, carbon fibers, basalt fibers, advantages and disadvantages of the composite materials is given. Chapter 1 contains more specific information about the academic work which has been done until now by the scientists in the scope of this study regarding the constituents of the composite materials, production and inspection of their mechanical properties using various mechanical techniques. It also shows the advantage of using basalt fibers instead of glass or carbon regarding cost and manufacturing simplicities. Chapter 2 has the materials and methods used for the manufacturing of the laminates. It contains the scientific methods used to manufacture the tested hybrid composite laminates and also gives the introduction to the machines which are used to investigate the impact and tensile behavior of the product. Chapter 3 possesses the second part of the study consisting of analyzing some of the mechanical properties of the manufactured samples using two tests which are tensile and the low speed drop weight impact test. Later the graph data extracted from these results and observations made from the results are provided in an organized manner. At the end of the chapter 3 a dedicated section collects and then evaluates the scattered results from both experiments for all the materials. This is followed by reviews and discusses them in detail to understand the reasons behind particular mechanical responses for all the hybrid composite laminates when a certain type of test was applied to them.

CHAPTER 1

LITERATURE REVIEW

Chapter 1 includes the background of the scientific work in the scope of this study. It basically has the work done by the other academicians regarding the production and the history of the basalt and carbon fibers which are the main constituents of the products used in this study. Tests to analyze the mechanical properties of the carbon and basalt based hybrid composites and the effect of incorporation of the basalt fibers in the carbon fibers is also described with the references of the literature studies. The first part tells the background, later the introduction of the basalt and carbon fibers is given which is followed by their comparison regarding their mechanical properties.

1.1 Background

Hybrid composites have advantages because it provides options to give more optimization to the mechanical and stability properties of the material. One of the techniques used change the properties of a composite materials is changing the nature of the matrix by introducing different elements. Another way of getting desired results is introduction of a totally new material in the main material which then is used collectively in the matrix. This is the main idea of the hybrid materials. In this study carbon and basalt fibers are used to create plain weave fabrics. These fabric layers are put together to create laminates of hybrid composite materials.

The manufacturing of the carbon fibers is complex and expensive as compared to that of basalt but it gives very promising properties. The use of carbon fiber reinforced plastics in the automotive industry is seen but due to its weight, it increases the weight of the vehicle by 40-60%. The more the weight the more energy is consumed as suggested by Fiore and Bella et al. [1].

Basalt fibers have become a potential candidate for the reinforcement fiber inside a hybrid because they are not only cheaper but also have good strength, modulus, high operating temperature range and good chemical and thermal resistance. They are said to have better tensile and compressive properties too as compared to glass fibers

confirmed by the studies carried out by Lopresto, Vione and Wang et al. [2-4] respectively. Cheaper manufacturing process, safer health measurements, similar mechanical properties to glass-fibers, non-combustibility and thermal stability are some of the key properties of basalt fibers which make them preferable to glass-fibers confirmed in the researches et al. [5-6].

Lopersto et al. [2] carried out some tests on the plastic laminates reinforced by basalt and E-glass fibers to compare the mechanical properties of both. The results showed the plastic reinforced with basalt fibers showed high performance in terms of young modulus, compression and bending strength, impact force and energy. Manikandan et al. [7] also showed basalt has superior properties than those of glass fibers.

Czigany et al. [8] made the hybrid composites of basalt-carbon, basalt hemp and basalt-glass with the poly-propylene as a matrix. Later he made the same composites this time not hybrid with basalt fibers but only carbon, hemp and glass with the poly-propylene as a matrix. The purpose was to understand the effect on the mechanical properties of composites when basalt is added as a secondary fiber in the composites. The experimental results showed that the mechanical characteristics improved in each case. A significant improvement in the mechanical properties was shown in case of carbon fiber and especially in the case of glass fiber composites when they basalt fiber is used as a secondary fiber in the composite.

In general, the main advantage of using fabric as reinforcement in the composite is that the laminates have balanced properties in orientations of 0°C and 90°C. However, the tensile strength and modulus of fabric-reinforced composites are lower than the unidirectional fiber (tape) reinforced composites.

When basalt is replaced with carbon fiber in a composite initially made by all carbon/epoxy composites, the substitution of 20% and 40% of basalt gives approximately same properties as those composites give with carbon. But basalt is cheaper as compared to that of carbon fiber. Then why not go for basalt, a cheaper fiber, as a reinforcement material which is giving almost same properties as carbon fiber? These experiments were carried by Chikhradze et al. [9] while he was making carbon, basalt and E-glass composites for the manufacturing of wind turbines.

Due to the high specific stiffness and strength, carbon fiber reinforced polymer composite is the material of choice in aerospace industry. However, the toughness of carbon fiber is quite low and the resulting damage resistance is poor. In this regard, several approaches have been successfully exploited to enhance the impact damage resistance of composite laminates. One approach consists in enhancing the properties of

the matrix material, as proposed by Reis et al. [58], who investigated the impact behavior as well as the damage tolerance of Kevlar/filled epoxy matrix with two different fillers, namely cork powder and nanoclays. They found that adding fillers increased the maximum impact load, which was very dependent on the filler type. Another approach is known as hybridization, usually with high strain to failure fibers to improve the damage resistance of composites to low velocity impact. This hybridization approach was followed in this study.

Lower tensile strength values of fabric reinforced polymeric composites are related to the bi-directional orientation and the undulations of the roving in the fabric confirmed in the studies by Schwartz et al. [15].

The stacking sequence; the arrangements of the laminae inside a composite material is thought to play an important role in the properties of the composites. That means inside a hybrid composite made by two fibers let's say A and B, the properties of the composite depend on the arrangement of A and B type fibers inside the matrix. During a study carried by Park and Jang et al. [10] they made a hybrid composite laminate made by Polyethylene and carbon fibers inside a matrix and concluded that the mechanical properties of the composite depended on the position of each fiber in the matrix. Highest flexure strength was seen when carbon was placed as the outermost layer as shown in the study by Park and Jang et al. [10].

Most of the studies regarding basalt fibers have focused on the improvement of the plastics reinforced with basalt and carbon fibers by introducing different reinforcements into it. For example, Lee et al. [11] introduced carbon nanotube (CNT] to the Basalt/Epoxy composites and examined the mechanical and thermal properties. Ying and Hong et al. [12] incorporated the rubber and silica nano-particles in the epoxy of the carbon fiber/epoxy laminates and did double-cantilever-beam tests to examine their fracture toughness. Scanning electron microscopy examination of the delaminated surfaces tests revealed the improvement in the interlaminar toughness is caused by the cavitation of nano-rubber particles and debonding of the nano-silica. The same type of work is done by incorporating filler fibers by Hao et al. [13] who carried out surface modifications to improve properties of composites.

However other than Ary and Yonjig et al. [14] who examined the effect of changing in the stacking sequences of woven carbon and basalt laminae on the mechanical properties of the hybrid composites, not much is discussed stacking sequence and its effect on the mechanical properties. The possibility of incorporating basalt fibers into carbon fiber reinforced composite and effect of stacking sequence on the flexural properties of the hybrid composite was discussed by Ary and Yonjig. The samples were

created using VARTM technique and post flexure tests samples were examined by the Scanning Electron Microscopy images. The results showed that higher flexural strengths and modulus were obtained when carbon layer was stacked on the outer layer. Carbon fibers bear most of the fatigue stress. Both sides layered with basalt, i.e. basalt on the compressive and tension sides, made the material more ductile.

In the study done here in this thesis, a similar approach is followed to Ary and Yonjig et al. [14]. The fibers used in this study are plain weave basalt, carbon and plain weave hybrid basalt-carbon woven fabrics. And here 24 layers of the fabrics are being used while the mentioned study used 10 layers of different sequences of the fabrics. Total 4 different arrangements of the composite material are used in this study. 3 of these composite materials are made by different stacking sequences of the 100% carbon and 100% basalt fibers. The last and fourth composite material is prepared by using the plain weave hybrid fabric of carbon-basalt. Details of these fabrics is given in the materials and methods section. A total of four different arrangement sequences are adopted to create basalt/Carbon/epoxy hybrid composites where each one is symmetric around carbon fiber except the one made by plain weave hybrid carbon-basalt fabric. Three of the laminates have carbon fibers in the middle of them while the fourth one is made of plain basalt-carbon hybrid laminae stacked just one by one on each other.

What's interesting is that all the plain weave carbon and basalt fibers are arranged in such a way that same amount of material is used to produce the laminate and the only difference they have is their stacking sequence. The common property of these samples is the amount of material and that the carbon fabric is present in the middle while basalt is at the compressive side. The laminate made by plain weave basalt-carbon fibers are just stacked on each other and have the same amount of material used in them too as compared to the other plain carbon basalt hybrid composites.

It is planned to do the tensile test and low-speed impact tests on all 4 different laminates and the post impact composites will be examined to see the effect of in-plain hybridization (1B1C, 2B2C and 3B3C composite laminates) and hybridization through thickness hybridization (plain weave carbon-basalt hybrid composite laminates) on the mechanical properties of the material.

1.2 Basalt Fibers

A brief but wide introduction to the basalt fiber and its main properties is given in this section. Basalt is an inorganic fiber, basalt fiber has good strength, modulus, and better strain to failure than carbon fiber, high operating temperature range, good chemical

resistance, can easily be processed, eco-friendly, and inexpensive as shown by studies in [17-19] respectively.

1.2.1 Origin, Constituent and History of Basalt Fibers

Basalt is a natural, but not biodegradable material which is found in the volcanic rocks all over the globe in the study by Militky et al. [16-17]. The condition and the quality of the rocks depend on the rate change of temperature during the quenching process eventually causing crystallization. By analyzing the chemical composition of the basalt it can be seen that mostly the main constituent is SiO_3, which is followed by the Al_2O_3 and Fe_2O_3 with the percentages of 43.3-47%, 11-13% and less than 5% respectively and these values are taken from the references [16-19].

Paul Dhé from Paris in 1923 was one of the first persons to give the idea of developing Basalt fibers. Then around 60s, a high-tech Basalt fiber was developed by Moscow Research Institute of Glass and Plastic during 1953 to 1954. Its first industrial production furnace that adopted 200 nozzles drain board combination oven bushing process was completed in 1985 at Ukraine fiber laboratory as shown in the study by Morova et al. [20]. Both the U.S. and the former Soviet Union [USSR) investigated the basalt fiber applications, especially in military hardware.

Owens Corning is one of the companies that had research on the basalt fibers but then such companies eventually halted such researches favoring their own glass-fiber products for marketing purposes. Their focus on the core products resulted in successful development of S-2 glass fiber by Owens Corning.

1.2.2 Manufacturing of Basalt Fibers

Like every product, the cost depends on the quality of the core material used in the process as the studied showed that the temperature difference during the quenching process which leads the total or partial crystallization plays major role in the quality of the basalt rocks as shown in the study by Militky et al. [16-17]. Elements' concentration in the chemical composition gives different chemical and mechanical or physical properties in the product in the study by Novitskii et al. [21].

The manufacturing of the basalt fibers is cheaper and less energy consuming as compared to that of glass or carbon as it needs no additives. The basalt rock is melted at 1450-1500°C and then forced through platinum/rhodium bushings for the formation of continuous or chopped fibers as reinforcement material. The conventional manufacturing process also needs no additives which has advantages in the cost as told in in the study by Sim et al. [22].

Other manufacturing processes for the formation of basalt include blowing melt technology for the formation of cheaper but bad mechanical properties possessing fibers shown by Deak et al. [18], melt-spinning method to produce fibers on laboratory scale based on dielectric heating shown by Kim et al. [23].

There is a method called spinneret method to form continuous fibers basically used to form glass fibers too as shown in Fig-1.1. This process can be used to form Basalt continuous fibers which have applications in the textile industry as shown in the study by Deak et al. [18].

1.2.3 Health Issues and Basalt

A naturally occurring mineral called Asbestos was once mainly used in different fields. Its durability and heat resistance, applications in building and pipe insulation, friction products and anti-heat products were overwhelming and justified it being favorite of US military as they used it to anti-fire vests and other military gears. But then studies showed that it caused lung cancers and was hazardous to health as inhaling those causes lung cancer, mesothelioma, laryngeal cancers and pulmonary fibrosis. Asbestos related fibers are banned in 50 countries except US.

Basalt fibers have the similar compositions to that of Asbestos and it was mandatory to

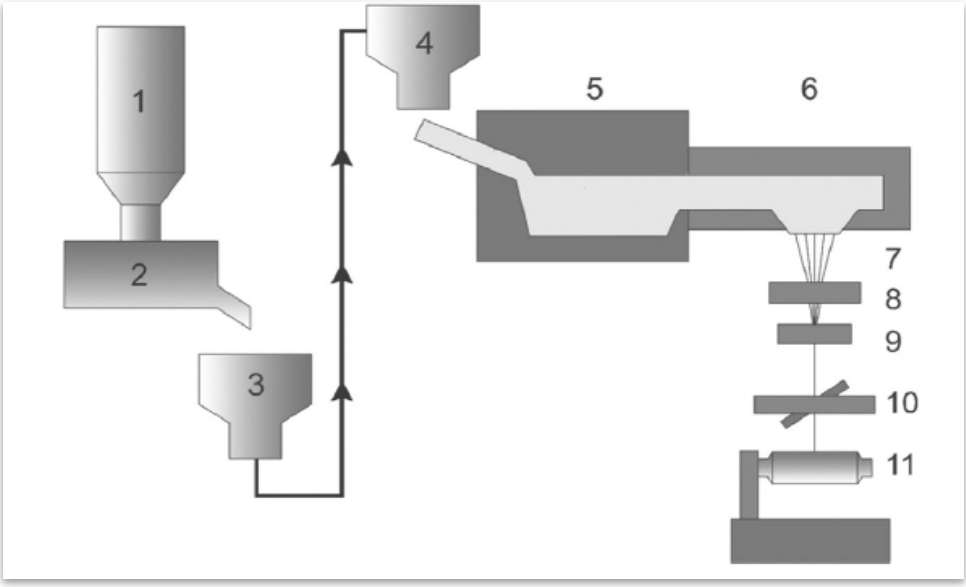


Fig-1.1 basalt fiberization processing line. 1) crushed stone silo; 2) loading station; 3) transport system; 4) batch charging station 5) initial melt zone; 6) secondary heat zone; 7) filament forming bushings; 8) sizing applicator; 9) strand formation station; 10) fiber tensioning station; 11) automated winding station

confirm if they had properties injurious to health. The morphology and surface properties of basalt ensures it is safe as compared to that of asbestos fibers as shown in the study by Quagliarini et al. [25].

Specially, Kogan et al. [26] in detail examined the effect of basalt fibers and chrysotile asbestos on the rats by making them inhale the air filled with asbestos and basalt for a period of 6 months. Asbestos fibers at a dose of 1.7 g/kg [body weight of the rat] killed 1/3 of the rats. While the 2.7 g/kg amount of asbestos killed all the rats. While in case of basalt fibers no rat died even when the dose was at the level of 10 g/kg. Such results showing that basalt is totally safe were re-confirmed by MConnell et al. [27] and causes no threat to human.

1.2.4 Advantages of Basalt Over Glass

The basalt and glass fibers have similar mechanical properties thus they do address the common fields in which basalt can be an advantageous alternative such as marine, automotive, sporting equipment and civil fields. Table-1.1 compares mechanical properties of glass and basalt fibers taken from the study by Fiore et al. [28].

Basalt fibers are non-combustible, possess higher chemical stability as sown in studies by Wei B. et al. [19, 29] and good resistance to weather, alkaline and acids exposure. Moreover, basalt fibers can be used from very low temperatures [i.e. about -200°C) up to the comparative high temperatures (i.e. in the range 600-800°C) and this data is taken from studies et al. [18, 21-32].

The thermal stability depends on the composition of the raw material of origin and the presence of micro-pores that prevent convection and thermal radiation of the air makes basalt a candidate for products serving the purpose of thermal insulation. [21-33, 34].

The chemical durability of basalt fiber was studied by Ramachandran et al. as early as 1981 [35]. The authors stated that this fiber has excellent resistance to alkaline attack, but it has poor resistance to acids. The better mechanical behavior of the basalt fibers than glass ones after corrosion treatments was then shown by Nasir et al. [36].

In particular, the thermal gravimetric analysis performed by Hao and Yu et al. [33] shows that the mass loss occurs in the temperature range of 200-350°C for both basalt and glass fibers (Fig-1.2). However, the basalt fiber has better thermal stability than glass fiber.

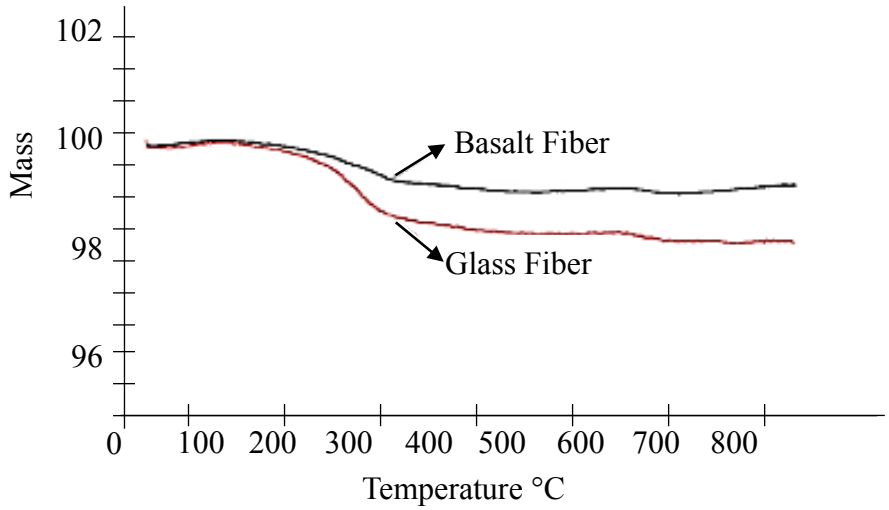


Fig-1.2 Mass loss of glass and basalt fibers [33].

1.2.5 Mechanical Properties of Basalt

The basic mechanical properties like high modulus, good strength and elastic behavior of the basalt fibers are similar to those of the glass fibers et al. [18]. The result of the tensile test applied on the short basalt fibers; relatively cheaper with not so good mechanical properties, continuous basalt fibers CB1, CB2, and CB3 from three different manufacturers is shown in Fig-1.3 As expected, the tensile modulus and strength of the continuous basalt fibers and glass fibers is similar while that of short basalt fibers is less stiff.

Table-1.1 Comparison of the basalt and glass fiberss

E glass and Basalt Fiber Properties Compared		
	E-Glass	Basalt
Density g/cm^3	2.56	2.8
Elastic Modulus GPa	76	89
Tensile Strength MPa	1.4-2.5	2.8
Elongation to Fracture	1.8-3.2	3.15
Specific E modulus (GPa per g/cm^3)	30	31.78
Specific Tensile Strength ((GPa per g/cm^3))	0.5-1	1

1.2.6. Applications of Basalt Fibers

Basalt fibers could be widely applied to many fields, such as corrosion resistance stuff in the chemical industry as seen in a study by Rabinovich et al. [37], wear and friction stuff in the automobile industry as shown in the study by Ozturk et al. [38], target area of anti-low velocity impact as seen in the study by Wang et al. [39], insulation of automobile catalysts as shown by Militky et al. [40], reinforcing material in construction as shown by Szbao et al. [6] and fire protection as shown by Landuci et al. [41]. In the automotive, basalt fibers are widely used for production of car headliners.

The main competitive advantage of basalt in this application is its outstanding recyclability, which is currently one of the key factors for automobile producers. In particular, a laminate for headliner is constituted by a core having an adhesive layer provided adjacent opposing sides thereof. Basalt fiber structural reinforcement layers are provided adjacent each adhesive layer. A scrim layer is provided next to one reinforcement layer while a film barrier and covering are provided adjacent the other reinforcement layer.

Moreover, basalt fibers are increasingly used in the following sections automotive brake disc pads and clutch facing applications. The technical advantages for their use in these applications than other typical materials are: 2-3 times longer service life of the break assembly; durable frictional contact with metal without its wear down; higher and more stable friction factor; increased shock resistance, extended working temperature range, resistance to chemically aggressive conditions.

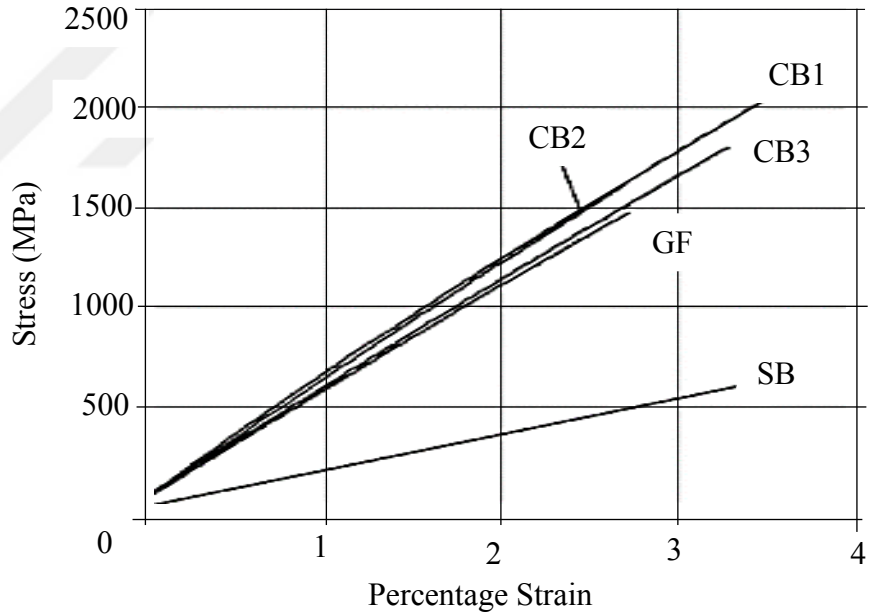


Fig-1.3 Stress-Strain diagram for Basalt Continuous/Short and glass

1.3. Carbon Fibers

1.3.1. History of Carbon Fibers

Thomas Edison was the first known person who used carbon fiber filaments in the year of 1879. He was working on incandescent light bulb baking the cotton threads. In the 50s, Akio Shindo et al. [43] worked on the polyacrylonitrile (PAN) treated with heat. In his work carbon fibers with tensile modulus of 140 GPa were formed while the fibers were based on Polyacrylonitrile.

In 1970, Toray Industries based in Japan obtained a license for Akio Shindo's patent rights, and by 1971 was manufacturing continuous PAN based Torayca T300 and M40 Carbon fibers at a production capacity of 1 ton/month with the tensile strength of 2.45 GPa which was increased to 3.30–3.43 GPa by 1985, and since 1988 has remained at

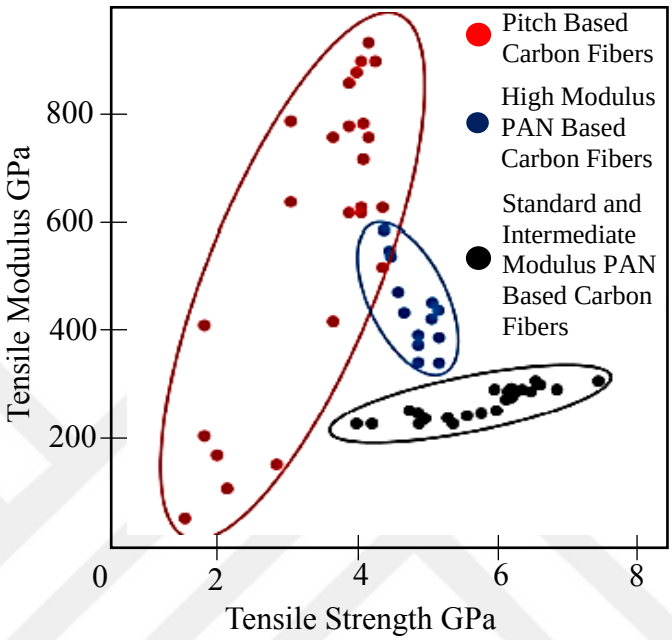


Fig-1.4 Different origin based carbon fibers and their tensile modulus

3.53 GPa. Toray also produced PAN based T8000H and T1000 carbon fibers while the later had tensile strength of 7.06GPa. Hexcel Corp. Inc. developed IM6, IM7 and IM8 carbon fibers with normal modulus. Fig-1.4 shows mechanical properties map of the carbon fibers manufactured by the different companies taken from the study by Bradly et al. [44] PAN and Rayon served as the origin of the manufacturing of the carbon fibers in the past. Despite the fact that currently almost 96% of the industry is utilizing the PAN based carbon fibers, in the past Rayon and pitch were also considered precursors of the carbon fibers. However, the cost of Rayon based fibers due to its costly processing techniques involving heat the price could reach to around 1000 euros per kg while the tensile strength was 2.25 GPa and modulus was 172 GPa, not very promising as compared to PAN based carbon fibers. The production of the carbon fibers from the precursors such as pitch and Rayon was decreased for these reasons. Sohim still produces the carbon fibers based on Rayon with carbonization at a temperature of 1500 and graphitization at a temperature of 2200. A study by Bradly shows that the carbon fibers based on pitch have unique properties such as their tensile modulus is 960 GPa although fibers with lower modulus are also available reference given at [44].

1.3.2 Manufacturing of Carbon Fibers

The manufacturing processes and techniques direct the properties of the product as per requirement. Carbon fiber ranges widely regarding its thermal and physical properties that can be tailored allowing the vast range of material properties. The manufacturing of the carbon fibers is mostly done by the PAN as precursor seen from the study by Das S. et al. [45]. During the processing of the carbon fibers based on PAN, higher tensile modulus, electrical and thermal conductivity is achieved by increasing the final heat treatment. In the studies by Edie and Qiu et al. [46, 47] shows that the commercially available carbon fibers based on the PAN have the properties like tensile modulus ranging from 230 to 588 GPa, electrical conductivities of 55-143 kS/m and thermal conductivities of 5-156 W/m/k. These improved properties decrease the tensile and compressive strength. ACording to Oya N et al. [48], Toray M60J carbon fiber possesses a tensile strength of 3.9GPa, tensile modulus of 588 GPa, thermal conductivity of 152W/m/K and electrical conductivity of 0.363 cal(c)m/s(c).

1.3.2.1 Pan Based Carbon Fibers

PAN based carbon fibers are prepared by the polymerization of the PAN or PAN copolymer. Fiber spinning and drawing is applied on them. Later they are stabilized in the air at a temperature of 200-300°C and carbonized in the inert environment at a temperature which ranges from 1000 to 1700°C. After these steps, heat treatment in an inert environment at the temperature of 3000°C defines the final amount of carbon in the final carbon fiber. Increase in the heat treatment temperature increases the fiber modulus and eventually the amount of carbon in fiber.

Toray T300 contains 93 wt% of carbon with not so good modulus. Toray T800 contains 96 wt % modulus and intermediate modulus. The high modulus carbon fiber contains more than 99 wt% carbon. The heat treatment temperature defines the amount of the carbon in the fiber and eventually its modulus.

1.3.2.2 Pitch Based Carbon Fibers

pitch based carbon fibers are also produced by the precursor as it is done for PAN based carbon fibers. The chain of the applied methods is fiber spinning, stabilization in the air, and carbonization in inert environment. Graphitization in argon at a temperature of 3000°C is also applied if needed.

Stabilization or thermosetting in the air is carried through for a temperature up to 350°C in an environment where oxygen is available. Carbonization is carried through again up to a temperature of 2000°C in an environment of nitrogen or argon as shown in the study by Morgan et al. [49] and Park et al. [50].

Pitch fibers are derived from the origins like melt spinning of isotropic pitch, natural sources like petroleum or coal. Properties of the resultant fibers depend upon the treatment temperature and the widely ranged origin of derivation. P25 carbon fiber manufactured by the pitch has a tensile strength of 1.56 GPa, Modulus of 172 GPa, thermal conductivity of 26 W/m/K and electrical conductivity of 77 kS/m. K-1100 pitched based carbon with a tensile strength of 3.10 GPa, tensile modulus of 965 GPa, thermal conductivity of 900-1100 W/m/K and electrical conductivity of 900 kS/m.

1.3.3 Carbon Fibers' Mechanical Properties

The mechanical properties of the carbon fibers like tensile strength depend upon the factors called flaw defects. Flaw defects can reside inside the fiber structure or on the surface of the carbon fibers during manufacturing and they limit the tensile strength of the carbon fibers. Crystal shear strength does put a limit to the tensile strength of the carbon fibers as studied by Reynolds and Sharp et al. [50]. They calculated the value of flaw size which puts a limit to the tensile strength of the carbon fibers. According to the studies of Reynolds et al. [50] and Honjo et al. [51] it's said that the carbon fiber tensile strength is a defect limiting property and the ultimate tensile strength values don't seem to be achieved if the typical processing methods are applied during manufacturing.

The structure-property relationships of the carbon fibers also affect their compressive properties. A study by Kumar et al. [52] shows that the compressive strength decreases inversely with the tensile modulus as long as the material is made of the identical precursor. Understanding such relationships can guide the manufacturing processes to get maximized properties.

The data values of the samples for G12 suggested that the higher carbonization temperatures and thus higher tensile modulus do not reduce the PAN carbon fiber shear modulus until sufficient carbonization temperature of 28000 degrees centigrade is reached as shown in the study by Bradly et al. [44].

1.3.4 Advantages-Disadvantages of Carbon Fibers

In this section, common properties of the carbon fibers are listed which might have advantages and the disadvantages in accordance with the use of these fibers.

1.3.4.1 High Strength to Weight

Strength of a material is the force per unit area at failure, divided by its density. Any material that is strong and light has a favorable Strength/Weight ratio. Materials such as Aluminum, titanium, magnesium, Carbon and glass fiber, high strength steel alloys all have good strength to weight ratios

Because of the way the crystals of carbon fiber orient in long flat ribbon or narrow sheets of honeycomb crystals, the strength is higher running lengthwise than across the fiber. That is why designers of carbon fiber objects specify the direction the fiber should be laid to maximize strength and rigidity in a specific direction. The fiber being aligned with the direction of greatest stress. Pan based precursor carbon fiber has higher strength than pitch based carbon fiber which has higher stiffness.

1.3.4.2 Rigidity

Rigidity or stiffness of a material is measured by its Young Modulus and measures how much a material deflects under stress. Carbon fiber reinforced plastic is over 4 times stiffer than Glass reinforced plastic, almost 20 times more than pin. For this reason, there are some ways to make these rigid carbon fibers reinforced materials flexible which include introduction of flexible fibers into it.

1.3.4.3 Electrically Conductivity

This feature can either be useful or be a problem. In Boat building conductivity has to be taken into account just as Aluminum conductivity comes into play. Carbon fiber conductivity can facilitate Galvanic Corrosion in fittings. Careful installation can reduce this problem. Carbon Fiber dust can accumulate in a shop and cause sparks or short circuits in electrical appliances and equipment.

1.3.4.4 Fatigue Resistance

Resistance to Fatigue in Carbon Fiber Composites is good. However, when carbon fiber fails it usually fails catastrophically without significant exterior signs to announce its imminent failure. Damage in tensile fatigue is seen as reduction in stiffness with larger numbers of stress cycles, (unless the temperature is high) Carbon fiber is superior to E glass in fatigue and static strength as well as stiffness.

The orientation of the fibers and the different fiber layer orientation, which we have done in this study by introducing basalt layers in the laminates, have a great deal of influence on how a composite will resist fatigue (as it has on stiffness). The type of forces applied also result in different types of failures. Tension, Compression or Shear forces all result in markedly different failure results.

1.3.4.5 Tensile Strength

Tensile strength or ultimate strength, is the maximum tensile stress that a material can withstand while being stretched or pulled before necking, or failing. Brittle materials such as carbon fiber does not always fail at the same stress level because of internal flaws which depend on the method of the manufacturing and information about this is also given in section 1.3.3 and reference of the study by Reynolds et al. [50]. They fail at small strains. In other words, there is not a lot of bending or stretching before catastrophic failure.

1.3.4.6 Thermal Conductivity

Thermal conductivity is the quantity of heat transmitted through a unit thickness, in a direction normal to a surface of unit area, because of a unit temperature gradient, under steady conditions. In other words, it's a measure of how easily heat flows through a material.

Because there are many variations on the theme of carbon fiber it is not possible to pinpoint exactly the thermal conductivity. Special types of Carbon Fiber have been specifically designed for high or low thermal conductivity.

1.3.4.7 Non Poisonous, Biologically Inert, X-Ray Permeable

These quality make Carbon fiber useful in Medical applications. Prosthesis use, implants and tendon repair, x-ray accessories surgical instruments, are all in development. Although not poisonous, the carbon fibers can be quite irritating and long term unprotected exposure needs to be limited. The matrix either epoxy or polyester, can however be toxic and proper care needs to be exercised

1.3.4.8 Carbon Fiber Price

Although it offers exceptional advantages of Strength, Rigidity and Weight reduction, cost is a deterrent. Unless the weight advantage is exceptionally important, such as in

aeronautics applications or racing, it often is not worth the extra cost. The low maintenance requirement of carbon fiber is a further advantage. You might need less of it compared to fiberglass and this might be a saving.

1.3.4.9 Brittleness

The layers in the fibers are formed by strong covalent bonds. The sheet-like aggregations readily allow the propagation of cracks. When the fibers bend they fails at very low strain. In other words, carbon fiber does not bend much before failing.

1.4 Carbon Fibers vs Basalt Fibers

Here properties of the carbon and the basalt fibers are compared in Table-1.2.

Table-1.2 properties of the carbon and the basalt fibers

Fibers	Density	Tensile Strength	Elastic Modulus	Elong. to Break
Basalt Fibers	2.7 g(c)m^3	4100-4840 MPa	93.1-110 GPa	3.1
Carbon Fibers	1.8 g(c)m^3	3500-6000 MPa	230-600 GPa	1.5-2.0

CHAPTER 2

MATERIALS AND METHODS

This chapter includes the nature, type and construction of the materials used in the study along with the methods of the fabrication of the product which will be tested. A detailed view of the production of the products and their geometry is given to understand and recognize the products.

2.1 Composites Manufacturing

2.1.1 Fabrics

There are three type of fabrics which are used in this experiment made of carbon and basalt fibers, for which a detailed overview, their properties, manufacturing processes and mechanical information is given in the previous chapter. Three fabrics are comprised of 100% carbon fibers, 100% basalt fibers and carbon-basalt hybrid plain weave fibers. Most fabrics are made by weaving or knitting yarns together. A fabric's appearance, properties and end use can be affected by the way it was constructed.

2.1.2 Carbon Weave Fabrics

The fabrics used in this project was based on the plain weave fabrics.

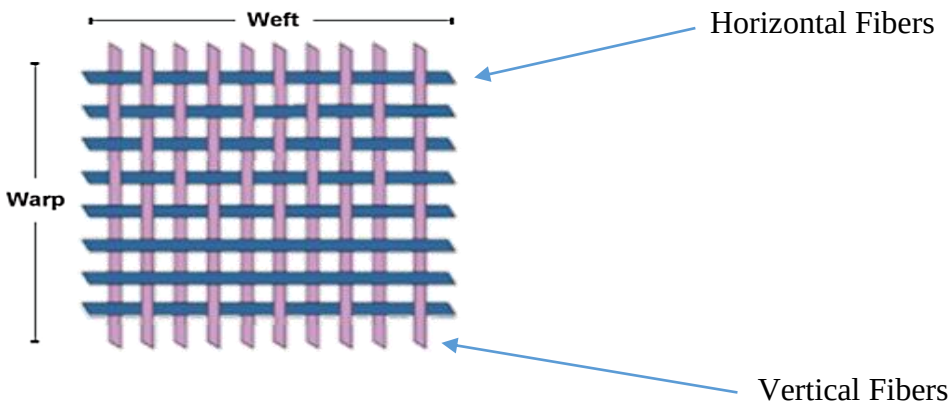


Fig-2.1(a) Plain weave arrangement of yarns in a fabric

In plain-weave fabric there is a complex arrangement of warp and weft threads, which allows longer float threads either across the warp or the weft. The long floats mean the light falling on the yarn doesn't scatter and break up, like on a plain-weave. Here both wrap and weft are made of carbon A-38 Figures-2.1(a), (b) and their properties are given in Table-2.1

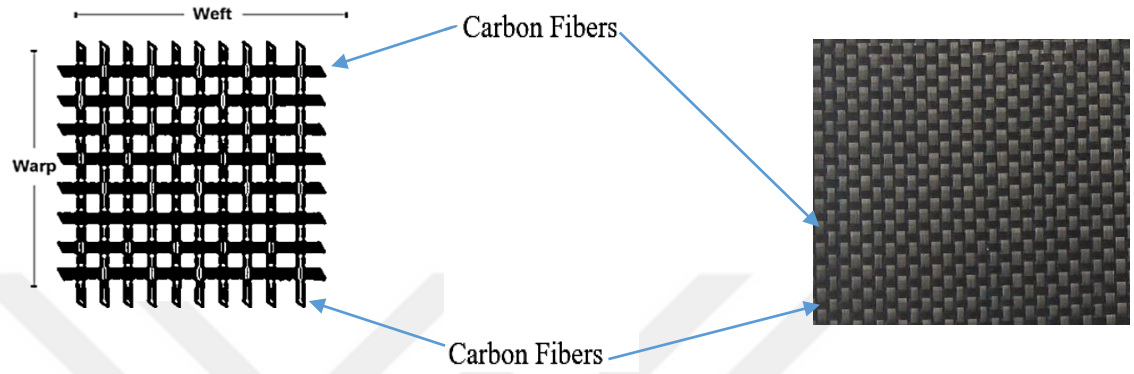


Fig-2.1(b) Arrangement of yarns in 100% Carbon Fabrics

The product name of these carbon fabrics is SPN B 200 P fabricated by the Spinteks Tekstil İnşaat Sanayi ve Ticaret A.Ş with the properties as given below.

Table-2.1 Properties of 100 % Carbon Fabrics

Product Code	**Weight**	**Warp and Weft**	**Width**	**Yarn**	**Tensile Strength**	**Thickness**
SPN B 200 P	200gr/m²	5 / cm	100/ cm	Carbon A 38	3800 MPa	0.20 ±%5 mm

The Yarn has a product name A 38 Carbon made by Dow Aksa and has the properties given in Table-2.2 giving the idea of the mechanical properties of the carbon fibers. Though a comparison between the mechanical, electrical and thermal properties is given in the last part of this chapter to have the idea of their properties.

Table-2.2 Properties of Carbon Fibers

Properties of Carbon Yarns	
Density g/cm^3	1.78
Tensile Strength MPa	3800
Tensile Modulus GPa	240

2.1.3 Basalt Weave Fabrics

These fabrics are also based on the stain weave plain fabrics made by the yarn of basalt which are arranged with the stain weave shape of warp and weft threads, which allows longer float threads either across the warp or the weft. Here both wrap and weft are made of basalt fibers as shown in Fig-2.2

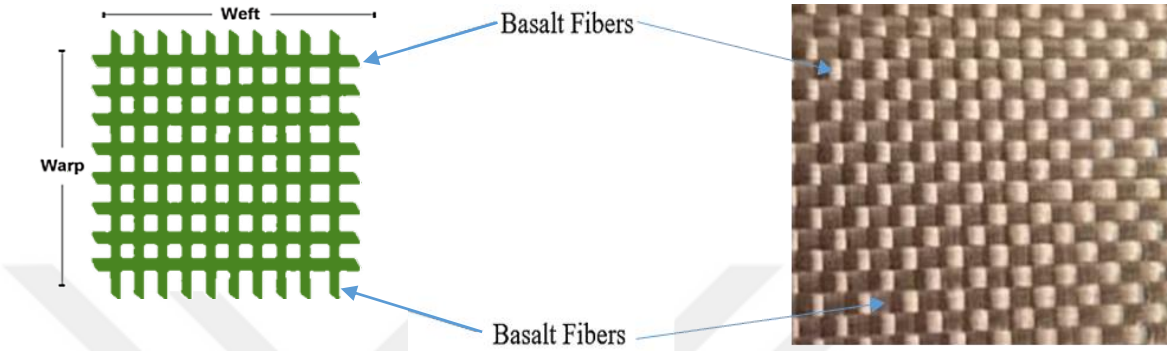


Fig-2.2 Arrangement of yarns in Basalt Fabrics

The basalt fibers at horizontal and vertical level both have 90°C angel with each other. The product factory name of these carbon fabrics is SPB 132 P fabricated by the Spinteks Tekstil İnşaat Sanayi ve Ticaret A.Ş with the product properties as in Table-2.3

Table-2.3 Properties of the basalt fabrics

Weight	**Warp and Weft**	**Width**	**Yarn**	**Tensile Strength**	**Thickness**
200 gr/m²	5 / cm	100cm	Basalt	4500 MPa	0.23 ±%5

The yarn is made of continuous basalt fibers with properties given in Table-2.4

Table-2.4 Properties of Basalt Fibers

Properties of Basalt Fibers	
Density [g/cm³]	2.6 - 2.8
Tensile Strength [MPa]	4100 - 4840
Elastic Modulus [GPa]	93.1 - 110
Elongation at break (mm)	3.1
Maximum Service Temperature	650°C

2.1.4 Basalt-Carbon In-Plane Weave Fabrics

The last type of fabric used in the experiment is the hybrid fiber composed of carbon and basalt fiber yarns arranged with plain weave. Hybrid Fabrics are woven by More than two kinds of different fibers materials (Carbon fiber, Aramid fiber, Fiberglass, Basalt fiber which have the great performance of composite materials in impact strength, rigidity and tensile strength. Hybrid Fabrics have extensive applications, such as automotive engineering, motor sports, the fashionable decorations, aircraft construction, ship construction, sports equipment, electronic products and other applications.

In this project the hybrid fabrics are composed of two different fiber materials which are basalt and carbon. The basalt and carbon fibers are arranged in a plain weave pattern and each is located at 90°C with each other. As shown in Fig-2.3 the carbon fibers in the black color and the basalt fibers in the softer color are evident. Both schematic and the real picture of the carbon-basalt fabric is given in Fig-2.3 to have a better understanding and recognizing the fibers with their color.

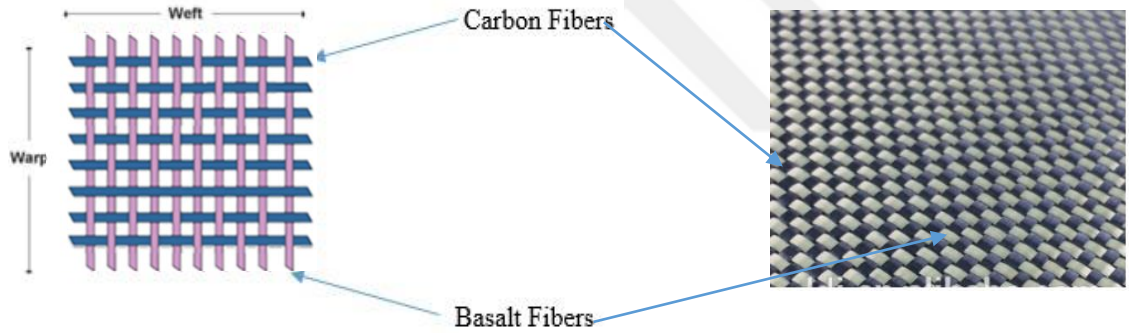


Fig-2.3 Arrangement of Yarns in Hybrid Carbon-Basalt Fabrics

The properties of the product and its mechanical properties are in Table-2.5, this product too, as 100% basalt and 100% carbon fabrics was fabricated by Spinteks Tekstil İnşaat Sanayi ve Ticaret A.Ş. The same company is creating other composite materials product including the 100% basalt and 100 carbon fabrics.

Table-2.5 the properties of Carbon Fabrics

Product Code	Weight	Warp and Weft	Width	Yarn	Tensile Strength	Thickness
SPN H	265 g/m^2	5 / cm	100/cm	Basalt/Carbon Fiber	unknown	0.25mm ±%5

2.1.5 Adhesive Resin and Hardener

The manufacturing of the laminates is actually based on the rule that mechanical strength of the laminate comes from the fibers used in it while the flexibility in the laminate is based on the epoxy resin or other adhesive material.

The adhesive resin used in the manufacturing of the laminates used in this project is Laminating resin MGS® L 285 manufactured HEXION. The properties of the product are in Table-2.6

Table-2.6 Laminating resin L 285 Properties

Laminating resin L 285 Properties	
Density [g(c)m³]	1.18 – 1.23
Viscosity [mPas]	600 - 900
Epoxy equivalent [g/equivalent]	155 - 170
Epoxy value [equivalent /100g]	0.59 – 0.65
Refractory index	1.525 – 1.5300

2.1.5.1 Effect of Hardener onThermosetting.

J.R.M. d'Almeida et al. [53] examined The Role of the Resin Matrix/Hardener Ratio on the Mechanical Properties of Low Volume Fraction Epoxy Composites. The mechanical performance of composite materials is usually associated with the properties of their reinforcement. However, the matrix materials also play an important role as is the case for thermoset resin matrix composite. In particular, it was observed that a significant change on the deformability of the composites can be obtained.

The hardener actually helps the easily setting of the laminates while the epoxy resin keeps them together. The ratio, usually 50/50%, defines the complete hardening the laminate while changing in the ratio can cause the setting of the product. In short, adding more or less hardener will not result in a faster or slower cure, but in incomplete curing with limited performance, that cannot be corrected in any way. In this experiment, 60% hardener and 40 % epoxy resin ratios are used.

The hardener used in this study is made by HEXION with the product name of MGS H260s and has the properties given in Table-2.7 which are measured at 25°C

Table-2.7 Properties of the H260S Hardener

Density (g/ cm³)	0.93-0.97
Viscosity (mPas)	80-100
Refractive Index	1.4980-1.4985

2.1.5.2 Effect of Temperature onThermosetting

The optimum processing temperature is in the range between 20 and 40°C for L 285. Higher processing temperatures are possible, but using higher temperature for the curing of the composite material reduces the operation by shortening pot life. Fig-2.4 shows temperature vs time to set for different hardeners for a sample of 100 g starting to set at a temperature of 20°C. It can be seen that temperature has serious effects on the time a laminate takes to cure completely. Hardener 285 takes lesser time to cure but needs a curing temperature of as high as 230°C. On the other hand, if the higher temperature is not available for the composite materials epoxy can take several hours to cure as in the case for Hardener 287. The Vacuum assisted resin infusion machine which was used in this study had heater which can provide continuous temperature which increases or decreases in steps to the laminates. The time for the epoxy I used in this study was heated till 100°C increased with steps and it took approximately one hour for the curing of the composites.

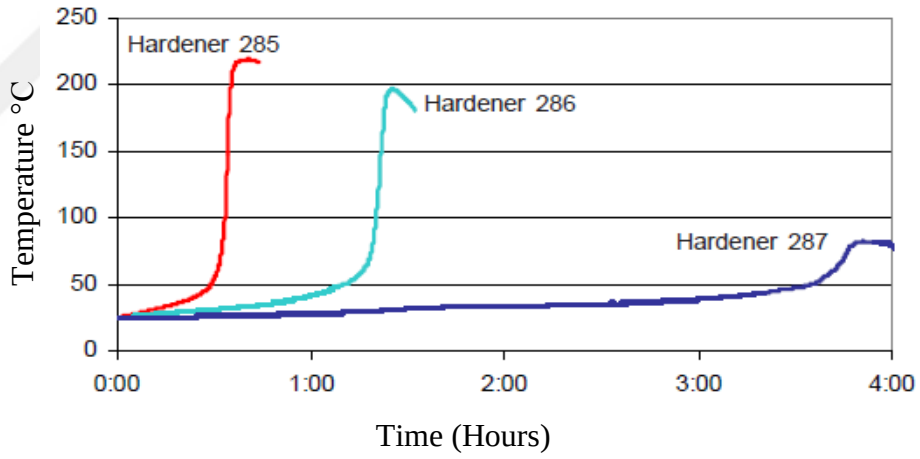


Fig-2.4 Temperature vs *Time* of curing for different Hardeners

2.2 VARTM (Vacuum Assisted Resin Infusion) Machine

In this project, the machine which is used for the manufacturing of the products is called VARTM machine with the dimension of 1500x1200x900 m^3. This specially designed machine is made to make laminates using vacuum assisted resin infusion and works on 9000 Watts Fig-2.5



Fig-2.5 VARTM Machine

2.2.1 Work Bench

This field work bench is the main interaction part made of steel and aluminum which has the property changing its temperature from 20°C-120°C. The temperature required for the curing of the composite materials using epoxy is 90°C-120°C. That's why the temperature values for the VARTM Machine are suitable for the production and curing of composite laminates.

The dimensions of the working area on the bench are 1.2m x 1.2m. The composite laminates had the dimension of 0.5m x 0.5m more than enough for the manufacturing of the laminates. The heaters under the working bench constantly change their temperature for the uniform availability of heat. Despite the large area of the work area I used lower dimensions for composite laminates which helped quick curing and easier infusion of epoxy laminate through the layers of the composite

2.2.2 Rotary Pump

The Rotary Pump is used to create a vacuum which goes as low as 1 atm which helps the perfect curing of the product with no air around and infusion of epoxy resin inside the fabrics. This vacuum is manufactured by VALUE. The properties of the Rotary Pump are given in Table-2.8. Fig-2.6 contains the picture of the Rotary Pump.



Fig-2.6 Rotary Pump

Table-2.8 Rotary Pump Properties

Model	VE260N
Free Air Displacement	7CFM
Ultimate Vacuum	15 micron
Voltage	230V / 50-60 Hz

Rotary Pump creates a vacuum which passes through some components of the VARTM machine and reaches the vacuum bag where it sucks the epoxy resin using the pipes which then due to vacuum is pulled through the composite laminates. The function of the Rotary Pump will be described in detail in the next sections.

2.2.3 Resin Trap

Another part of the VARTM machine called resin trap serves two purposes. The analogue clock on the resin trap gives a quick measurement of the vacuum in the vacuum bag. It also prevents the extra sucked up resin to enter in the vacuum. The vacuum pulls the resin from the laminate towards the vacuum causing the resin to sometimes all the way to vacuum that's why this resin trap serves to prevent that as



Fig-2.7 Resin Trap

shown in Fig-2.7

2.2.4 Temperature/Vacuum Control Panel

The panel in Fig-2.8 serves to control and successive increase in the temperature of the work bench. The setting allows the user to change the temperature gradually by 1 degree in 10 minutes. It turns the heaters on while the temperature of those heaters is distributed on the aluminum based work bench. The panel controls give the option of keeping the temperature constant after a particular value of the heat temperature is reached. This is needed mostly after the manufacturing of the composites is completed and the Rotary Pump is closed. The temperature of the work bench actually defines the time of the curing because different hardeners cure in different times under the various values of the temperature. This control panel helps the control of all these values.



Fig-2.8 Electric Control Panel

2.3 Laboratory Equipment

The lab equipment list used in the manufacturing of the materials is given as below.

- The pipe cut for the infusion of the epoxy resin inside the vacuum bag. Fig-2.9
- Normal pipe for the transportation of resin to and from vacuum bag. Fig-2.10
- The infusion matrix as shown in Fig-2.11
- Scissors
- Resin Mixing Cup
- Clips
- Sand Paper
- The vacuum bag
- Peel Ply/ Releasing Agent
- Two sided solution tape
- Vacuum bag whole filler solution tape



Fig-2.9 Cut Pipe



Fig-2.10 *Normal* Flow



Fig-2.11 Flow Matrix

2.4 Laminates Production

The manufacturing method used in the manufacturing of the samples for this study is called Vacuum Assisted Resin Infusion. As per name in this process the resin is infused in the laminates with the help of vacuum. The VARTM process of manufacturing has following basic steps listed below which are followed in the order.

The manufacturing is based on

1. Preparation of fabric lay-up
2. Stacking of the layers of fabrics
3. Cutting of excessive fiber-filaments
4. Application of the tapes
5. Sealing the mold with the vacuum bag
6. Creating a vacuum around the fabrics
7. Resin preparation and degassing
8. Resin impregnation.
9. Cure of fabricated panels
10. Removing with the help of releasing agent
11. Cutting of the laminates
12. Getting the laminates ready for the tests.

2.4.1 Preparation of The Fabrics

As discussed in the previous section there were in total 3 different types of the fabrics used in the preparation of the samples used here. Total carbon, total basalt and

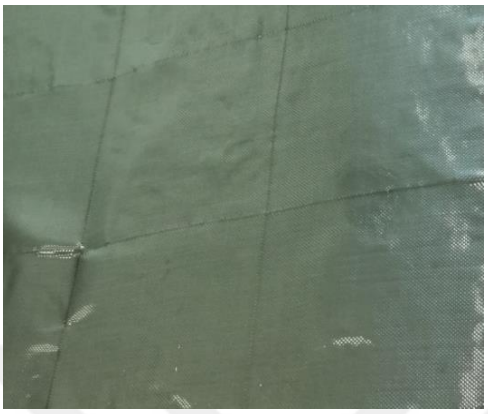


Fig-2.11(a) 100% Woven Basalt Fabric



Fig-2.*11*(b) 100% Woven Carbon Fabric



Fig-2.11(c) In-plane Carbon/Basalt Hybrid Fabrics

plain weave in-plane basalt/carbon hybrid fabrics. All the three fabrics were cut in from the role with the dimension of 100x100 cm Figures-2.11(a), (b), (c)

2.4.2 Stacking Sequences

The stacking sequence of the fabrics was changed to get 3 three different arrangements. The plies of these fabrics were put in a certain arrangement i.e. the number of carbon or basalt fibers put together was changed. It's good to color code the fabrics to easily identify them as well as to name these particular sequences Figures-2.12(a), (b)

Each arrangement is made of 24 layers out of which 12 belong to Carbon fabric and 12 belong to the basalt fabric. But in every arrangement, despite the number of the total number of layers is same, the stacking style is changed.

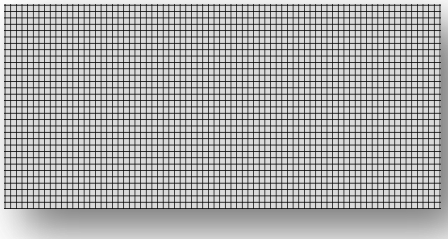


Fig-2.12(a) Carbon Fabric

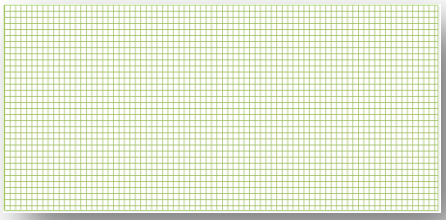


Fig-2.12(b) Basalt Fabric

2.4.2.1 1B1C Arrangement

B-C-B-C-B-C-B-C-B-C-B-C-C-B-C-B-C-B-C-B-C-B-C-B=12 Basalt + 12 Carbon Fabrics

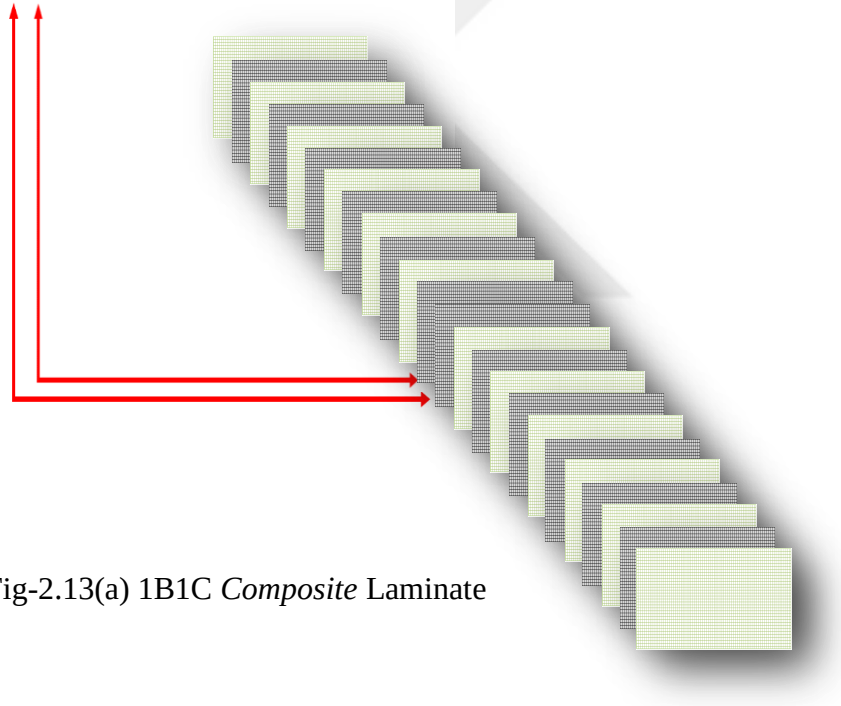


Fig-2.13(a) 1B1C *Composite* Laminate

In this arrangement of the plies or the cloths of carbon and basalt, only one ply of basalt and carbon is taken and all of it is put together. In totally there are 24 layers out of which 12 from carbon and 12 from basalt are stacked together. The first layer is taken from the basalt fabric while the second one is taken from the carbon fabrics. This goes on until the 6^{th} layer where the carbon fiber is put twice. It means that this arrangement is symmetric on the carbon fibers. Both sides of the sample are covered with a single fabric made of basalt fibers, while in the middle there are two fabrics of carbon. Fig-2.13(a) shows the arrangement in detailed view. If B stands for Basalt and C stands for Carbon fabrics the arrangement is as follows for this arrangement names as 1B1C.

It can be seen that right in the middle of the laminate there are two consecutive carbon fabrics and it is called symmetric around carbon fabrics. It is expected to play an important role in the mechanical properties of the laminate. The side view of the 1st Stacking Sequence is given in Fig-2.13 for schematic view.

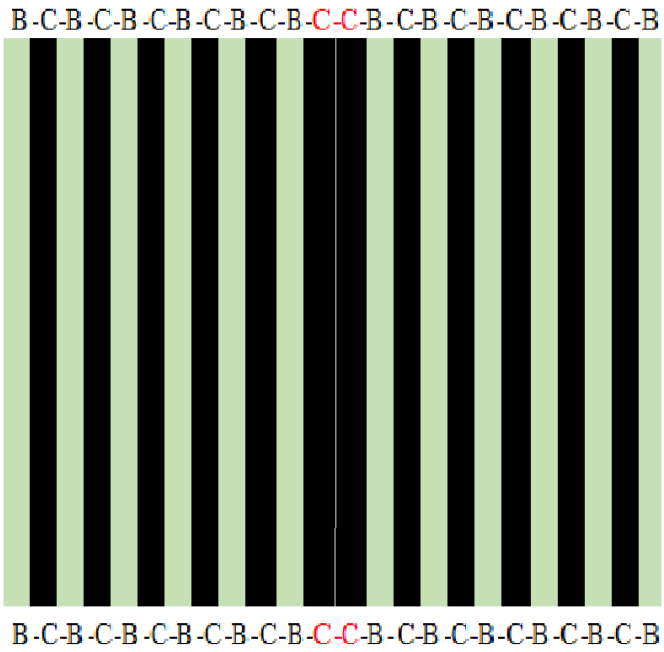


Fig-2.13(b) Side View of 1B1C *Composite* Laminate

2.4.2.2 2B2C Arrangement

In this arrangement of the plies or the cloths of carbon and basalt, two layers of basalt and carbon are taken and all of it is put together. In totally there are 24 layers out of which 12 from carbon and 12 from basalt are stacked together. The first two layers are taken from the basalt fabrics while the next two layers are taken from the carbon fabrics. This goes on until the 6th layer where the carbon fiber is put quadric, it means that this arrangement is symmetric on the carbon fibers too. Both sides of the sample are covered with double basalt fibers, while in the middle there are four carbon fabric.

It can be seen that right in the middle of the laminate there are four consecutive carbon fabrics and it is called symmetric around carbon fabrics. It is expected to play an important role in the mechanical properties of the laminate. The side view of the 2nd Type Stacking Sequence is given in Figures-2.14 (a), (b) for schematic view which shows a core of the carbon fabric is made which is evident due to is darker color as compared to the basalt fabric. This core is going to constitute the main part of its structure.

B-B-C-C-B-B-C-C-B-B-C-C-C-C-B-B-C-C-B-B-C-C-B-B = 12 Basalt + 12 Carbon Fabrics

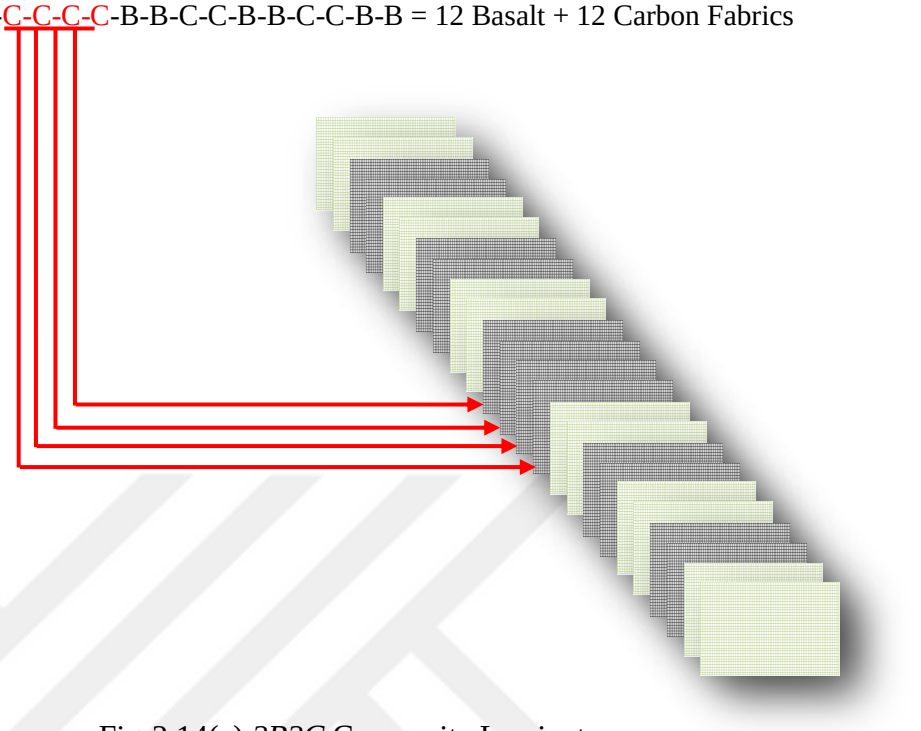


Fig-2.14(a) *2B2C* Composite Laminate

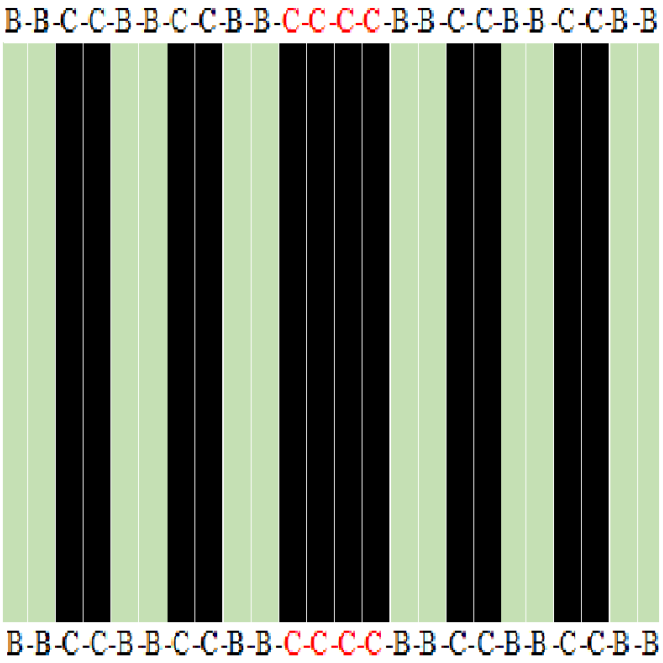


Fig-2.14(b) Side View of 2B2C Composite Laminate

2.4.2.3 3B3C Arrangement

In this arrangement of the plies or the cloths of carbon and basalt, three layers of basalt and carbon are taken and all of it are put together. In totally there are 24 layers out of which 12 from carbon and 12 from basalt are stacked together. The first three layers are taken from the basalt fabrics while the next three layers are taken from the carbon fabrics. This goes on until the 6th layer where six carbon fabrics are put together, it means that this arrangement is symmetric on the carbon fibers too. Both sides of the sample are covered with three basalt fibers, while in the middle there are four carbon fabric. Fig-2.15(a)

B-B-B-C-C-C-B-B-B-C-C-C-C-C-C-B-B-B-C-C-C-B-B-B = 12 Basalt +12 Carbon Fabrics

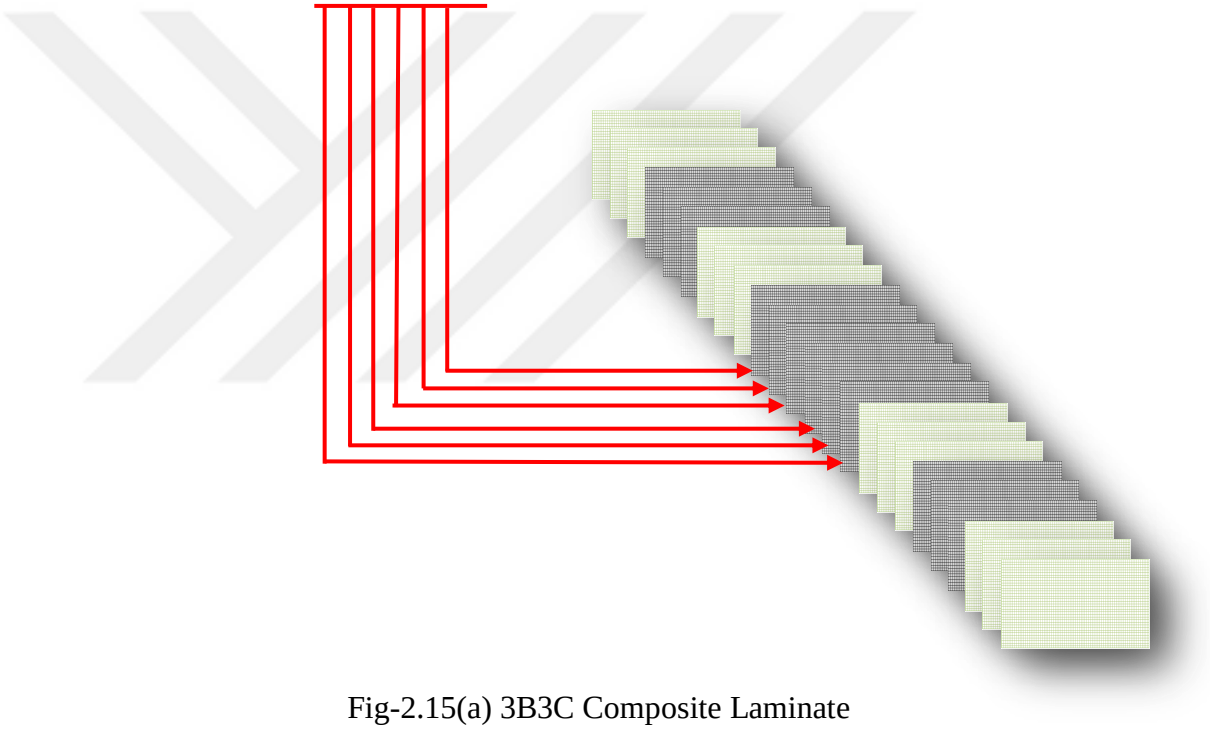


Fig-2.15(a) 3B3C Composite Laminate

It can be seen that right in the middle of the laminate there are six consecutive carbon fabrics. The arrangement of the fabrics is also shown with the red arrows to understand the location of each fabric in the structure. The upper and the lower side of this stacking sequence contains three consecutive fabrics of basalt. It is called symmetric hybrid composite laminate around carbon fabrics. The side view of the 2nd Type Stacking Sequence is given in Fig-2.15(b) for schematic view. The side view reveals that the carbon fabrics in the middle forms a thick core which is expected to play in important role in the shape of the structural behavior of the composite laminate. At this stage the fabrics are put on each other with the same dimensions.

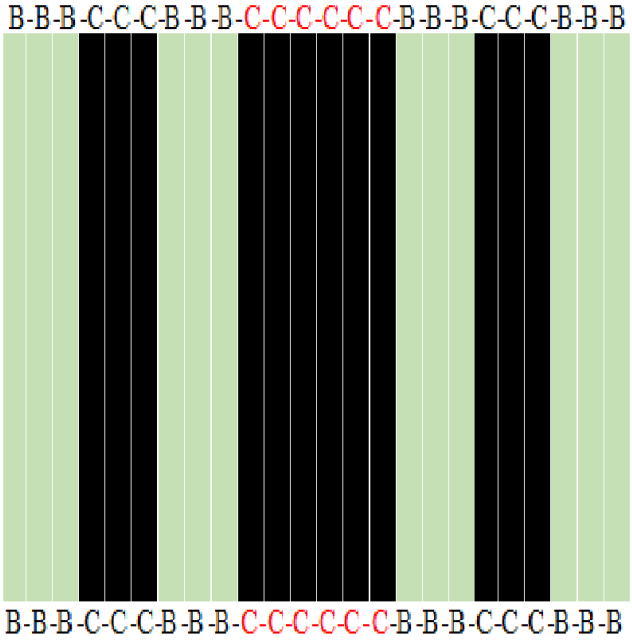


Fig-2.15(b) side *view* of 3B3C Composite Laminate

2.4.2.4 Carbon-Basalt In-Plane Hybrid Laminate (Hyb)

The 3 different types of stacking sequences of the 100% Carbon and 100% Basalt fabrics are ready and put on each other in the desired stacking manner. Details of their preparation are given in the previous section in detail. The 4th arrangement of the hybrid composite material which is called the in-plane hybrid composite laminate is made from the hybrid plain weave Carbon-Basalt fabrics. All the fabrics are same in this arrangement so there is no question of the stacking sequence. In total 24 fabrics are stacked on each other.

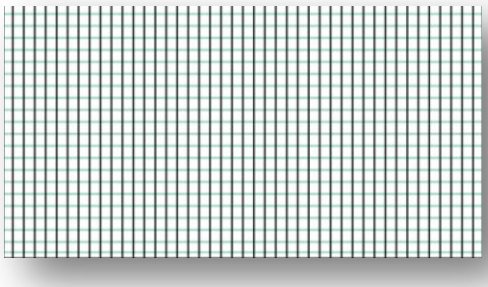


Fig-2.16(a) Carbon-Basalt Hybrid Fabric

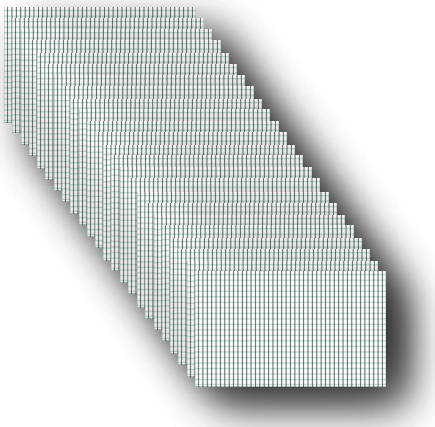


Fig-2.16(b) Hybrid Composite Laminate

The sample of the one fabric is given in Fig-2.16(a). To be noted is the longitudinal basalt fiber in basalt color and the verticals one in the black carbon color.

2.2.3 Preparation of Epoxy Resin

The Laminating resin MGS® L 285 is mixed with the hardener MGS H 260s to create the epoxy resin. The proportion for the mixing is kept 40 percent resin 60 percent hardener. Keeping in mind the dimensions of the laminates that are 50x50x2.50±0.15 cm^2, the following formulae are used to determine the total amount of the resin to be used in the laminates.

$$\frac{m}{V} = \ density\ of\ the\ resin = \ 1.20\ g/cm^3$$

$$volume\ of\ the\ sample = 50\text{x}50\text{x}h\ cm^3$$

$$h\ stands\ for\ the\ height\ of\ the\ laminate$$

$$width\ of\ singel\ fabric = 0.20\ mm$$

$$h = 0.20mm\ \text{x}\ 24 = \ 4.2\ mm = 0.42cm$$

$$the\ amount\ of\ mass\ to\ be\ used\ is\ calculated\ by$$

$$m = Volume\ \text{x}\ density$$

$$m = (50\ \text{x}\ 50\ \text{x}\ 0.42)(1.20) = \frac{g}{cm^3}\ .cm^3.1260 = 1260\ g$$

The amount of epoxy to be used for the laminate of 50x50 cm^2 in grams is 1260 g. 60 percent of which must be taken from hardener while the 40 percent must come from the resin.

$$mass\ of\ the\ Hardener = 1260\ \text{x}\ \frac{60}{100} = \ 756\ g$$

$$mass\ of\ the\ Resin = 1260\ \text{x}\ \frac{40}{100} = \ 504\ g$$

With this formulation the amount of hardener and resin is 756 grams and 504 grams respectively.



Fig-2.17 Mixing of resin and *hardener* with 40-60 %

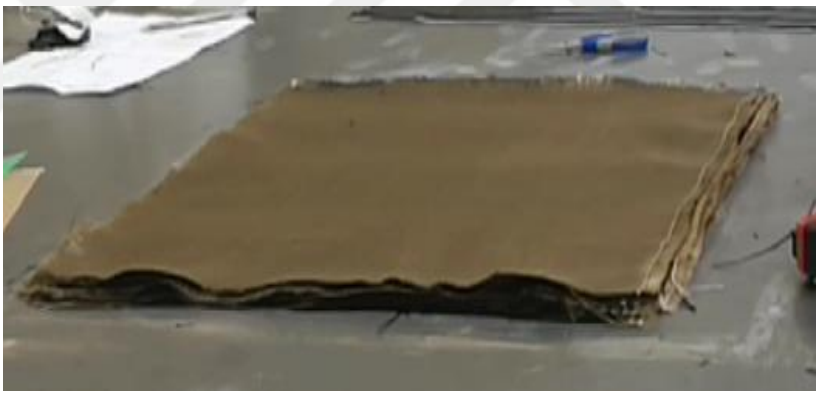


Fig-2.18 *Stacking* of the Fabrics

2.2.4 Equipment Arrangement

All the fabrics are stacked together as per their particular sequence defined above on the work bench as shown in Fig-2.18

First of all, the clothes of fabrics are stacked together. Then a two faced solution tape is applied around these fabrics on all four sides as show in Fig-2.19(b). The pipe used for the resin flow in the clothes is cut as show from Fig-2.9. The cut faces in the pipe ensure the smooth transportation of the resin. The cut pipes are pasted on both sides of the stacked fabrics. One of them serves as the collection and infusion of the resin while the other one is used for the removal of excessive resin from the layers as shown in Fig-2.19(a). The smooth flow is ensured by the green matrix Fig-2.10, A; and put on top of

the layers which also serves as the monitoring of the resin infusion's location in the layers.



Fig-2.19(a) Green Flow Matrix

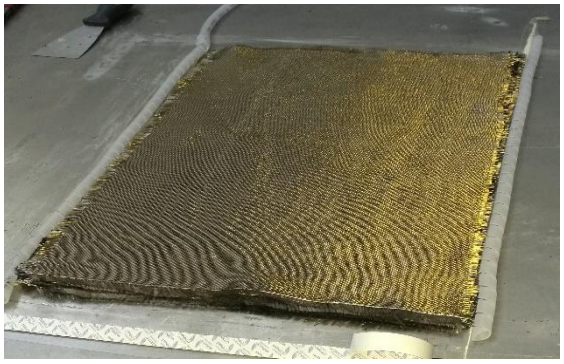


Fig-2.19(b) Pasting of Flow Pipe

The vacuum bag is a bit tiresome as not a single whole is permitted which can easily break the vacuum. The whole vacuum bag is applied carefully around the fabrics. The schematic view of the arrangement until now is given in Fig-2.20(b). The real view of the arrangement prepared for the vacuum assisted resin infusion is shown in Fig-2.20(a). The pipes which are cut ensuring the smooth flow of the resin through the fabrics are shown with the yellow color.

The vacuum bag is visible in the schematic view despite it is transparent in nature. The

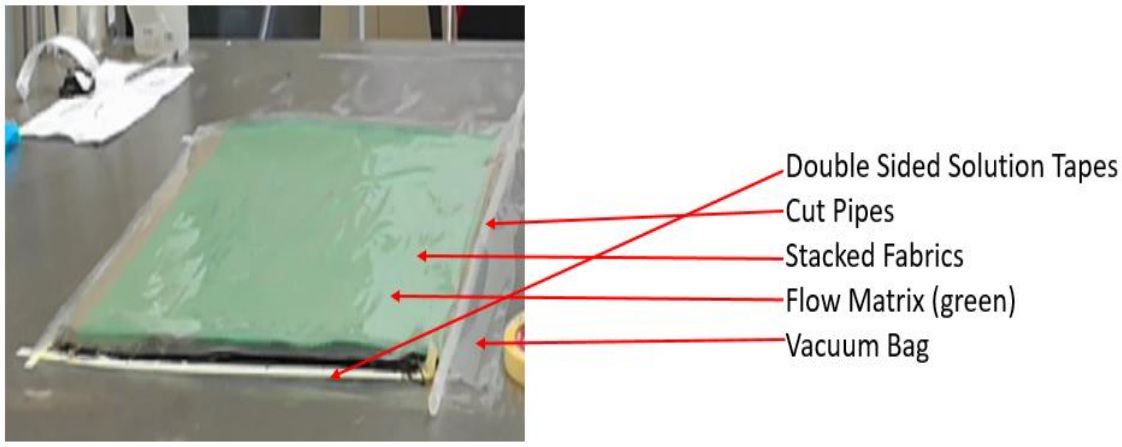


Fig-2.20(a) Real view of arrangement of and flow of resin and fabrics

green color matrix helps tracking the flow direction through the fabrics.

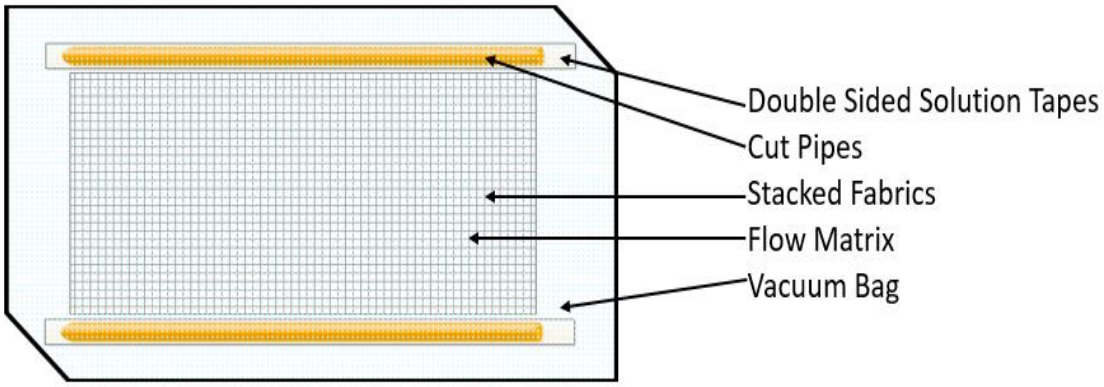
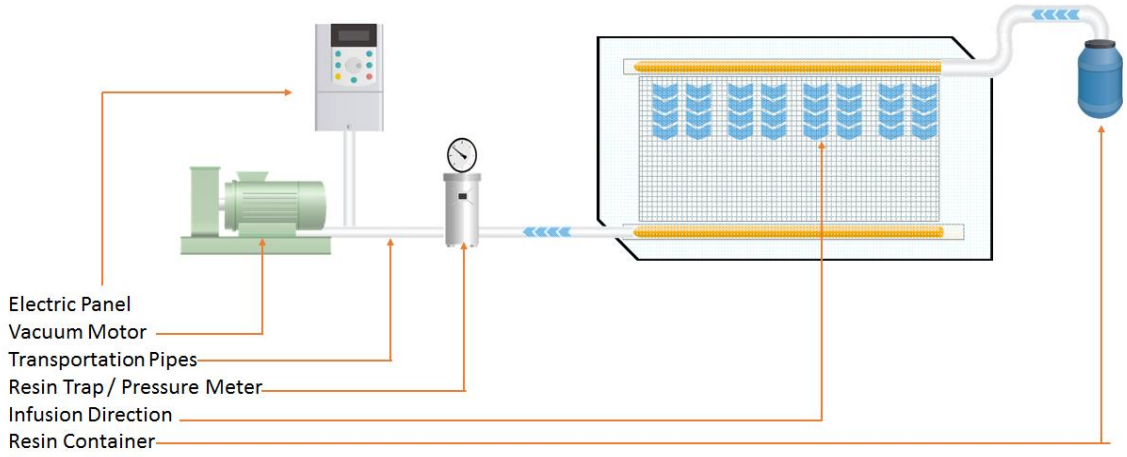


Fig-2.20(b) Schematic view of arrangement of the flow of resin and *fabrics*

The resin is prepared by the mixing of the resin and hardener with the proportion of the 60-40. The flow pipe connects the resin container to the 1st cut pipe from where the resin is introduced to the vacuum bag and later upon opening the Rotary Pump, it is infused in the layers. The pipes have holes in it which ensure the easy flow of the resin. The other side of the fabrics where the second cut pipe is connected the connection pipe is connected to the resin trap which further is connected to the Rotary Pump.

When the motor is turned on, it first pulls out all the air in the vacuum bag and tightens the fabrics together. Later the air pipes which connect the resin container to the cut pipes from where the infusion of the resin takes place the epoxy resin starts entering the layers of the fabrics in the shown direction. The direction of the flow depends on how good the vacuum is formed. The better the vacuum the better and smooth flow of the resin is possible. Fig-2.21(a) for schematic and Fig-2.21(b) real view of the VARTM



Process

Fig-2.21(a) the schematic view of the whole VARTM process and machine parts.

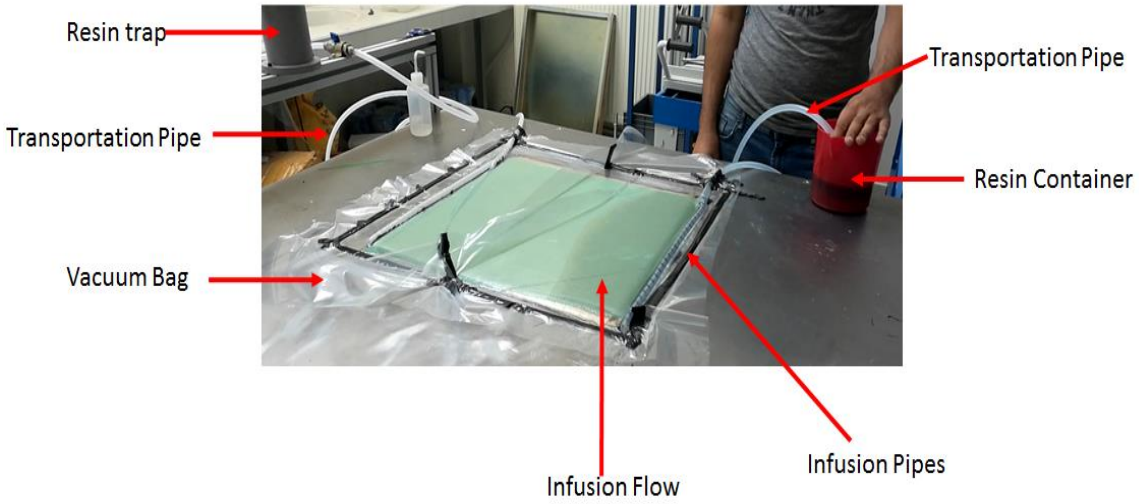


Fig-2.21(b) the process of *infusion* of the resin into

After the vacuum is totally established, the resin is introduced in the layers of the fabrics which smoothly distributes itself in the fabrics. The high temperature till 100°C ensures the full and quick gelling of the layers together. The heaters under the work bench are turned on using the electric panel and the Rotary Pump is turned off after resin is distributed totally.

2.2.5 Curing of The Fabrics

The temperature of 100°C is kept under the arranged fabrics for a period of 1 hour. The heaters under the work bench automatically turn themselves off after the desired temperature is reached. Complete curing turns the laminates in Fig-2.22

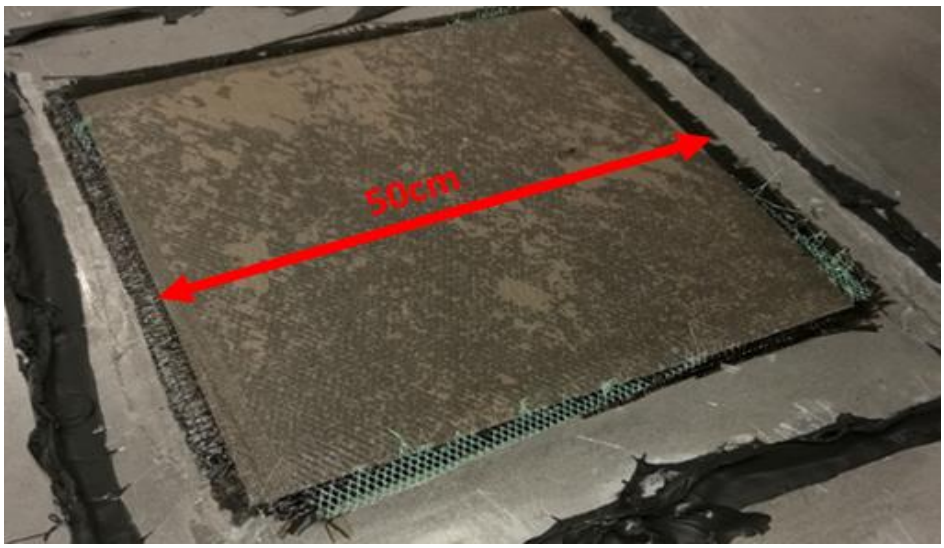


Fig-2.22 Fabrics after complete curing

The laminate is carefully removed from the work bench with the help of a scrapper without the damaging the surface of the workbench. The 50x50x2.50±0.15 cm² need to be cut in the appropriate size for the low speed drop weight test and tensile test.

The machine used for cutting of the fabrics Fig-2.23 is called D24000S from DEWALT. It is basically used for cutting stones, ceramics and other composite materials. The saw motor tilts and has the options to operate at 45 or 22.5 degrees. Alignment on Table is possible by using adjustable rollers. The Machine possesses a 24-inch ripping capacity. Two adjustable water nozzles spray on the blade to reduce friction during cutting and the nozzles collect water from the pan and then it recycles back to tub with a small pump after passing through the blade.



Fig-2.23 D24000S by *DEWALT* cutting machine

It has an efficient 1.5 HP engine, flip-style edge guide for 90° and 45° set-ups, and a tub-style bottom with four molded sections that fit into the included stand. It has an internal stainless steel rail-system. The operational properties of the machine are given in Table-2.9.

Table-2.9 Properties of the D24000S Cutting Machine

Power	Voltage	Length of Cut	Arbor	Blade Capacity	Weight	Dimensions
Direct Drive - (15 amps)	120V	60.96 cm	1.59 cm	25.4 cm	31.2979 kg	91.45 x 73.66 x 50.80 cm³

After the sample is removed from the work bench it looks like Fig-2.24. While stacking the fabrics on each other they might get slip on the edges which need to be cut and removed from there. The process of the cutting is shown in Fig-2.25. The edges of plates were smoothened with the sandpaper after begin cut with the help of wet cutter machine. The 50x50x2.50±0.15 cm² samples are cut into the maximum number of 100x100x2.50±0.15 mm^3 and 15x250x2.50±0.15 mm^3 as shown in Fig-2.26

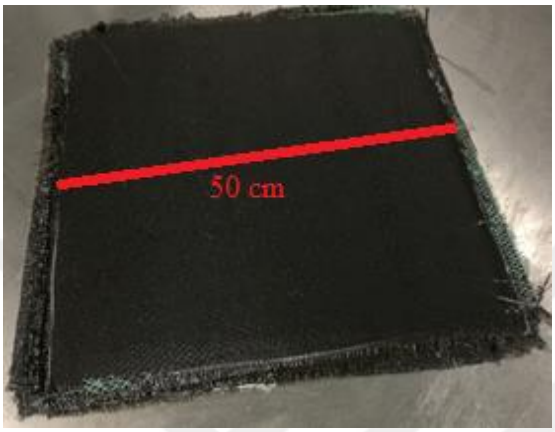


Fig-2.24 Ready to *cut* laminates



Fig-2.25 Cutting of the Laminates

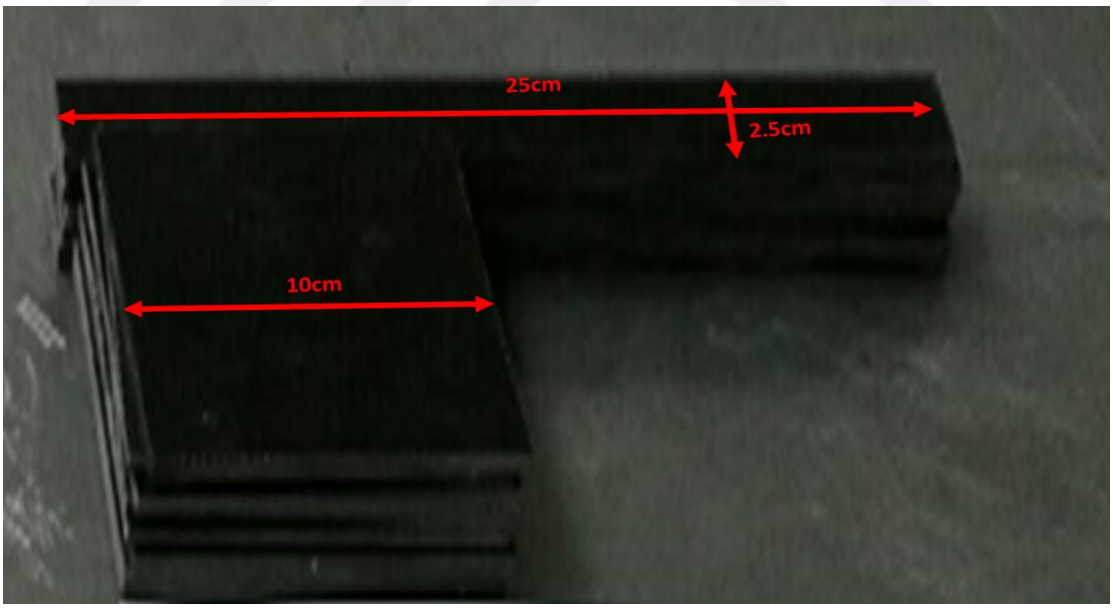


Fig-2.26 Ready for the tensile and impact test samples

2.5 Drop Weight Impact Test

2.5.1 Test Preparation

Although the 4 arrangements of the laminates are cut into the dimensions of 15x250x2.50±0.15 mm^3 and 50x50x2.50±0.15 mm^3 were ready for the tensile and drop weight test but product samples are further modified mechanically. For example, the samples which have the dimensions of 15x250x2.50±0.15 mm^3 needed modification for it to be appropriate to machine. The cutter machine uses water to reduce friction between the product and the saw of the machine. The continuous flow of the water on the cutter causes the water to infuse through the laminate samples and make them wet after cutting. The water above the laminates can be cleaned by the cloth but moisture through the fabrics is hard to clean. The water might change the structure or damage the laminate from the inside because of its reaction to the epoxy and if we keep it waiting for an extended period of time the moisture inside the epoxy might reduce adhesiveness changing mechanical properties of the material. The removal of the water after the laminates are cut to be ready for the test is necessary. The removal of moisture from the laminate is completed by using the air pump with high pressure of air which easily gets through pores and removes the water out of laminate

Despite the fact that laminates were prepared in a very good condition in the sense that the epoxy was cured completely and no area was wet (uncured) upon the removal of the composite laminate from the work-bench, but still clearing the laminate edges was needed after they were cut using the saw machine. The laminates are made by the fabrics which are plain weave arrangement of the carbon and basalt fiber yarns. The fibers in the fabric are also attached with the epoxy material after the curing. When the laminate is cut using saw cutter, edges of these fibers are pulled out of the laminate. One of the reason is that at some places the epoxy is not uniformly distrusted and the friction between the saw and the laminate causes the fibers to show this behavior. It is important to clear those pulled out fibers with something to make the edges of the laminate samples smoother. This is achieved by using appropriate sand paper.

After removing the moisture from the laminates using pump and removing pulled out fibers using sand paper, 50x50x2.50±0.15 mm^3 and 15x250x2.50±0.15 mm^3 samples were prepared for tests.

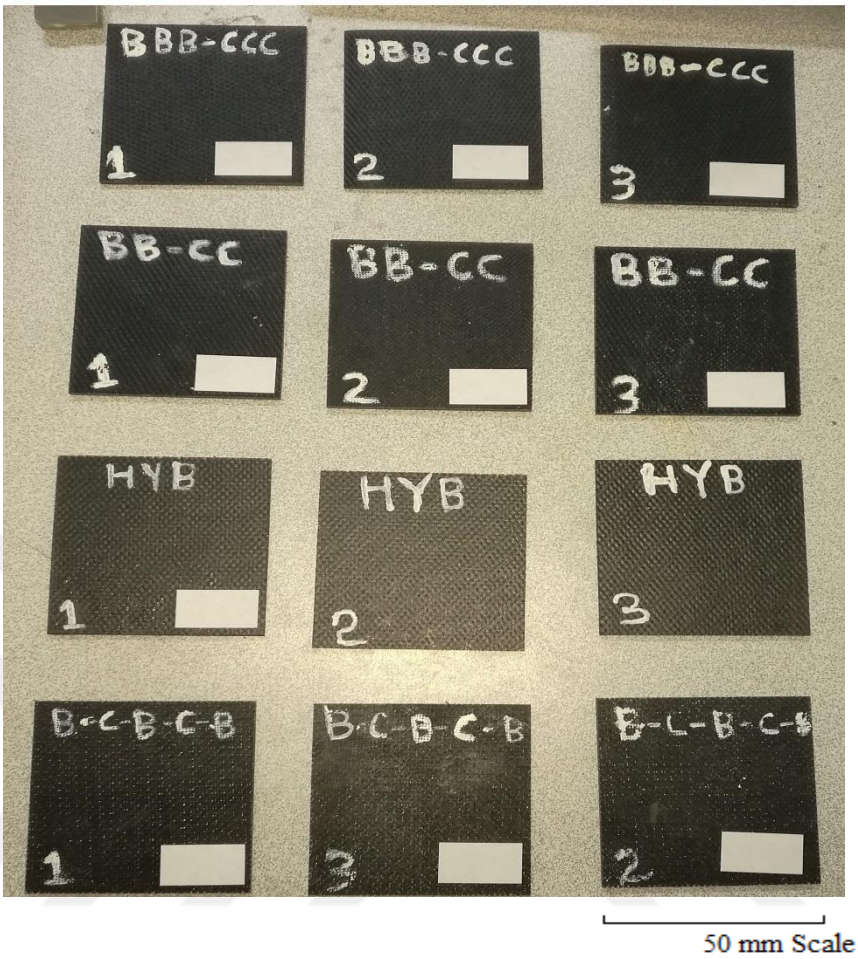


Fig-2.27 Naming the Composite Laminates

2.5.2 Naming of The Samples

The drop weight test was carried through on the samples which were cut were named as follows:

1B1C two laminates arranged as one basalt and one carbon fabric stacked together.
2B2C two laminates arranged as one basalt and one carbon fabric stacked together.
3B3C two laminates arranged as one basalt and one carbon fabric stacked together.
HYB two laminates of in-plane Carbon/Basalt fabrics stacked together.

All 4 laminates are cut in 100x100 cm^2 and were tested at 4, 6 and 8 m/s. The resultant plots are named in such way that V4 stands for the sample which was tested at 4 m/s, V6 for 6 m/s and V8 for 8 m/s. For example, 1B1C-V6 stands for the laminate which is stacked in a way that first fabric is basalt and the second fabric is carbon which continues till the 24^{th} layer of basalt and this laminates is tested at 6 m/s. All the samples are labelled carefully to recognize them easily as shown in Fig-2.27The coding is based on their structures and the stacking sequence of their fabrics.

2.5.3 Drop Test Machine

The machine used for the low speed drop weight impact test has a product name of CEAST-Fractovis Plus as shown in Fig-3.1. A simple control panel is attached with the machine to give input data without the need of the PC but the plots and the results are still shown on the computer attached with the machine. The test execution is controlled by the microprocessor. The main features are the ability to check speed right before the impact and automatic specimen clamping system. Clamping of the samples are shown in Figures 3.2(a) and 3.2(b)



Fig-2.28 Drop Test Machine

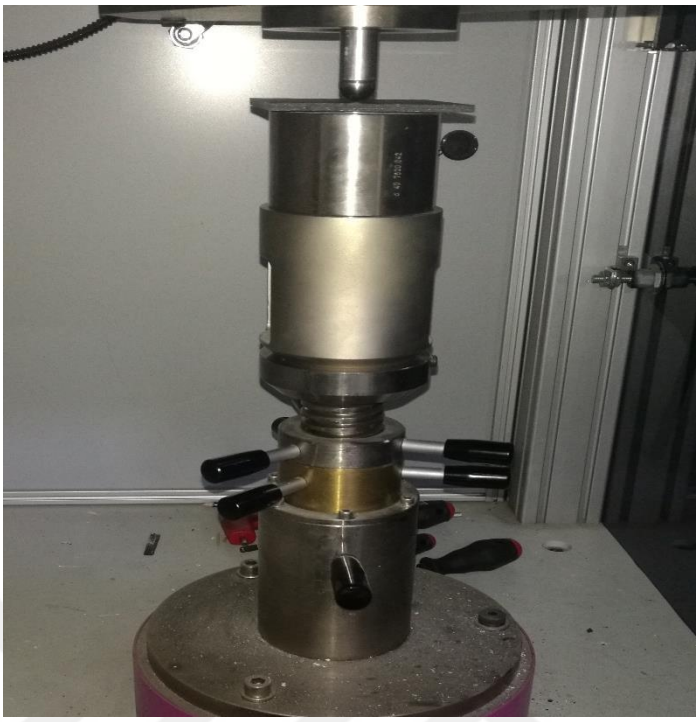


Fig-2.29 (a) Clamping of the laminate

The mass of the impactor here the low speed drop weight impact tests is 5.045 kg. The diameter of the head of the impactor is 10mm. Low speed impact tests were done at the speed of 4 m/s, 6 m/s and 8 m/s.

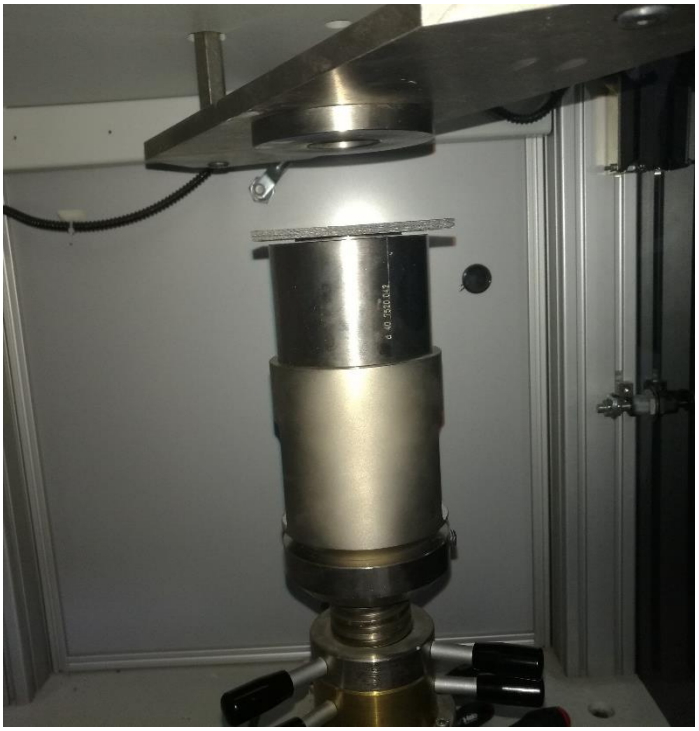


Fig-2.29 (b) Clamping of the laminate

2.6 Tensile Test

The tensile test of the samples is done to calculate some mechanical properties of the material like tensile strength and elongation to break values of the composite materials. The metals show a graph of the under the tensile test in which the shape of the graph explains the ductility, brittleness and modulus of elasticity. These comments are made because particular shape of the graph actually is a resultant of a specific inner structure and the response of the material which went under tensile test. This is valid for the metals and its alloys because a particular failure phenomenon is seen in the sample which then can be reviewed with the stress-strain graph. Composite materials however do not behave like this because of their inner structure and the stress-strain graph does not resemble to the conventional stress-strain plots. The main difference is the absence of the graph shape in the plastic region. It means that the fiber reinforced composite materials don't show any plot in the plastic region and after the material reaches its yield point, the material just fails. This can be seen in Fig-3.11

2.6.1 Naming of The Samples

The samples to be tested are named 1B1C, 2B2C and 3B3C for the hybrid through thickness HYB composite laminates based on their structure and the stacking sequence. The in-plane hybrid composite laminate is labelled as HYB. Two samples of each composite laminate is tested here too to compare their similarity. One of them is taken as reference to review the results since all the samples tested under the tensile test showed acceptable similarity. The samples contain the names as BBB-CCC which indeed means 3B3C and same names were used while the data was fed to the tensile machine.
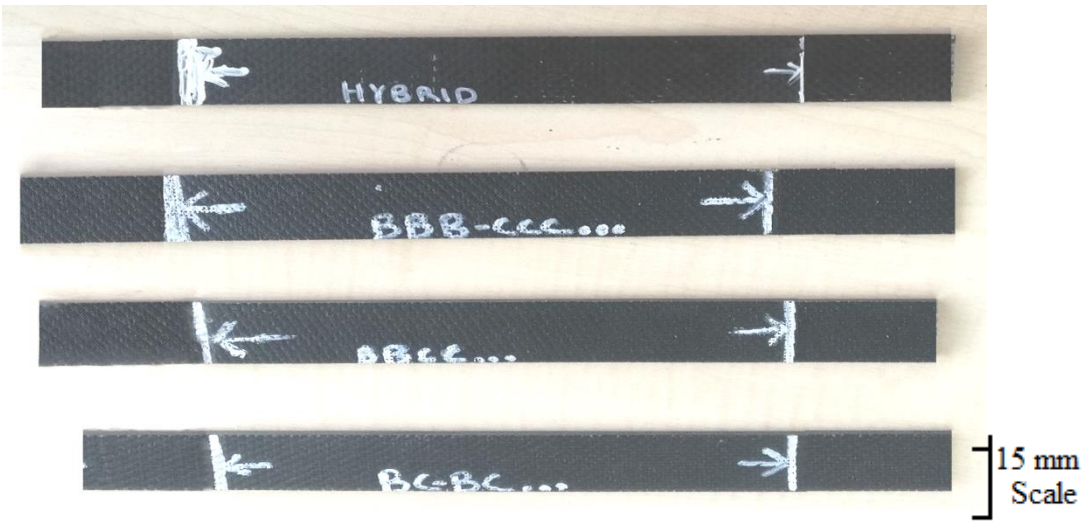


Fig-2.30 Naming of the samples before the tensile test.

2.6.2 Dimensions of The Samples

Despite the fact that the field of the composite materials and their tensile tests is not too old, there are some ASTM standards which involve complex preparation methods for example attachment of tabs on the edges of the samples. So, it is no seen necessary to make the whole procedure difficult and the samples used for the tensile test are not modified to match any particular testing standards. The gauge length for the samples is kept 70 mm while the total length of the sample for the tensile test is 250 mm. The width of the sample is kept 15 mm. The white lines on the samples guide the gauge length on the samples as shown in Fig-2.30. The purpose of the tensile testing was to *compare* their properties and review their failure phenomenon to understand the effect of the hybridization on the mechanical properties of the hybrid composite laminates.

2.6.3 Tensile Testing Machine

The tensile testing machine used in the tensile test was made by Shimadzu with the product name of AGS-XD with the capacity of 50kN. This machine provides a vast range of configurations for different tests with the attachment of accessories like tensile grips, compression plates, environmental chambers and extensometers. The grips used in this study were appropriate for the straight edges of the composite laminates. The tensile testing machine is shown in Fig-2.31 and clamping of sample in Fig-2.32, respectıvely.



Fig-2.31 AGS-X Shimadzu Tensile Strength Machine



Fig-2.32 Tensile test of the hybrid composite laminates

CHAPTER 3
RESULTS AND DISCUSSION

This chapter addresses the mechanical tests carried on the hybrid composite laminates and the discussion on the results. Initially, both tests' preparation and parameters are given later the results gained from these tests are organized which is followed by the observations from these results. Evaluation of the results is given at the end of the chapter to see why a particular behavior is seen by the composite laminate.

3.1 Impact Test Results

Three graph types for each laminate gained by the drop weight impact test in this study.

3.1.1 Force-Time Plots

The data obtained by the machine is first calculated in the form of Force-Time Plot which later is converted into other plots. Two samples from all laminates are tested and create by putting time on x-axis and force on the y-axis. The maximum value of the graph curve gives the value of the peak force. The area of the curve after the peak force value depicts the behavior of the laminate upon unloading.

3.1.2 Force-Displacement Plots

Force in units of Newton and Displacement in units of the millimeters is placed on y-axis and x-axis in Force-Displacement plots. Area under the graph of these curves give us the work done in the units of Joules. The test results give a number of data values which are rendered into shorter number of data values without altering the results. The value of the maximum peak force, displacement and area under curve can be found from these plots.

3.1.3 Energy-Time Plots

The energy time plots are given to check the value of the energy of the impactor when the impact with the laminate starts and the amount of the energy when the impactor bounces back due to elastic behavior of the laminate. The amount of the absorbed energy can be calculated by the difference of the impact and the released energy from the graph.

3.1.4 Two Samples' Tests

Two samples of each laminate is tested. In order to see whether the results are acceptably similar or not, any two tests of one sample are plotted on each other. Here selected for convection 1B1C, 2B2C, 3B3C and Hybrid laminates impacted at the speed of 8 m/s. Fig-3.1 shows that both test plots are laying on each other with acceptable same values. It means any one of them can be taken as the reference. I am taking the results of second tests as a reference here in this study. The Force-Time Plot for 1B1C and 2B2C were tested for 8 m/s. The low speed drop weight impact test is used for two samples. It can be seen from the plots in the figures that both samples show acceptable similarity.

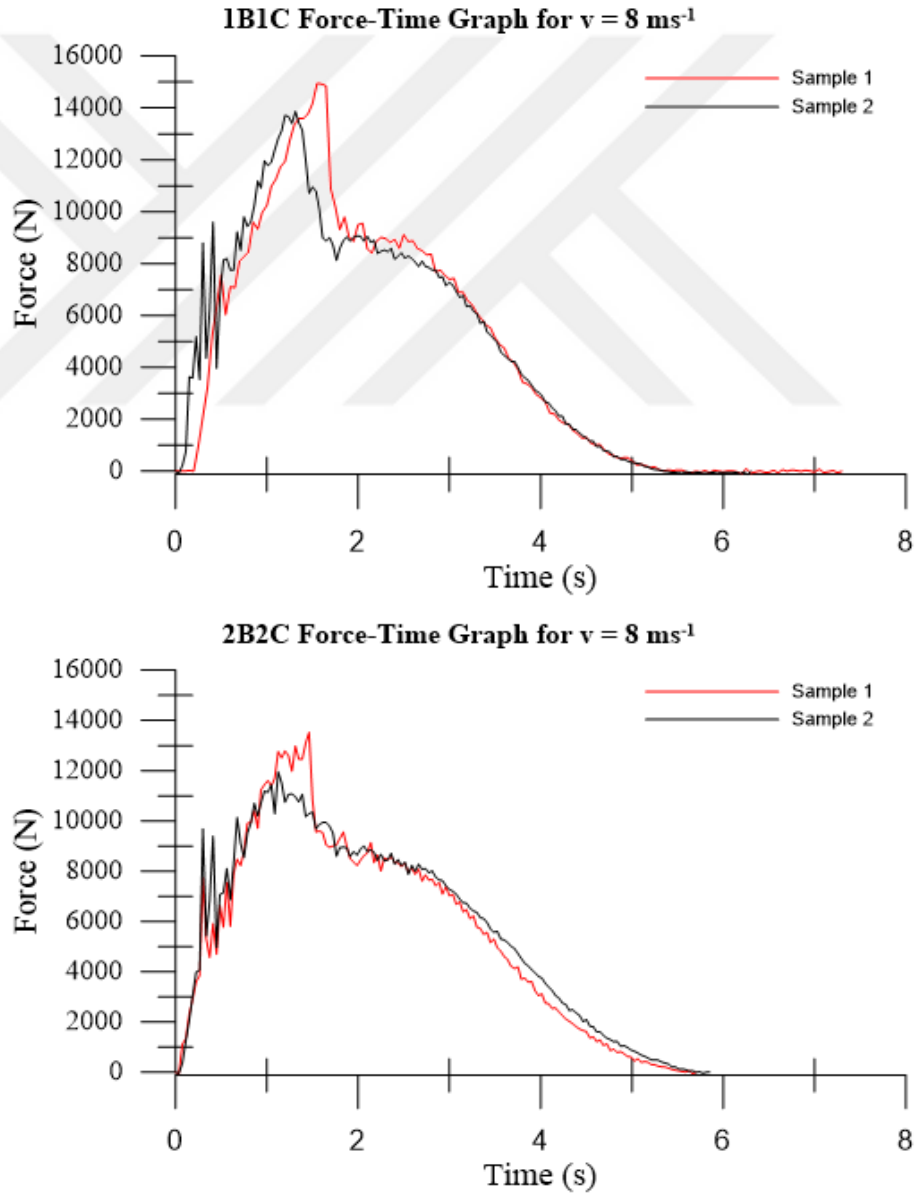


Fig-3.1(a) Overlaying Force-Time Graph for two samples

For this reason, any one of these plots can be taken as the result graph to comment or review the results. The Force-Time Plot for 3B3C and HYB for two different samples are shown in Fig-3.1(a) and 3.5(b). The drop weight impact test for 8 m/s for two similar samples was applied. It can be seen from the plots that they have acceptable similarity and anyone of them can be taken as a reference for evaluation and review.

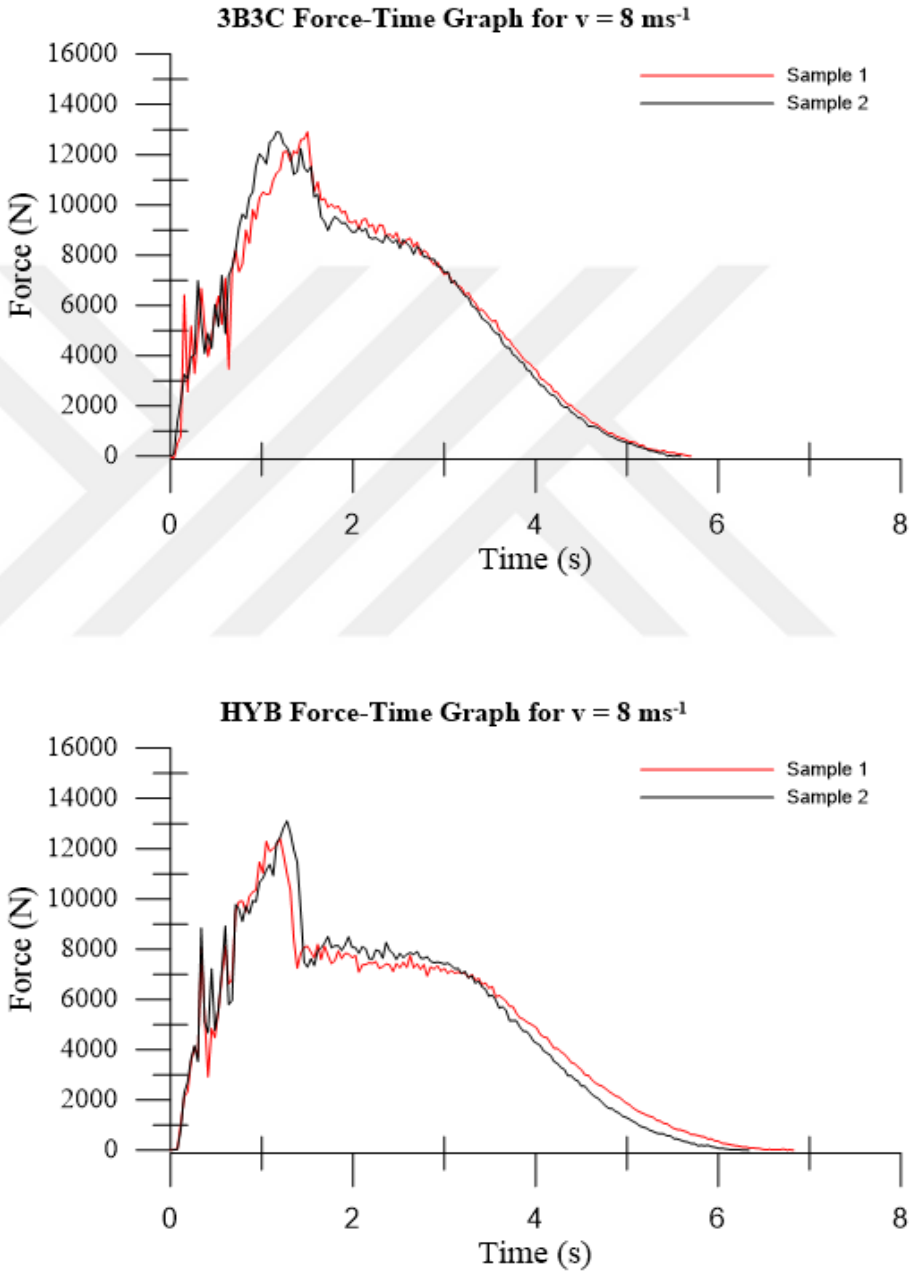


Fig-3.1(b) Overlaying Force-Time Graph for two samples

3.1.5 Results for Each Laminate

In this section results gathered from the data of the impact tests are listed. First of all, each hybrid composite is taken into consideration and its Force-Time, Force-Displacement and Energy-Time plots are given. A brief observation of the results is given under the plots. In order to understand the theme map of the plots, a chart in Fig-3.1(c) is given. This section deals with *observation* only which is given under each graph. *Results based on each composite laminate* means that each structure is taken into consideration and the related plots for this particular laminate are prepared for all the drop weight impact speeds.

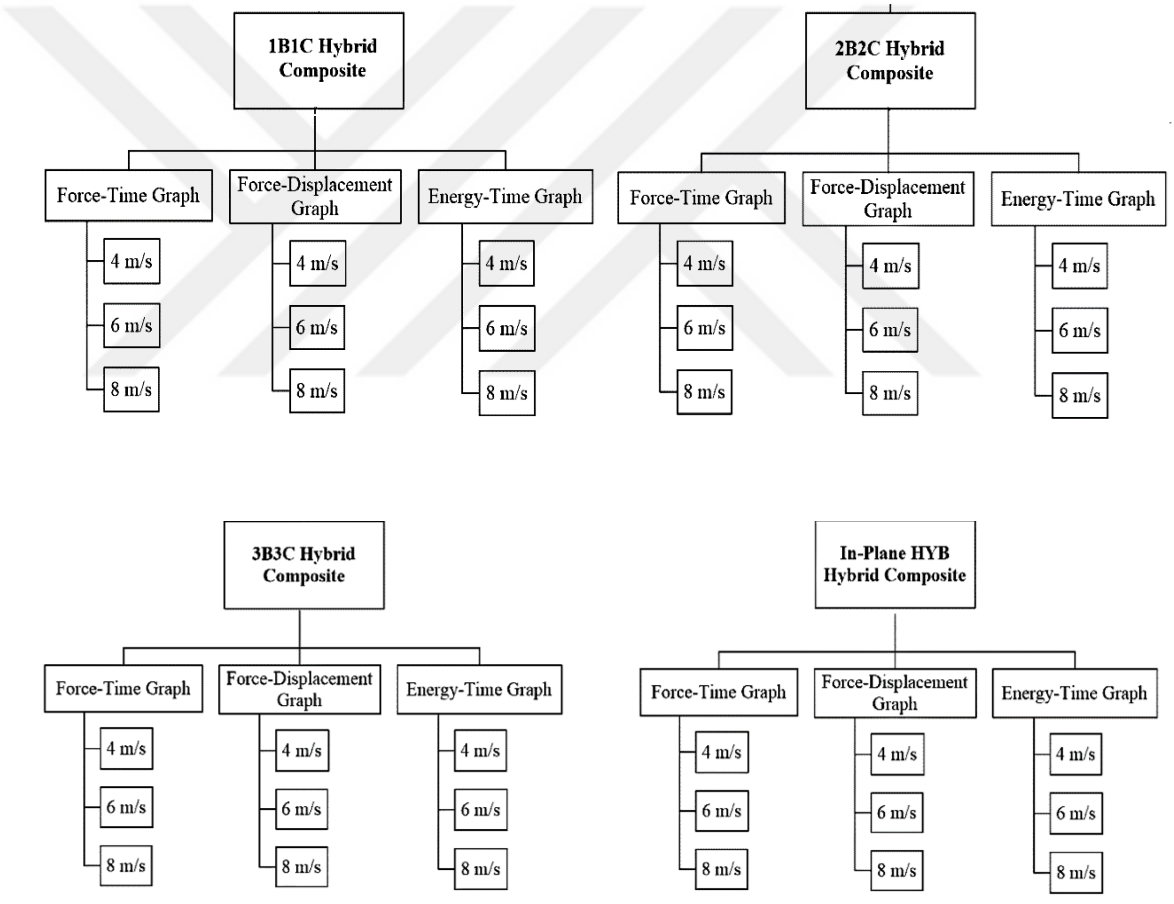


Fig-3.1(c) Results Based on Each Composite Laminate

3.1.5.1 Plots For1B1C

In this section only 1B1C hybrid through thickness composite laminate also known as the 1st type stacking sequence hybrid composite material's results from the low speed impact test are given. The plots are overlaying for the impact tests of speeds like 4 m/s, 6 m/s and 8 m/s which are labelled in different colors like red, blue and black. This makes the recognition of a particular material easier while looking that graph. The y-axis stands for Force and Energy values gained for the test while the x-axis stands for the displacement and time based on the specific plots. The standards for the x-axis are kept same which will make the review easier.

3.1.5.1.1 Force-Displacement Plot for 1B1C

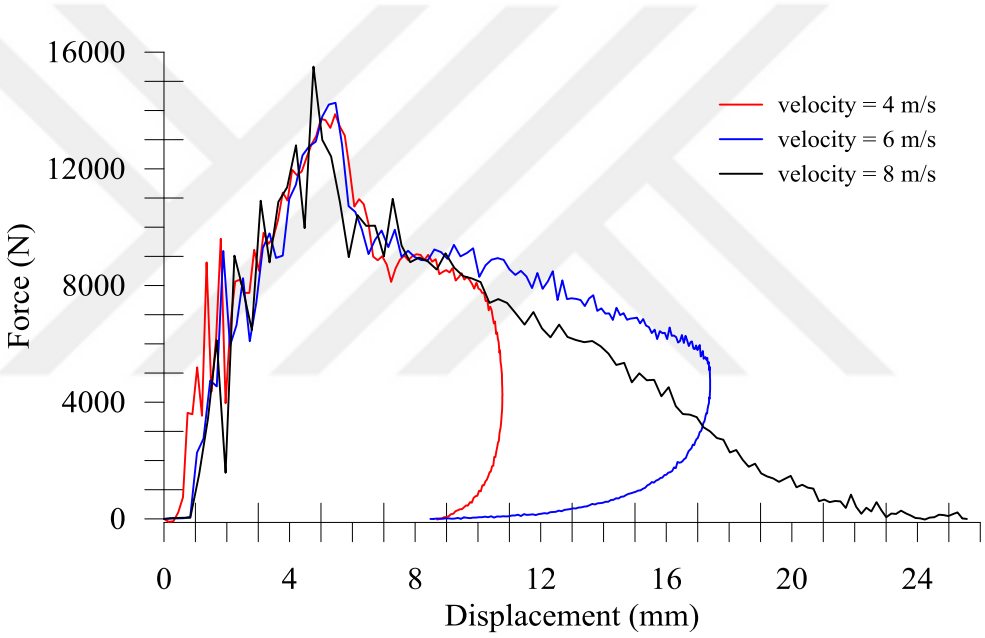


Fig-3.2(a) Force-Displacement Graph for 1B1C

The area under the Force-Deformation gives the work done in the units of Joules. The numerical values for Peak Force and the Area under the curve is given in Table-3.1

Table-3.1(a) Force-Deformation Graph Values for 1B1C

Specimen	Velocity m/s	Peak force (N)	Max Displacement (mm)	Area Under Curve (J)
1B1C	4	13877.06	10.78	93970.96
	6	14267.83	17.40	144437.17
	8	15505.24	25.57	131204.21

3.1.5.1.2 Force-Time Plot for 1B1C

The values for the force-time plots for 1B1C are given in Fig-3.2(b). The peak force values are the same as Force-Displacement Plot. The only difference between the Force-Displacement and the Force-Time Plot is the shape of the plots.

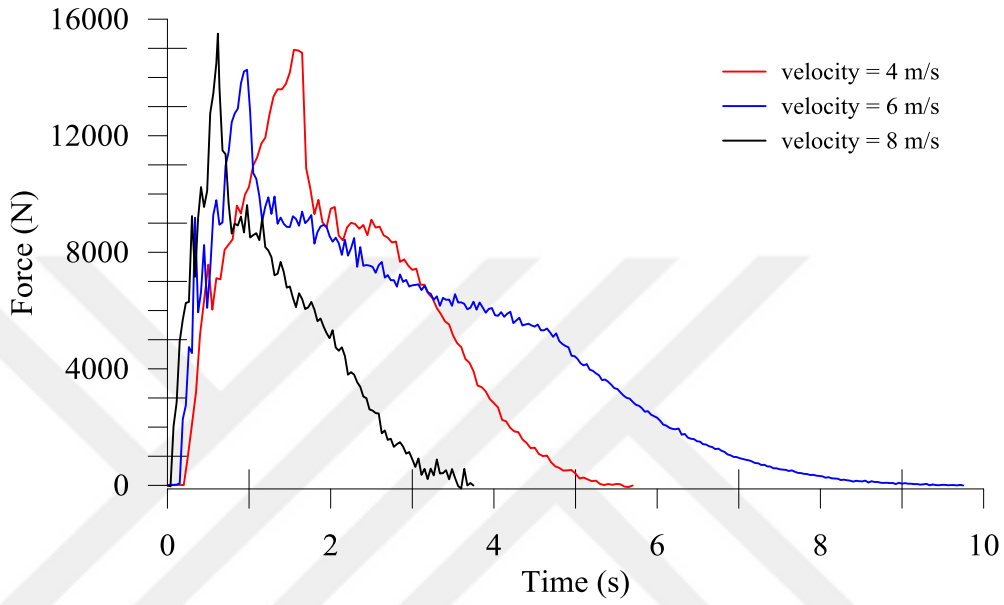


Fig-3.2(b) Force-Time Graph for 1B1C

It can be seen that there is no recovery in the force value in the Force-Time Plot. The value of the force reaches zero with the time. The impactor touches the impact face and the value of the Force increases with the time and after the impactor discharges it's all energy to the laminate sample, the impactor either bounces back for the impact speeds of 4 m/s and 6 m/s and the value of the force reaches zero. As for the case of impact test done at 8 m/s, the impactor causes penetration through the sample. This penetration takes less time that is the reason it has the smallest value of the time on the x-axis.

3.1.5.1.3 Energy-Time Plot for 1B1C

The graph of the Energy-Time for 1B1C hybrid through thickness composite laminate under the drop weight impact test three different impact speeds labelled with colors on the graph is given in the Fig-3.2(c). Numerical values from this graph are extracted for maximum impact Energy and the absorbed energies which are given in Table-3.1(b) in each tab for the impact speeds of 4 m/s, 6 m/s and 8 m/s for the 1B1C hybrid composite laminate.

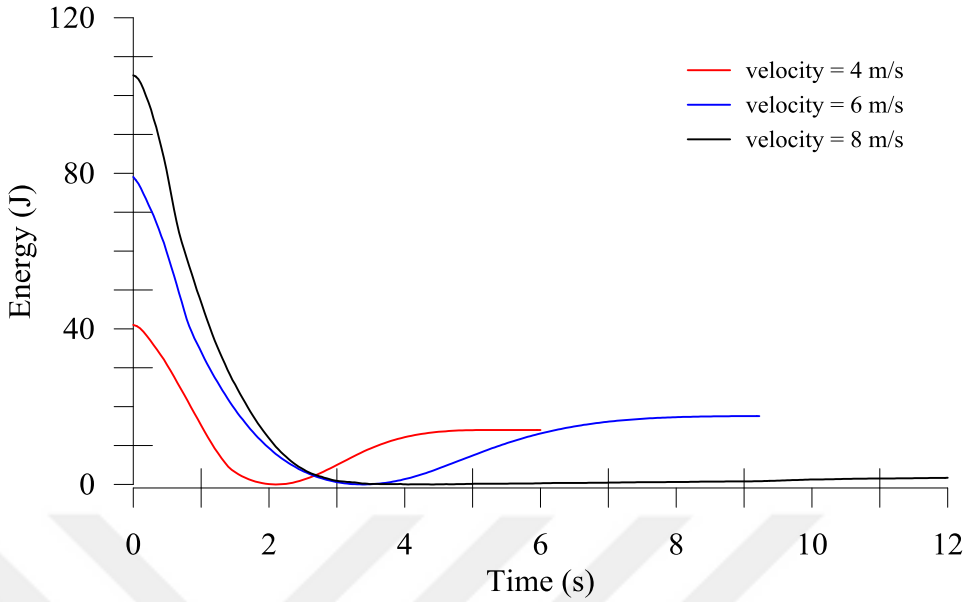


Fig-3.2(c) Energy-Time Graph for 1B1C

Table-3.1(b) Energy-Time Plot Values for 2B2C

Specimen	Velocity of Impactor (m/s)	Impact energy (J)	Absorbed energy (J)
1B1C	4	39.88	24.48
	6	79.76	64.73
	8	98.61	97.89

The value of the impact energy increases as the speed of the impactor increases same is valid for the absorbed energy. The amount of the absorbed energy is found by the difference of absorbed and the impact energy as shown in the following formula:

$$E_{Absorbed} = E_{Impact} - E_{Released}$$

3.1.5.2 Plots for 2B2C

The value of the plots for the second type sequence 2B2C hybrid composite laminates are given in the 3.6(a), 3.6(b) and 3.6(c) for Force-Displacement, Force Time and Energy-Time plots respectively.

3.1.5.2.1 F-d Plot for 2B2C

Graph for the 2B2C hybrid through thickness composite laminate is given in Fig-3.3(a).

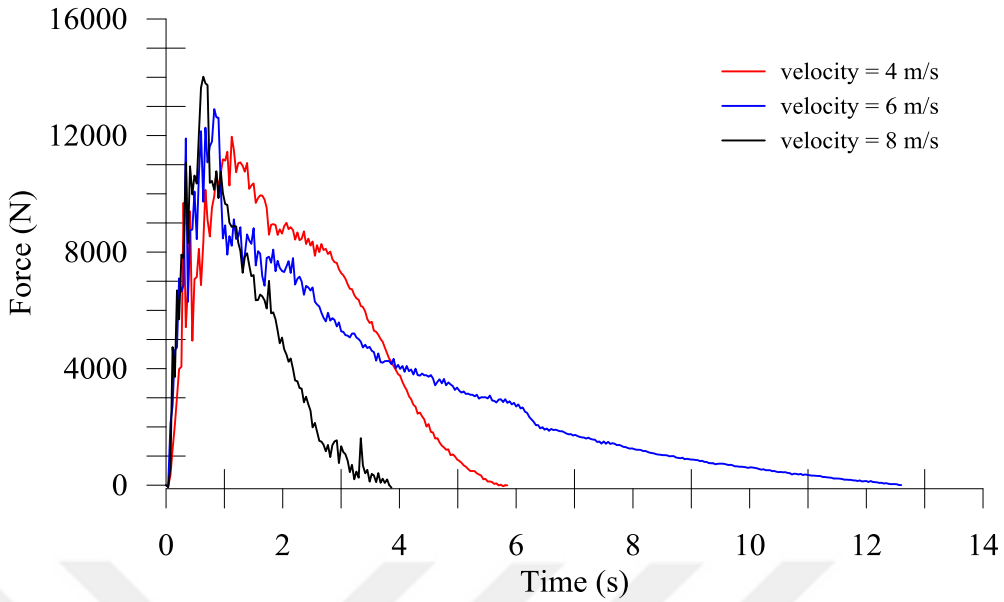


Fig-3.3(b) Force-Time Graph for 2B2C

The numerical values of the Peak Force, Maximum Displacement and Area under the Curve are given in Table-3.2(a)

Table-3.2(a) Force-Deformation Graph Values for 2B2C

Specimen	Velocity (m/s)	Peak force (N)	Max Displacement (mm)	Area Under Curve (J)
2B2C	4	13531.39	10.85	92.96080
	6	12905.17	18.49	141.320.51
	8	13710.76	26.69	136.13019

3.1.5.2.2 Force-Time Plot for 2B2C

The values of F-t graph are given in Fig-3.3(b) for all impact speeds. Peak force values are same as for F-d Plot. But force values don't return as was seen in the F-d Plot. It can be seen that there is no recovery in the force value in the Force-Time Plot. The value of the force reaches zero with the time. The impactor touches the impact face and the value of the Force increases with the time and after the impactor discharges it's all energy to the laminate sample, the impactor either bounces back for the impact speeds of 4 m/s and 6 m/s and the value of the force reaches zero. As for the case of impact test done at 8 m/s, the impactor causes penetration through the sample. This penetration takes less time that is the reason it has the smallest value of the time on the x-axis.

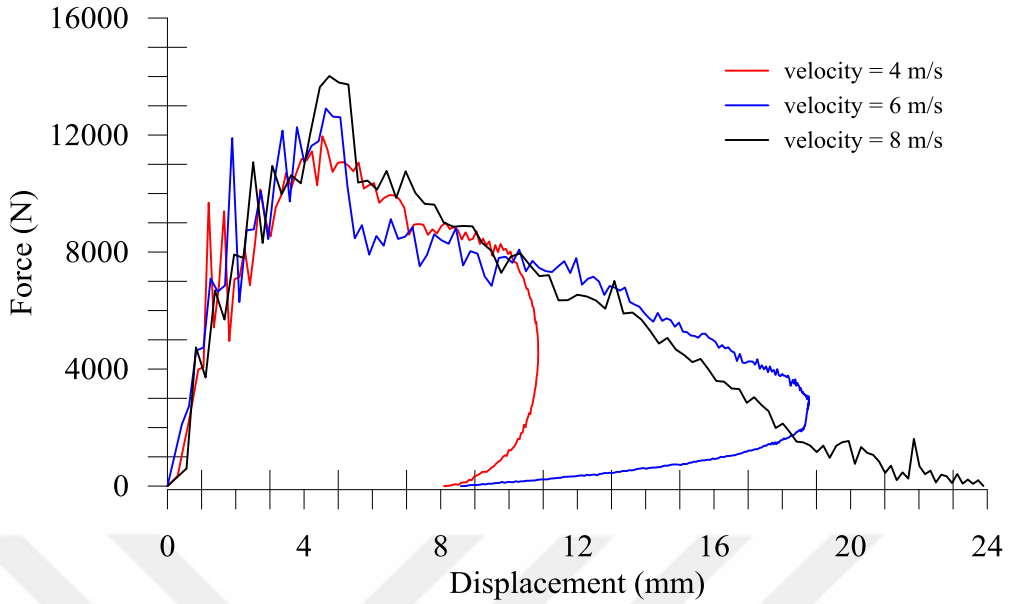


Fig-3.3(a) Force-Displacement Graph for 2B2C

3.1.5.2.3 Energy-Time Plot for 2B2C

The values of the Energy-Time Plot for 2B2C hybrid through thickness composite laminate which was tested for drop weight impact test for the impact speeds is given in Fig-3.3 (c). The color codes for three impact speeds are red, blue and black for the quick recognition of at a glance on the graph.

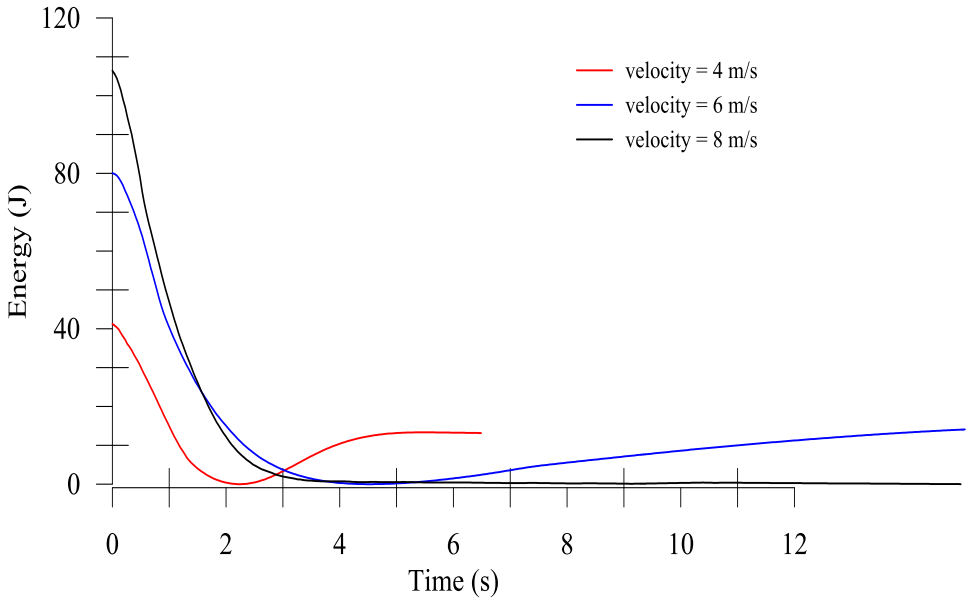


Fig-3.3(c) Energy-Time Graph for 2B2C

Table-3.2(b) Energy-Time Plot Values for 2B2C

Specimen	Velocity of Impactor (m/s)	Impact energy (J)	Absorbed energy (J)
2B2C	4	41.25	28.08
	6	80.01	71.51
	8	106.43	106.42

The numerical values of the impactor for impact energy and absorbed energy which are gained from these plots are also given for all three speeds at which the drop weight impact test was done are given in Table-3.2(b).

3.1.5.3 Plots for 3B3C

This section carries the plots of the Force-Displacement, Force-Time and the Energy-Time plots for only 3rd Type stacking sequence labelled as 3B3C. The plots are made in such a way that all 3 impact speeds for the drop weight impact test can be seen in plots.

3.1.5.3.1 F-d Plot for 3B3C

Force-Displacement Plot for 3B3C for all speeds of the impact tests are given in Fig-3.4(a). Force-Displacement Plot contains color codes of red, blue and black for the impact speed of 4 m/s, 6 m/s and 8 m/s for quick recognition at a glance on the graph. y-axis gives the peak force value of the force during the impact test while the x-axis shows the maximum distance for each speed for 3B3C through thickness hybrid laminate.

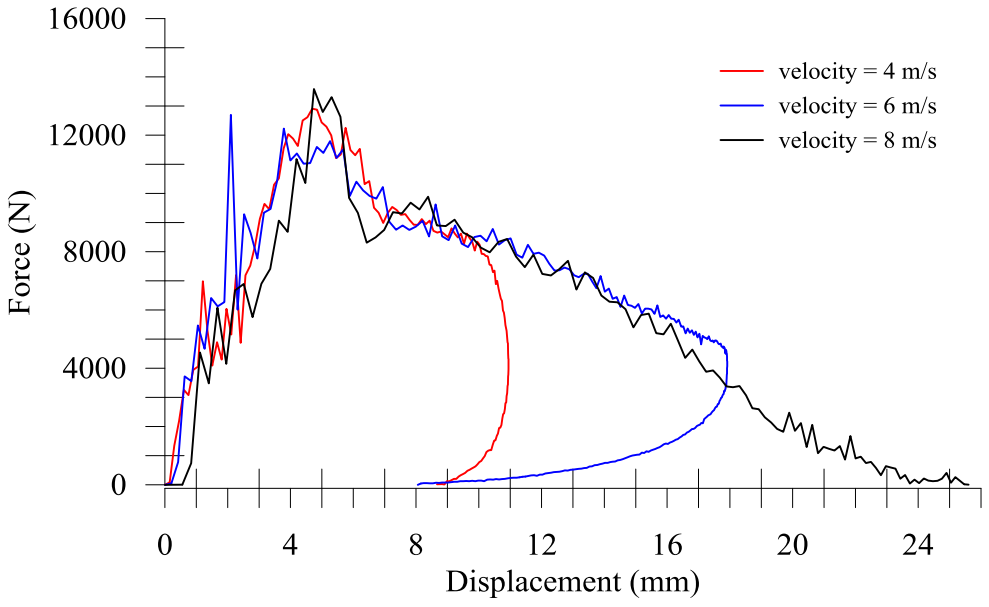


Fig-3.4(a) Force-Displacement Graph for 3B3C

Table-3.3(a) Energy-Time Plot Values for 3B3C

Specimen	Velocity (m/s)	Peak force (N)	Max Displacement (mm)	Area Under Curve (J)
3B3C	4	12905.17	10.94	94.06631
	6	12694.76	17.87	146.94941
	8	13581.49	25.61	138.77429

The numerical values of the maximum displacement, peak force and the area under the curve calculated from the graph of the 3B3C under impact for three different impact speeds are given in Table-3.3(a)

3.1.5.3.2 Force-Time Plot for 3B3C

The values of F-t graph are given in Fig-3.4(b) for all impact speeds. Peak force values are same as for F-d Plot. But force values don't return as was seen in the Force-Displacement Plot.

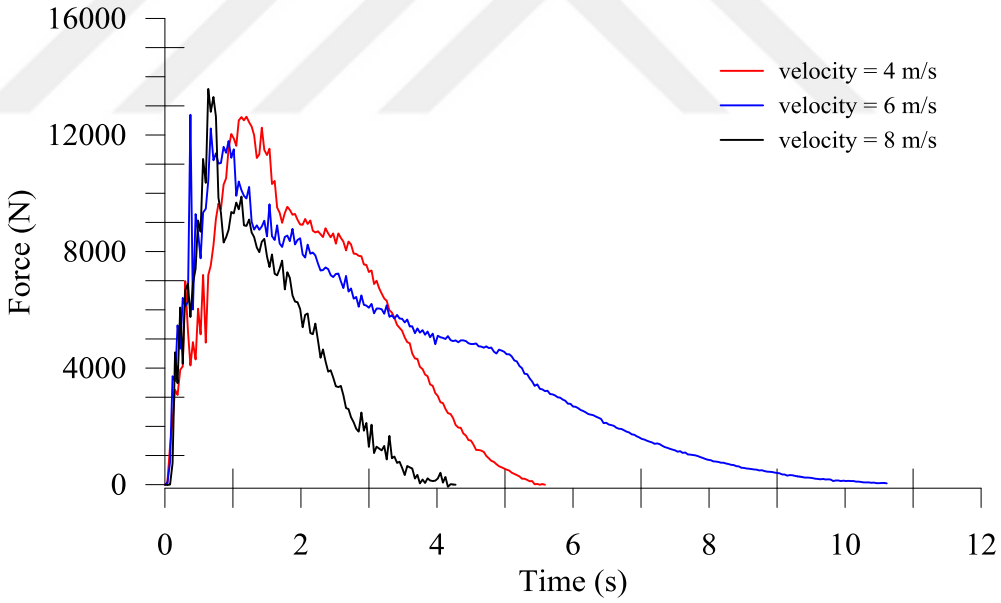


Fig-3.4(b) Force-Time Graph for 3B3C

3.1.5.3.3 Energy-Time Plot for 3B3C

The values of the Energy-Time Plot for 3B3C composite laminate is given in Fig-3.4(c). Drop weight impact test which was done for the impact speeds of 4 m/s, 6 m/s and 8 m/s is labelled with red, blue and black colors respectively for quick recognition. The values of the peak force are same as in the Force-Displacement Plot.

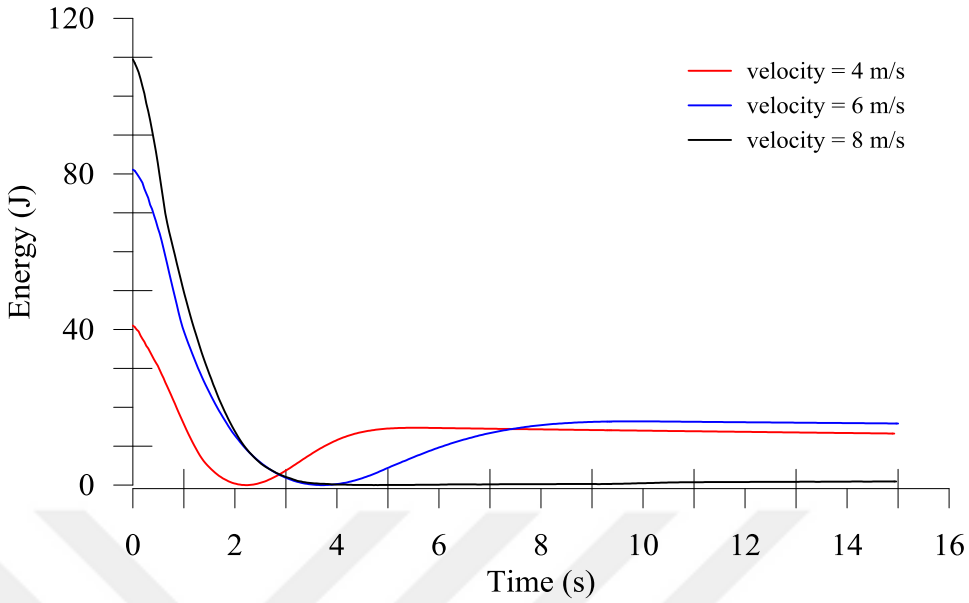


Fig-3.4(c) Energy-Time Graph for 3B3C

Values of the impact Energy and the absorbed energies for three impact speeds of 4 m/s, 6 m/s and 8 m/s which are gained from the graph for 3B3C given in Fig-3.4(c) are extracted from graph and given in Table-3.3(b)

Table-3.3(b) Energy-Time Plot Values for 3B3C

Specimen	Velocity of Impactor (m/s)	Impact energy (J)	Absorbed energy (J)
3B3C	4	41.01	27.76
	6	81.09	65.26
	8	109.05	108.59

3.1.5.4 Plots for HYB

Force-Displacement, Force-Time and Energy-Time plots for the in-plane hybrid composite are given separately with the brief description under them. These plots are gathered from the low speed drop weight test. 4 m/s, 6 m/s and 8 m/s speed tests were done on the 2 samples for each speed. These speeds are labelled in plots.

3.1.5.4.1 F-d Plot for HYB

Force-Displacement Plot for HYB in-plane hybrid composite laminate for all speeds of the impact tests are given in Fig-3.5(a). Force-Displacement Plot contains color codes of red, blue and black for the impact speed of 4 m/s, 6 m/s and 8 m/s respectively for quick recognition at a glance on the graph. y-axis gives the peak force value of the force

during the impact test while the x-axis shows the maximum distance for each speed for HYB in-plane hybrid composite laminate.

Table-3.4(a) Energy-Time Plot Values for HYB

Specimen	Velocity (m/s)	Peak force (N)	Max Displacement (mm)	Area Under Curve (J)
HYB	4	39.88	24.48	89.57053
	6	79.76	64.73	141.53843
	8	98.61	97.89	126.22934

The numerical values of the maximum displacement, peak force and the area under the curve is given in Table-3.4(a) which are extracted from the graph given in Fig- 3.9(a)

3.1.5.4.2 Force-Time Plot for HYB

The Force-Time Plot for HYB in-plane hybrid composite laminate for all speeds of the impact tests are given in Fig-3.5(b) for all impact speeds. Peak force values are same as for F-d Plot. But force values don't show recovery as was seen in the Force-Displacement Plot for 4 m/s and 6 m/s because these values are plotted versus time on the x-axis. The *shape* of the graph plot for the impact test for 8 m/s speed of the impactor are same for both Force-Displacement and Force-Time plots. For the impact speed of 8 m/s total penetration through the laminate occurs. The impactor does not bounce back as there is no elastic recovery at this impact speed.

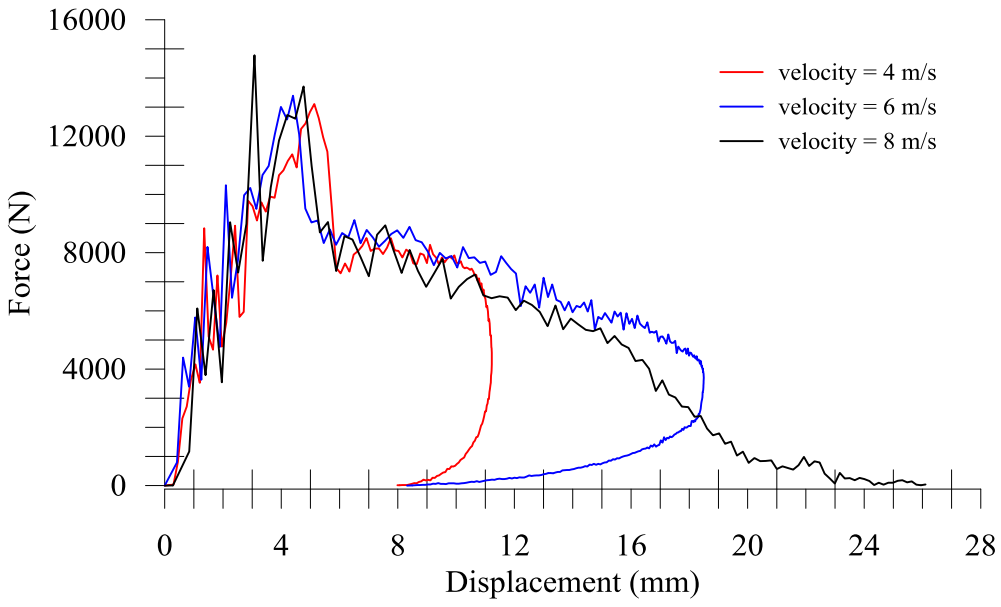


Fig-3.5(a) Force-Displacement Graph for HYB

3.1.5.4.3 Energy-Time Plot for HYB

The values and graph of the Energy-Time Plot for HYB hybrid composite laminate for all three drop weight impact speeds are given in Fig-3.5(c) and Table-3.4(b)

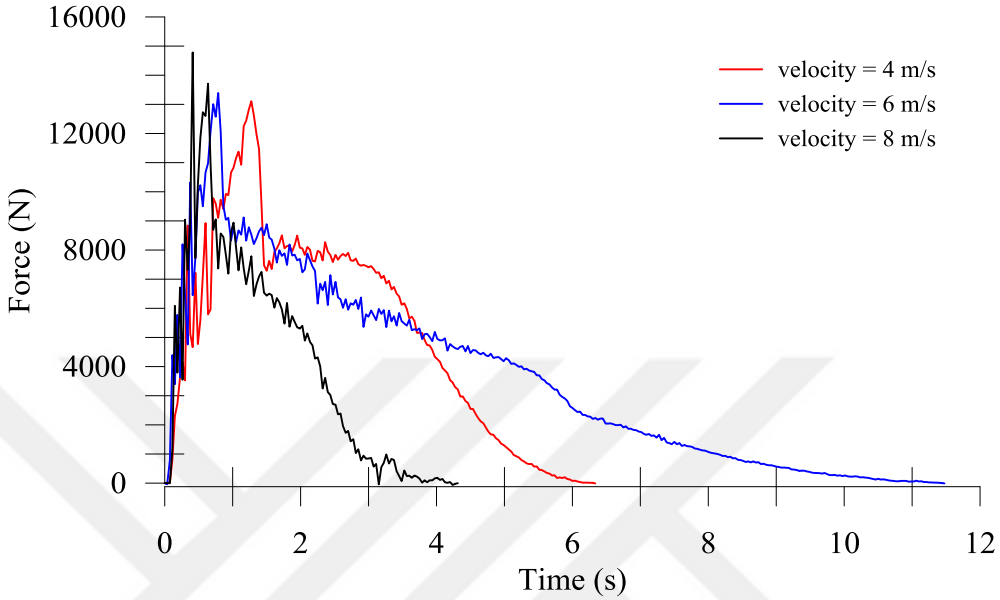


Fig-3.5(b) Force-Time Graph for HYB

Table-3.4(b) Energy-Time Plot Values for in-plane Hybrid Composite

Specimen	Velocity of Impactor (m/s)	Impact energy (J)	Absorbed energy (J)
HYB	4	39.88	24.48
	6	79.76	64.73
	8	98.61	97.89

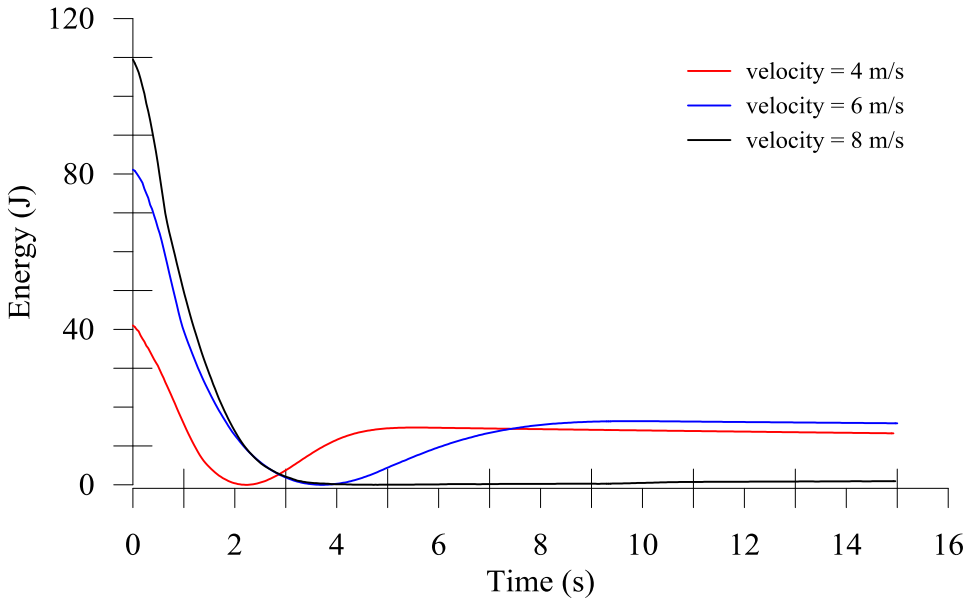


Fig-3.5(c) Energy-Time Graph for HYB

3.1.6 Results for Impact Speed

This section gives the plots for Force-Displacement, Force-Time and Energy-Time for all the laminates. The color labelled names of all laminates makes the quick recognition possible from the legend. This helps to see the behavior of each laminate when the low speed impact test is applied on the different speeds. Here again the quick observations from the plots is made and the is written under each particular graph. The detailed review of these observations, reasons behind these behaviors and conclusions are given in the next chapters. Low speed drop weight impact test speeds are kept constant and the graph plots for all four hybrid composite laminates are plotted on the same graph in under to understand their behavior for each speed. Fig-3.5(d) gives the schematic view of these plots. The number of the plots is a bit high so this theme chart helps understand the flow of these plots.

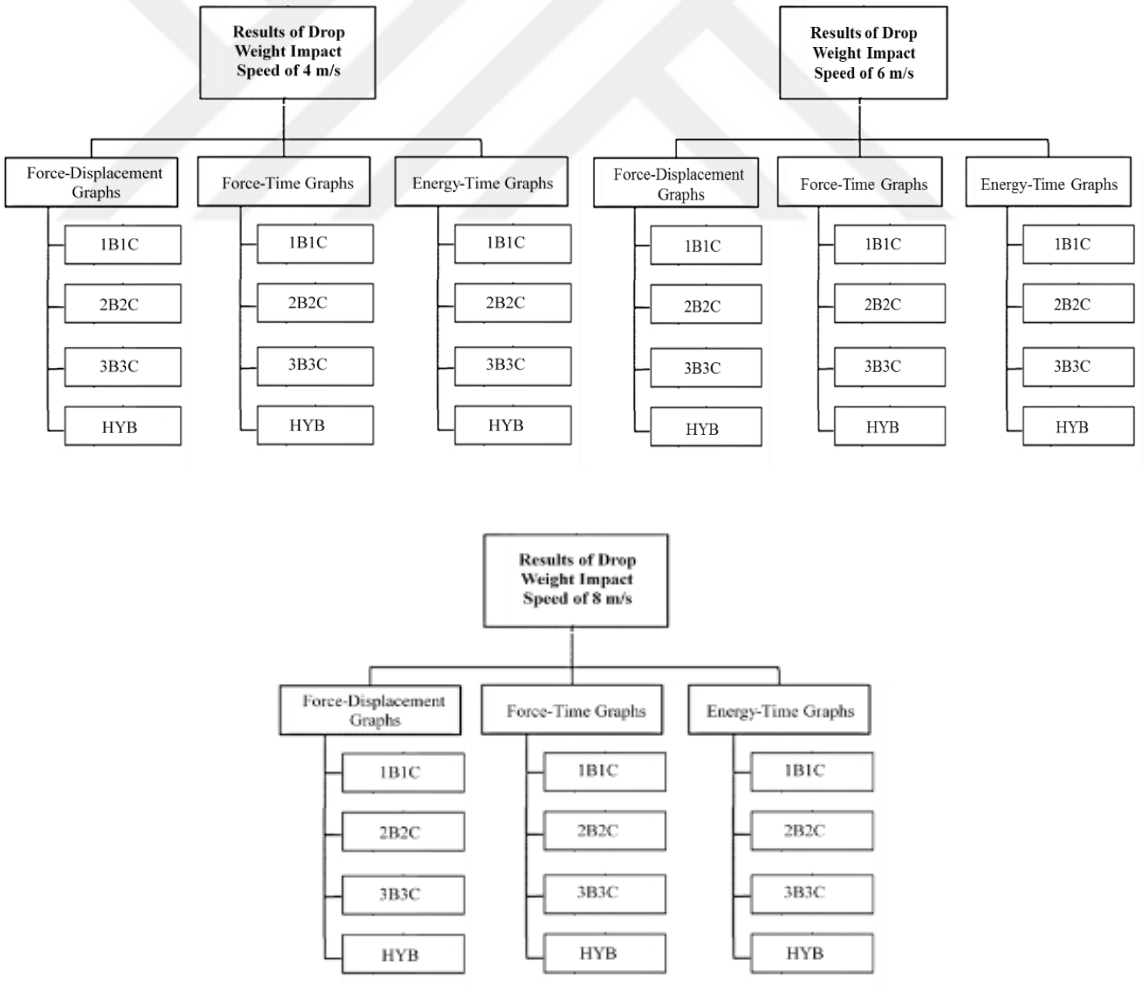


Fig-3.5(d) Results Based on Each Composite Laminate

3.1.6.1 Plots for 4 m/s

Plots for the low speed drop weight impact test for 4 m/s are given in the in this section. These plots have Force-Displacement, Force-Time and Energy-Time plots for 1B1C, 2B2C, 3B3C hybrid through thickness and HYB in-plane hybrid composite laminates are given. Limit values of the plots on the x-axis and y-axis are kept same for the *plots based on each laminate.* This is done to have an easier review or comment on the plots.

3.1.6.1.1 Force-Displacement Plot for 4 m/s

The Force-Displacement Plot for drop weight impact test applied for the speed of 4 m/s is given in this section. Table-3.1 contains the numerical values of the peak force and the area under the curve for all laminates extracted from the graph given in Fig-3.6(a).

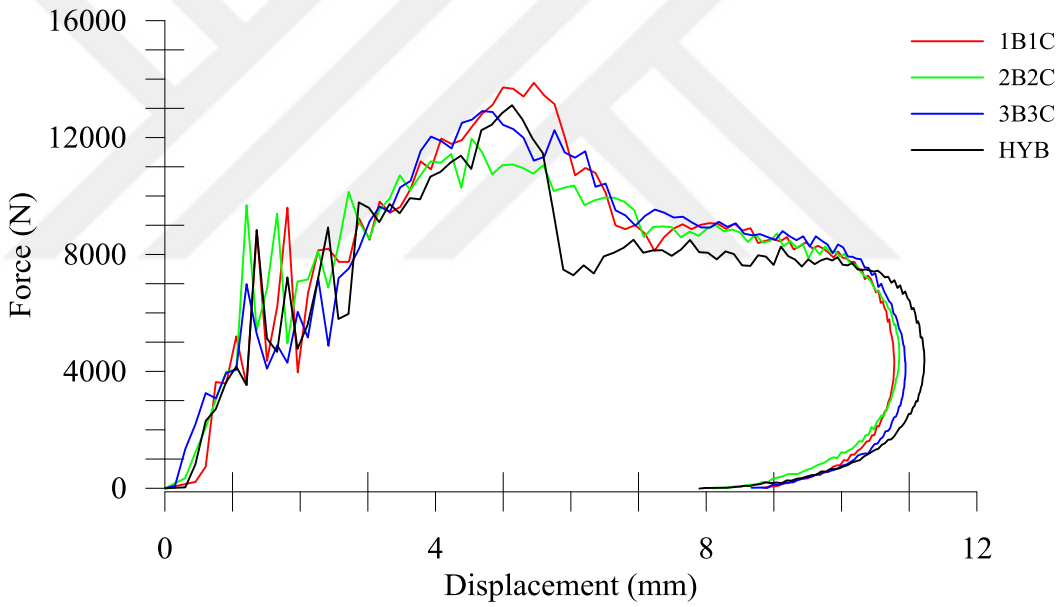


Fig-3.6(a) Force-Displacement Graph for 4 ms^{-1}

Table-3.5(a) Peak Force, Maximum Displacement and Area under Curve for 4 m/s

Specimen	Peak force (N)	Maximum Displacement (mm)	Area Under Curve (J)
1B1C	13877.06	10.78	93.97096
2B2C	13531.39	10.85	92.96080
3B3C	12905.17	10.94	94.06631
HYB	13105.56	11.17	89.57053

3.1.6.1.2 Force-Time Plot for 4 m/s

The Force-Time Plot for 4 m/s is given in Fig-3.6(b). The colors ensure the quick recognition of the samples tested for low speed drop weight impact test.

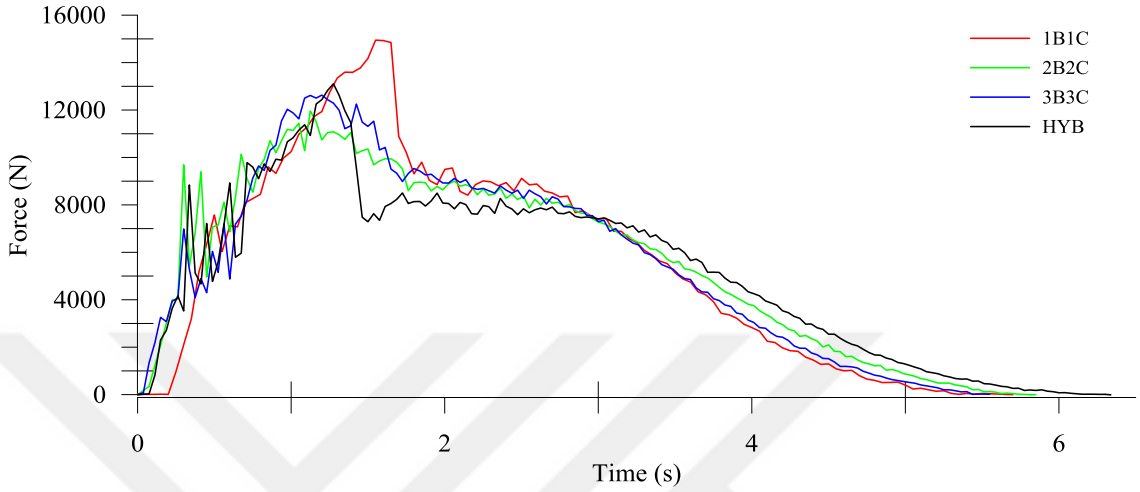


Fig-3.6(b) Force-Time Graph for 4 ms^{-1}

3.1.6.1.3 Energy-Time Plot for 4 m/s

The plots for the Energy-Time values of all the laminates which are tested for the low speed of 4 m/s drop weight impact test are given in Fig-3.6(c). Each hybrid composite is labelled with different colors for quick recognition.

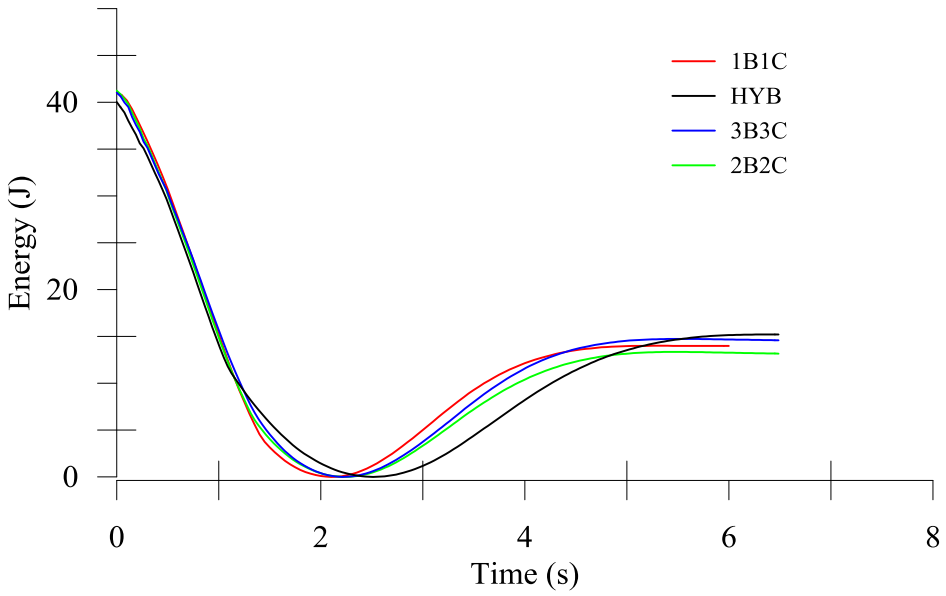


Fig-3.6(c)Energy-Time Graph for 4 ms^{-1}

Table-3.5(b) Impact energy and absorbed energy for 4 m/s

Specimen	Impact energy (J)	Absorbed energy (J)
1B1C	41.03	27.05
2B2C	41.25	28.08
3B3C	41.01	27.76
HYB	39.88	24.48

The values of the impact energy and the absorbed energy for all the laminates when the impact test was carried on for 4 m/s are given in Table-3.5(b)

3.1.6.2 Plots for 6 m/s

Plots for the low speed drop weight impact test for 6 m/s are given in this section. Force-Displacement, Force-Time and Energy-Time plots for the impact tests of 6 m/s are given in Figures -3.7(a), (b) and (c) respectively. The numerical values of these plots are also given in 3.6(a) and (b).

3.1.6.2.1 Force-Displacement Plot for 6 m/s

The Force-Displacement Plot for 4 m/s is given in Fig-3.7(a) and the values of the peak force, maximum displacement and the area under the curve are given in Table-3.6(a)

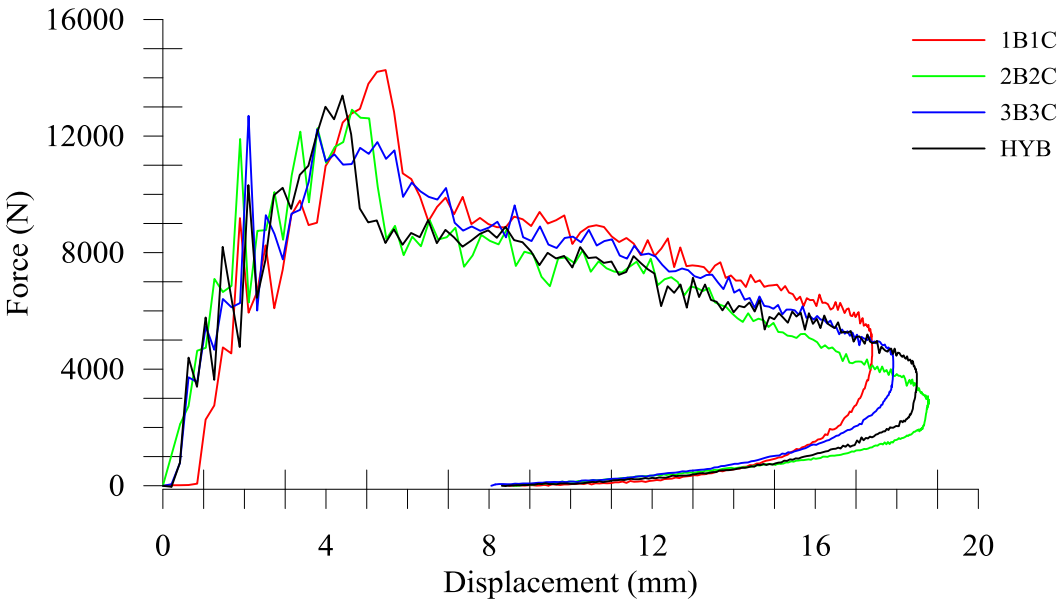


Fig-3.7(a) Force-Displacement Graph for 6 ms^{-1}

Table-3.6(a) Peak Force, Maximum Displacement and area under the curve for 6 m/s

Specimen	Peak force (N)	Maximum Displacement (mm)	Area Under Curve (J)
1B1C	14267.83	17.40	144.43717
2B2C	12905.17	18.49	141.32051
3B3C	12694.76	17.87	146.94941
HYB	13391.12	18.49	141.53843

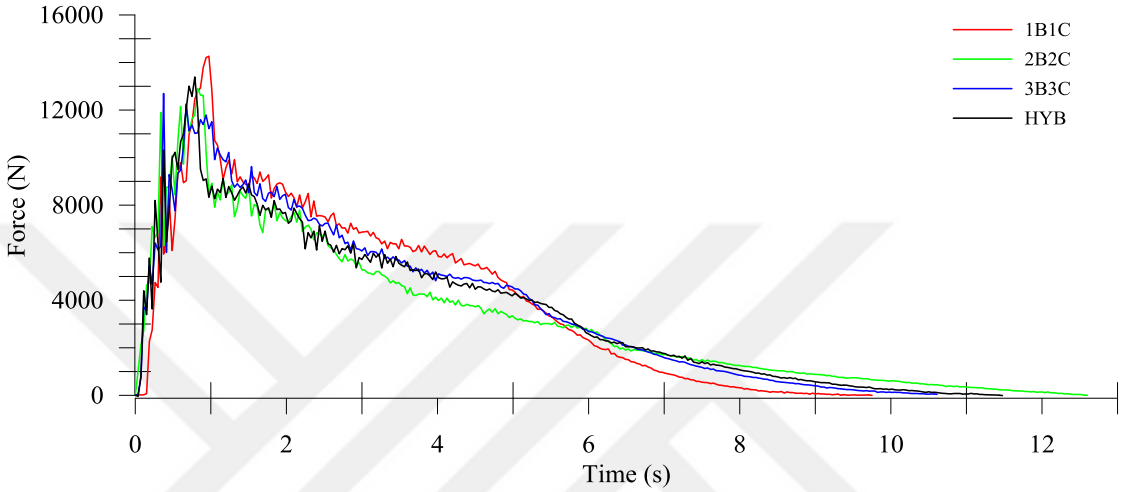


Fig-3.7(b) Force-Time Graph for 6 ms^{-1}

3.1.6.2.2 Force-Time Plot for 6 m/s

Force-Time plots for all laminates labelled with different colors which were tested with the low speed of 6 m/s drop weight impact test in Fig-3.7(b)

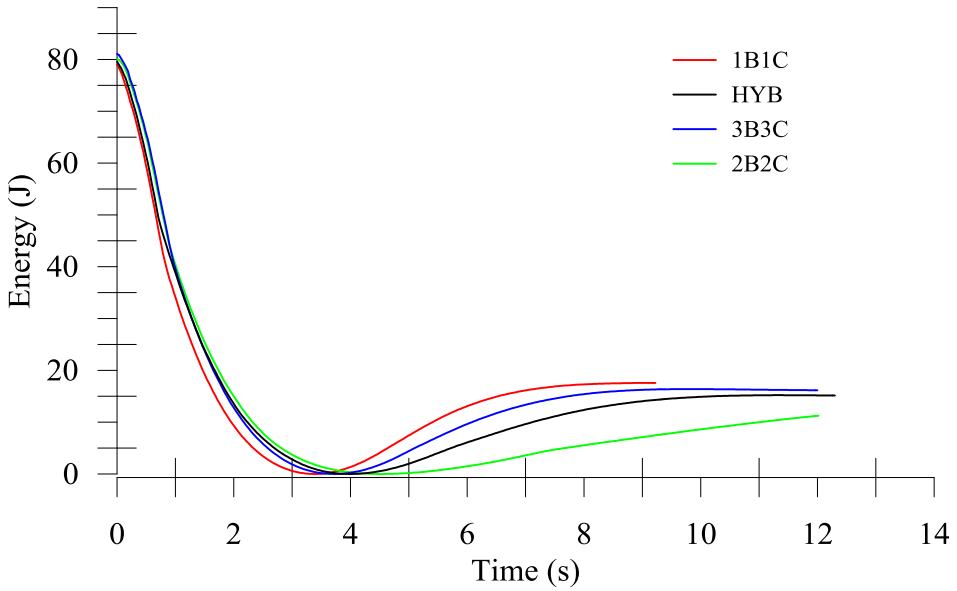


Fig-3.7(c) Energy-Time Graph for 6 ms^{-1}

3.1.6.2.3 Energy-Time Plot for 6 m/s

The plots for the Energy-Time values of all the laminates which are tested for the low speed of 6 m/s drop weight impact test are given in Fig-3.7(c). Each hybrid composite is labelled with different colors for quick recognition.

Table-3.6(b) Impact energy and absorbed energy for 6 m/s

Specimen	Impact energy (J)	Absorbed energy (J)
1B1C	79.05	61.46
2B2C	80.01	71.51
3B3C	81.09	65.26
HYB	79.76	64.73

The values of the impact energy and the absorbed energy for all the laminates when the impact test was carried on for 4 m/s are given in Table-3.6(b)

3.1.6.3 Plots for 8 m/s

This section contains the Force-Displacement, Force-Time and the Force-Energy plots for 1B1C, 2B2C, 3B3C and in-plane Hybrid Composite laminates labelled the different colors impacted at the speed of 8 m/s.

3.1.6.3.1 Force-Displacement Plot for 8 m/s

The Force-Displacement Plot for 8 m/s is given in Fig-3.8(a) and the values of the peak force, maximum displacement and the area under the curve are given in Table-3.7(a)

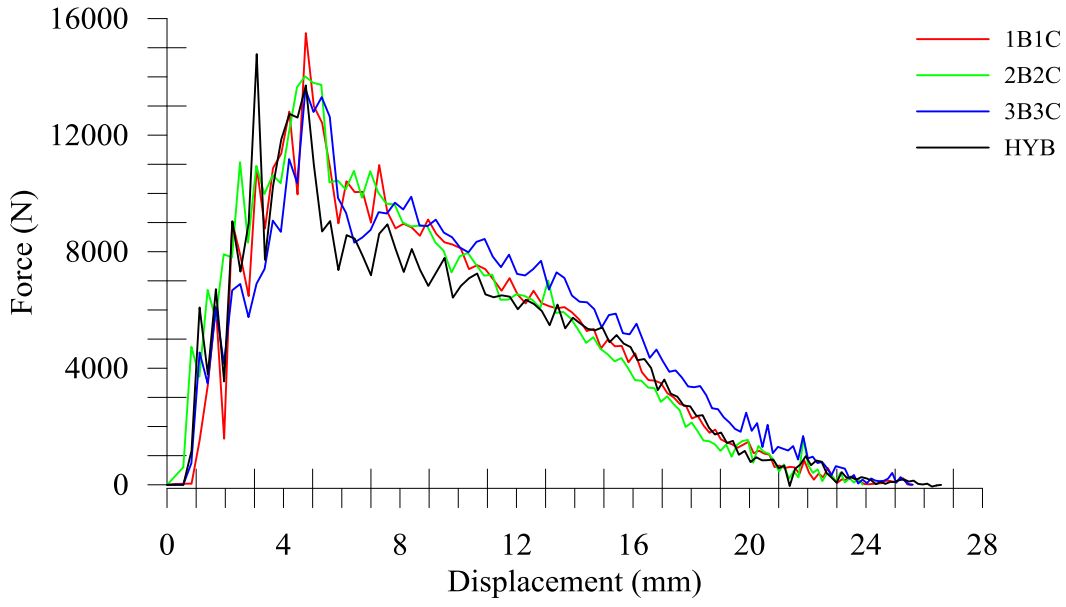


Fig-3.8(a) Force-Displacement Graph for 8 ms^{-1}

Table-3.7(a) Peak Force, Maximum Displacement and area under the curve for 8 m/s

Specimen	Peak force (N)	Maximum Displacement (mm)	Area Under Curve (J)
1B1C	15505.24	25.57	131.2042053
2B2C	13710.7645	26.687432	136.1301858
3B3C	13581.4875	25.606262	138.7742905
HYB	14783.8324	26.582067	126.2293362

3.1.6.3.2 Force-Time Plot for 8 m/s

Fig-3.8(b) has the plots of Force-Time for 1B1C, 2B2C, 3B3C hybrid through thickness and HYB in-plane hybrid composite laminates which were tested under the low speed of 8 m/s drop weight impact test. Vertical axis gives the peak force value while the horizontal axis gives the value of time.

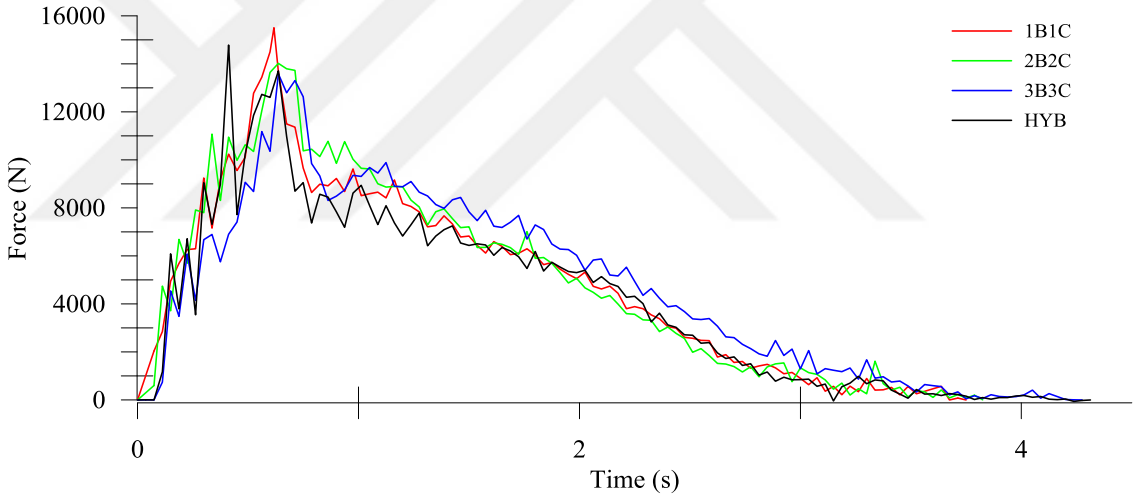


Fig-3.8(b) Force-Time Graph for 8 ms^{-1}

3.1.6.3.3 Energy-Time Plot for 8 m/s

The values of the impact energy and th e absorbed energy for all the laminates when the impact test was carried on for 8 m/s are given in Table-3.7(b) and graph is given in Fig-3.8(c).

Table-3.7(b) Impact energy and absorbed energy for 6 m/s

Specimen	Impact energy (J)	Absorbed energy (J)
1B1C	105.20	103.06
2B2C	106.43	106.42
3B3C	109.05	108.59
HYB	98.61	97.89

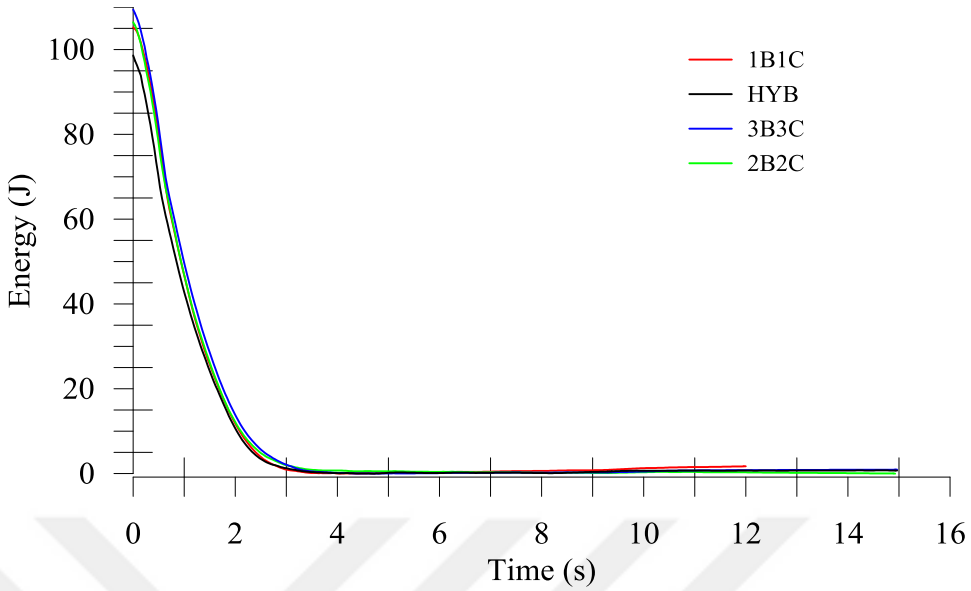


Fig-3.8(c) Energy-Time Graph for 8 ms^{-1}

3.1.7 Failure Observations

This Section contains the pictures of the front and back side of the impacted samples. 1B1C, 2B2C and 3B3C and in-plane Hybrid Composite laminate. The front and the backsides have different patterns which change under the effect of various factors such as impacted energy, geometry and the nature of the laminates. In this study the main factor which needs to be checked is the change in the macroscopic impact patterns on the front and the backside of the laminates with the change in the stacking sequences.

In-plane hybrid composite laminates are made from the plain weave carbon-basalt hybrid fabrics which have basalt fibers on 0^o and 90^o. 60x zoomed area of the back side of the in-plane hybrid composite, labelled as HYB, is given in Fig-3.9.

According to Fig-3.10 the following observations are made from the impact patterns of the tested samples.

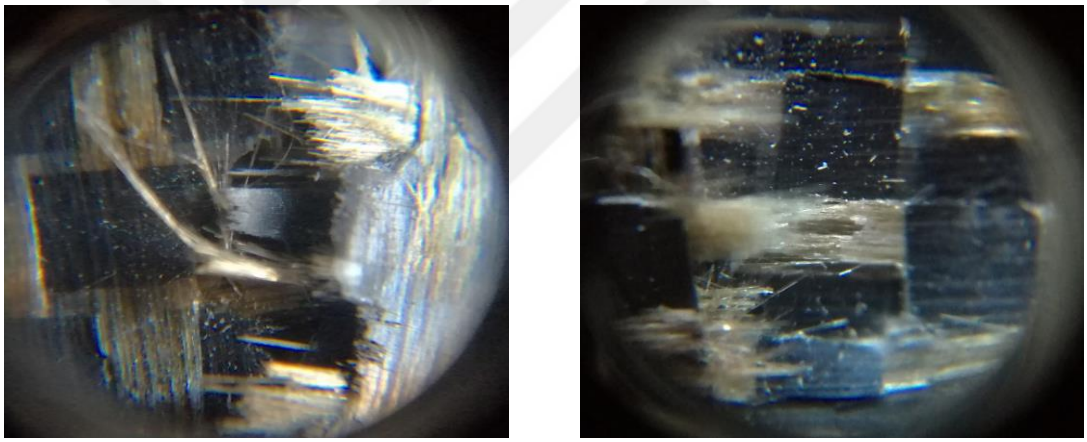
i. Impacted area shows a cross shaped impact pattern for all the laminates. This pattern is most evident for 1B1C and least evident for 3B3C.
ii. Elastic behavior for all the laminates is observed for 4 m/s, 6 m/s low speed drop weight impact test. There is no full penetration for these speeds and the impactor does not go through the laminate. The impactor bounces back for 4 m/s and 6 m/s
iii. Perforation is observed for all the laminates which are impacted at 8 m/s. The impactor does not bounce back and go through the laminates. The cross shaped impact pattern is most evident here for 1B1C and least evident for 2B2C.

iv. Area of the impacted area is similar for all the laminates however the backside of the impacted laminate for 3B3C does not show a clear cross-shaped damaged area.

According to Fig-3.9 the following observations are made from the breakage of the fibers inside the laminate.

i. Backside of the impacted HYB composite (for 6 $^{m/s}$ speed) shows basalt fibers leave small filaments when they crack due to their ductile nature and also the longer tension to breakage length. It could also be because of the inner structure and the constituents of the basalt fibers. The closer inspection of the material shows that basalt fibers do not have good adhesive properties that's why it is pulled out easily.

ii. Carbon fibers break in a brittle way again due to their brittle nature. Absence of the filaments on the breakage also emphasizes they have shorter tension to breakage lengths. Their better adhesive properties with the epoxy even after the breakage on the backside of the laminate due to the impact test.



60x zoom

Fig-3.9 Back face of the Hybrid Laminate at 6 m/s (left) no perforation has occurred here but the lowest layer in the sample is broken. Other layers showed elastic behavior and pushed the impactor back. The carbon fiber is broken in a brittle way while the basalt in a ductile way. On the right is the layer next to the broken layer which shows the basalt fibers

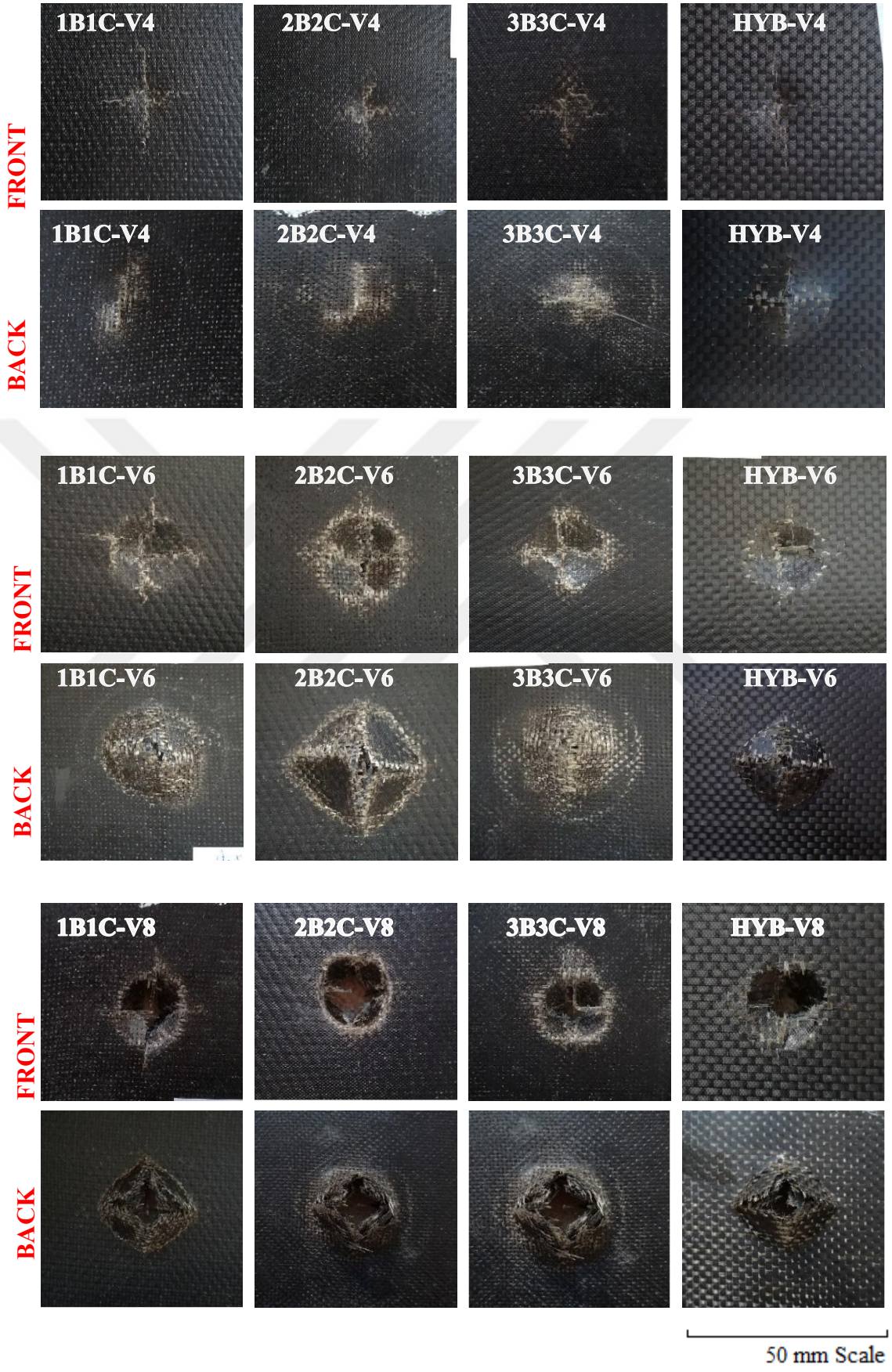


Fig-3.10 Front and back side of the impacted samples for 4 ms^{-1}, 6 ms^{-1} and 8 ms^{-1}

3.2 Tensile Test Results

3.2.1 Results Gained from The Tensile Test

The results acquired from the tensile test consist of Stress-Percent Elongation graph for the tested samples. The y-axis gives the values of the load and the x-axis show the value of the percent elongation as it is measured by the tensile loading.

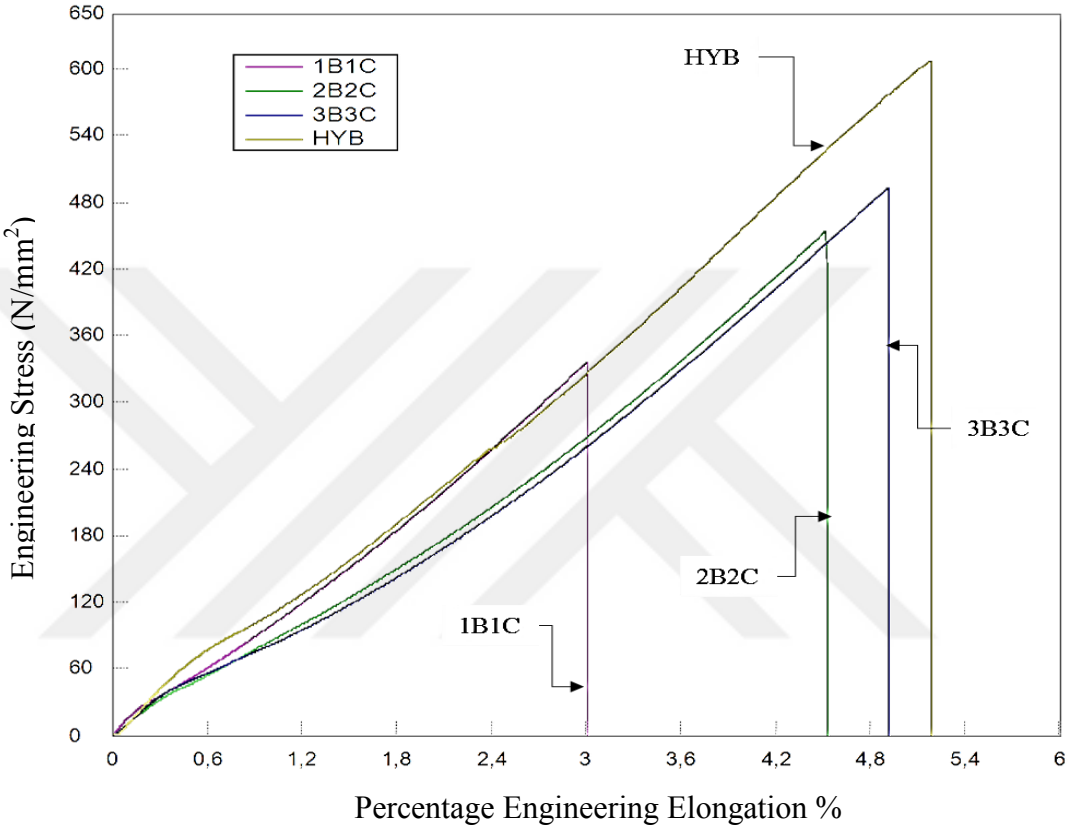


Fig-3.11 Tensile Test results and the Stress-Percent Elongation of all laminates

The color labelled hybrid through thickness 1B1C, 2B2C, 3B3C and in-plane hybrid composite laminate HYB show the maximum stress values on the graph through y-axis. The numerical values extracted from the graph are given in Table The numerical values extracted from the graph are given in Table-3.8(a).

Table-3.8(a) Numerical values of Maximum Stress

Name of the Laminate	Maximum Tensile Stress (N/mm^2)	Maximum Percent Elongation
1B1C	335.7	3.01
2B2C	453.6	4.51
3B3C	491.9	4.91
HYB	606.8	5.1

It is evident from the numerical values and from the graph that *the 1B1C hybrid structure shows the minimum stress value and 3B3C shows the maximum Stress value in the group of the hybrid through thickness structures.* On the other hand, in-plane hybrid composite laminate *HYB shows the maximum stress among all the hybrid composite laminates.* This value is almost two times higher than that of 1B1C.

Values of the stress are calculated by dividing the area of the laminate to the force/load values. The only difference between the hybrid through thickness laminates (1B1C, 2B2C,3B3C) in-plane hybrid composite laminate is the thickness. Remaining dimensions (250x15 mm^2) are same for all the laminates. The detailed review of these results and evaluation of the possible reasons behind such mechanical behaviors are discussed in chapter 3. The conclusion based on the results gained from both results is given in the next section.

3.4 Evaluation of Results

This section includes the discussion and the evaluation of the results from the two tests used for the examination of the mechanical properties of the composite materials of two types, in-plane hybrid composite (named as HYB) and hybrid through thickness composite laminates (named as 1B1C, 2B2C and 3B3C). These results are gained from the plots from the previous sections which are Force-Displacement, Force-Time and Energy-Time plots.

3.4.1 Results of Impact Tests

A detailed information about the results is given in the section 3.2. The plots for all 3 impact speeds are plotted on the same graph for Force-Displacement, Force-Time and Energy-Time values labelled with different colors. Reference was taken for each hybrid composite. The purpose was to understand the impression of speed for all laminates on a single graph. The graph plots of all 4 hybrid composite laminates are plotted on the same graph for Force-Displacement, Force-Time and the Energy-Time values for each impact speed labelled with colors. The low speed drop weight impact test speeds were taken as reference and for all three speeds, separate plots were made. The purpose was to see the behavior of the laminates for each speed on the same graph.

3.4.1.1 Force-Displacement Plots

Plots of the data from the low speed drop weight impact test were used which gave the value of the Peak Force, Maximum Displacement and the Area under the curve. Values of these entities are given in Table-3.8(b). This Table is created by gathering the values of all the Force-Displacement Plots for 1B1C, 2B2C, 3B3C and in-plane HYB hybrid composite laminates tested with the impact speeds of 4 m/s, 6 m/s and 8 m/s.

Table-3.8(b) Values of Peak Force, Max Displacement and the area under the curve

Impact Speed	Specimens	Peak force (N)	Maximum Displacement (mm)	Area Under Curve (J)
4 m/s	**1B1C**	13877.06	10.78	93.97
	2B2C	11958.32	10.85	92.96
	3B3C	12629.63	10.95	94.07
	HYB	13105.56	11.22	89.57
6 m/s	**1B1C**	14267.83	17.40	144.44
	2B2C	12905.17	18.78	142.32
	3B3C	12694.76	17.91	146.95
	HYB	13391.12	18.49	141.54
8 m/s	**1B1C**	15505.24	25.57	131.20
	2B2C	14022.35	24.04	136.13
	3B3C	13581.49	25.61	138.77
	HYB	14783.83	26.58	126.23

3.4.1.1.1 Observations on the F-d Plots

Impactor starts exerting the force on the laminate and the impact shows deformation. The value of the peak force increases so does the deformation till a point. After that particular point the force shows a quick decrease and reaches to zero. If the material is elastic and no perforation has occurred, impactor bounces back. The value of the distance decreases as the impactor leaves the laminate. This recovery is seen only for 4 m/s and 6 m/s only. For 8 m/s, perforation occurs, no recovery is witnessed and the impactor does not bounce back.

Peak Force values from the force-displacement plots are gathered and a graph of these values is made to see the effect of different stacking sequences on the peak force values in Fig-3.12. Area under the curve of the Force-Displacement Plot gives the work done in units of joules.

Following observations were made from the Force-Deformation Graph.

Peak Force Values

The value of the peak force is highest for 1B1C hybrid composite and in-plane HYB hybrid composite value has the peak force value between the 1B1C and 2B2C laminate and minimum of peak force for all laminates (this is more evident in Fig-2.29) for 6 m/s and 8 m/s. These values are calculated from the Force-Displacement plots and the particular numerical value of the bar graph in Fig-3.12 are given in Table-3.8 which can be checked if needed to have a better understanding of the peak values for force as peak values for force as seen in all the different structure arrangements. The values are

grouped for each speed and sub-group contains labelled names for each structure. Fig-3.12 is created to have a quick check on the peak force values.

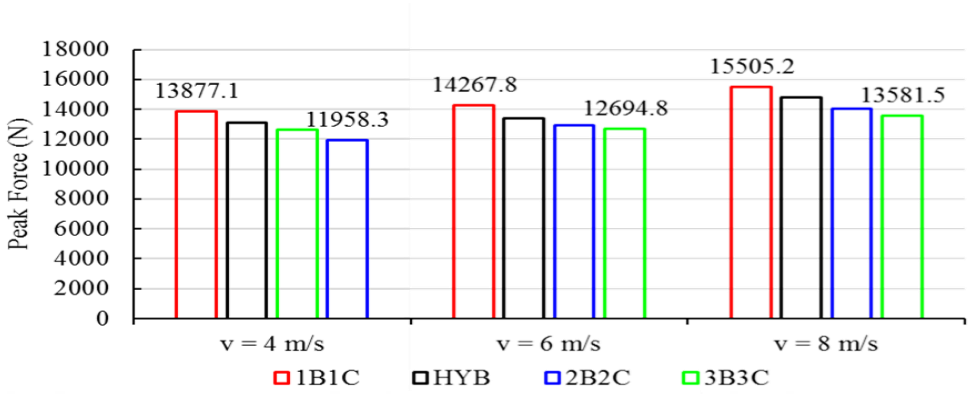


Fig-3.12 Peak Values for all laminates for 6 m/s and 8 m/s

and the laminates of interest, for example 1B1C which has the maximum peak force 3B3C which has the minimum peak force value valid of 6 and 8 m/s impact speeds also contains tags of their numerical values on the top of the bar graph.

Area under the F-d curve and Maximum Displacement

The value of the F-d area is highest for 3B3C hybrid composite and is lowest for in-plane HYB hybrid composite. The displacement or the deformation has the largest value for in plane hybrid composite labelled as HYB due to the lower relative thickness as compared to any other of the through thickness hybrid composite laminates. Other than that there is no strict pattern for maximum displacement in the laminates.

Sudden Decrease in the Force

The hybrid composite laminate of 1B1C, 2B2C and 3B3C are symmetric around the carbon. It means all of them have carbon-layers in the middle of the laminates. However, 1B1C has only two consecutive carbon fabric layers in the middle, 2B2C has four and 3B3C has a total of 6 carbon fabric layers in the middle of the structure. This is shown in Fig-3.13 for both schematic and the real view of the laminates.

Now if we compare the F-d plots of 1B1C with the F-d plots of 3B3C for any speeds, one thing is very clear that there is a sudden decrease in the force for 1B1C, in-plane HYB composite which is not present in the F-d Plots of 3B3C. This is because the middle layer of carbon fabrics is larger for 3B3C hybrid composite laminates. Please check Fig-3.6 for the comparison of the plots. The blue line for 3B3C has no quick decrease in the force in the region of 4mm-6mm in the x-axis.

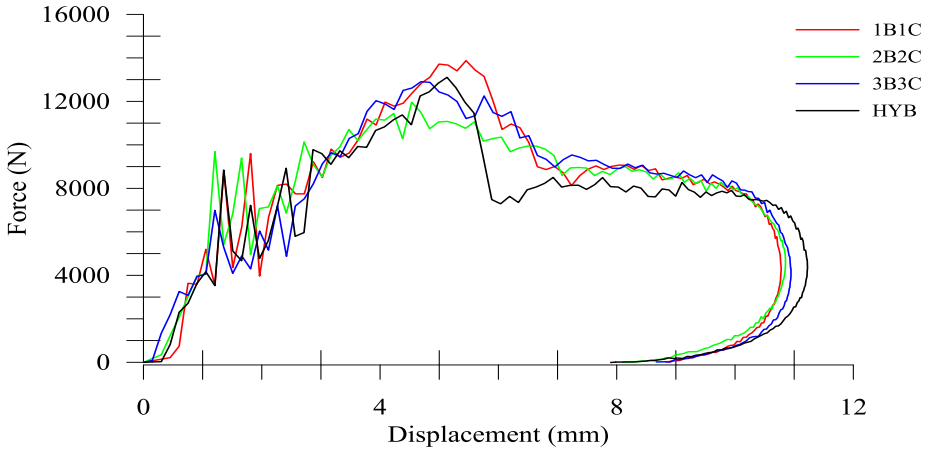


Fig-3.10(a) Force-Displacement Graph for 4 ms^{-1}

3.4.1.2 Force-Time Plots

Force-Time Plot for all the laminates show the maximum value of the force giving the peak value of the load. The values of the peak load are in consistency with the F-d plots. Detailed values of the Force-Time plots for each laminate for three different impact speeds is given as well as for each impact speed. Following observations from the plots are made.

3.4.1.2.1 Force-Time Plots Observations

Following observations from the Force-Time plots were made.

Symmetry of the Force-Time Plot

If the shape of the graph is same before and after the peak force, the graph is called symmetric. There is no symmetry in the Force-Time plots of any laminate.

Ductility Index

The Force-Time plots for all the specimen show the linear increase in the amount of the force with time which reaches maximum and then decreases. If we look at the area under the curve for Force-Time Plot for 1B1C and in-plane HYB hybrid composites before the peak force and after the peak force values as shown in Fig-3.14(a) and Fig-3.14(b). The area under the curve before PF is higher for 1B1C and lower for HYB meaning a large fraction of the energy is absorbed in the 1B1C before the fracture and vice versa for HYB. Energy absorbed before the peak-load is called the initiation energy and the after the load is called the propagation energy. The ratio of the propagation energy to the initiation energy is called the *Ductility Index* as given in the following formula.

$$Ductility\ Index = \frac{Inititation\ Potential\ Enery}{Propagation\ Enery}$$

This has something to with the load bearing capacity of the material. Ductility index is a theoretical value which can be calculated using the Force-Time plots to have the idea about the ductility of the laminate. Area under the curve is calculated above the x-axis with a single command but in this case following formula is used.

$$Ductility\ Index = \frac{Area\ under\ the\ Force\ vs\ Time\ Curve_{before\ peak\ force}}{Area\ under\ the\ Force\ vs\ Time\ Curve_{after\ the\ peak\ force}}$$

The maximum value of the peak force was taken as reference and the graph was plotted till the peak force. Then with the computer program area under the curve till this point is calculated. This process is shown in Fig-3.14(a) for 1B1C hybrid through thickness and HYB in-plane hybrid laminates. The second step is the calculate the are under the Force-Time Plot after the peak force value. The graph is plotted from the highest y-axis value which is the peak load value for the graph, to the zero value on the y-axis. Then again with the help of the computer program area under this second half of the original graph is calculated. This is shown in Fig-3.14(b). This process is repeated for 2B2C and 3B3C hybrid through thickness composite laminates and their Force-Time plots are used for this process. The color codes of Hybrid and 1B1C in-plane and hybrid through thickness composite laminates are used to distinguish between the laminates.

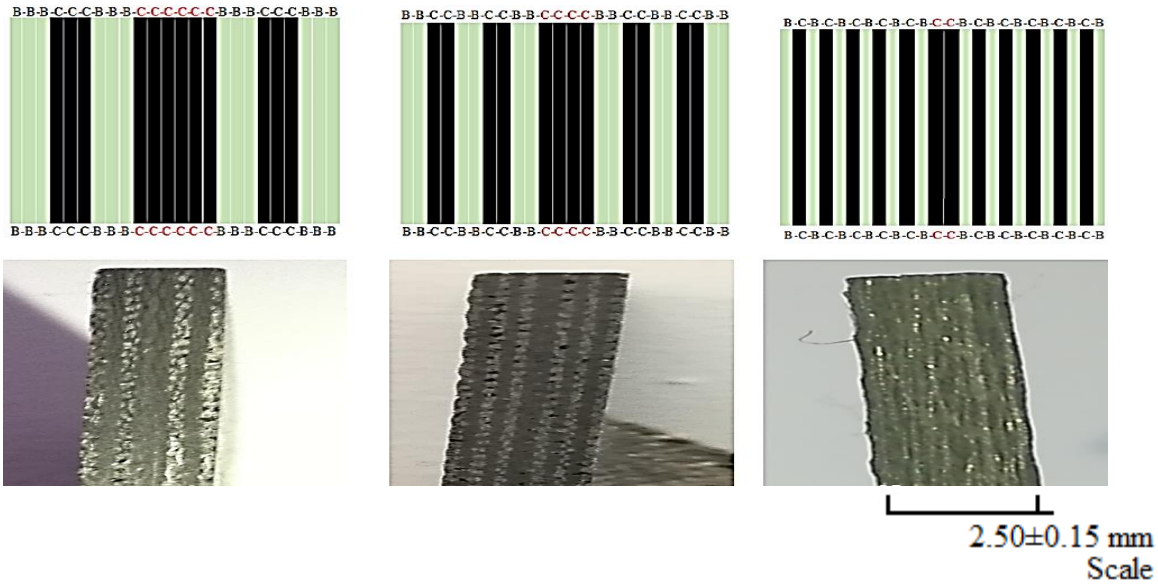


Fig-3.13 The symmetric layers of carbon fabrics in the middle of the Laminates

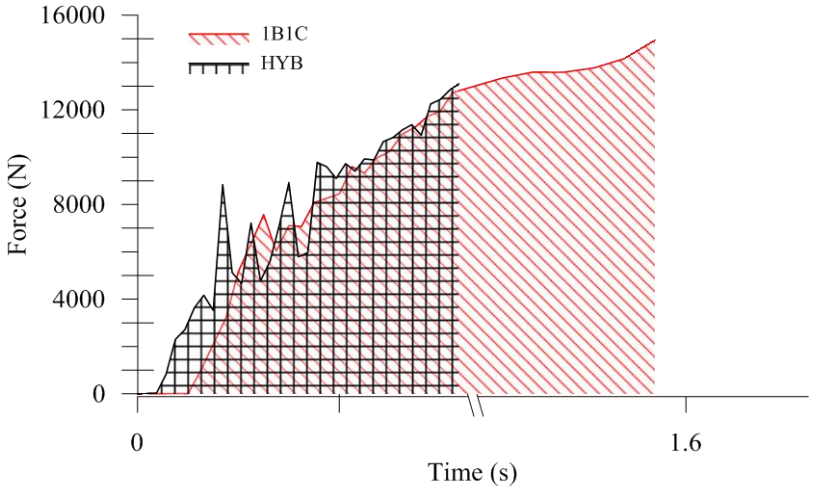


Fig-3.14(a) Area under Curve before Peak Load for Force-Time Graph for 4 ms^{-1}

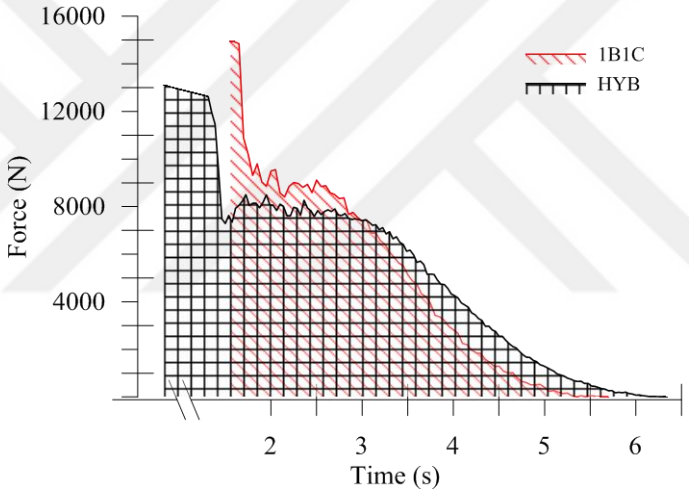


Fig-3.14 (b) Area under Curve after Peak Load for Force-Time Graph for 4 ms^{-1}

The larger area before the peak force value shows that the material is brittle and lower area conversely predicts the ductile nature of the material. Here one by one for each material, the ductility index value from the Force-Time plots for each laminate under the impact speed of 4 m/s, 6 m/s and 8 m/s are calculated. Values of the area under the curve before and after the peak force are given in Table-3.10

Table-3.9 Values of the Ductility index for all laminates at different impact speeds

	Specimens	Area Under Curve Before Peak Force	Area Under Curve after Peak Force	Ductility Index
4 m/s	**1B1C**	12208.06	20133.01	1.65
	2B2C	8159.88	24919.54	3.05
	3B3C	7202.99	25119.33	3.49
	HYB	9288.68	23440.28	2.52
6 m/s	**1B1C**	7152.07	34651.67	4.84
	2B2C	6594.58	33903.59	5.14
	3B3C	1626.92	38031.77	8.68
	HYB	5910.24	35424.43	5.99
8 m/s	**1B1C**	4689.32	13916.08	2.88
	2B2C	4928.96	14195.56	2.97
	3B3C	3700.97	16128.71	4.36
	HYB	4261.28	13121.70	3.08

In order to better understand the pattern of the ductility index values, a bar graph in Fig-3.15 is made to show the value of the maximum and minimum ductility values for all the laminates. These value are calculated from the numerical values of Table-3.9 and are readily available for the reader if area under the F-t curve is needed before or after the peak force.

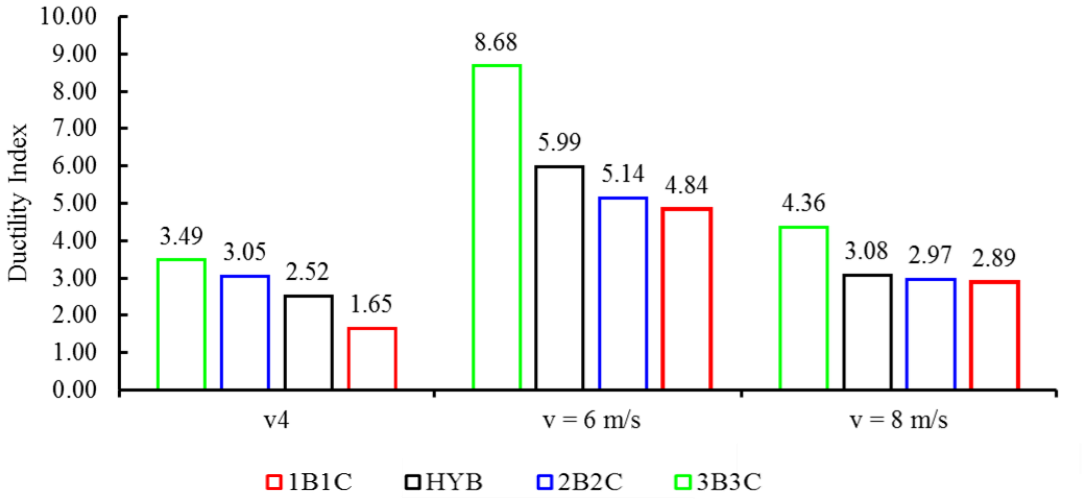


Fig-3.15 Values of the Ductility index calculated from Force-Time plots

Though a strict pattern cannot be seen from the ductility index value calculated from the Force-time plots. But the 1B1C laminate has the least ductility index for 4 m/s and 6 m/s. As far as the value of the ductility index is concerned for the drop weigh impact test for 1B1C which at the speed of 8 m/s, the value of the ductility index is not the lowest in the series. But for the drop weight impact test for 4 and 6 m/s the hybrid

composite laminate 3B3C shows the maximum ductility index. The graph for the Force-Time tests of 8 m/s showed total penetration for all the laminates.

3.4.1.3 Energy-Time Plots

The energy-time plots for all four laminates of impact tests are given in the previous chapter. First for each for each speed keeping he laminate constant, and then laminate keeping the speed constant. Each graph also contains a Table which has the values of their impact energies and absorbed energies. Table-3.10 shows the numerical values of energy of the impactor when it hits the surface defined as the impact energy and the remaining energy with which the impactor leaves/pushed back from the sample surface (due to elastic behavior of the laminate) which is defined as the released energy. This detailed Table is gathered from all the energy-time plots for all the hybrid composite laminates. The difference of these two energies (impact energy of the impactor and the energy released after the impactor bounces back) gives the energy amount which is absorbed by the laminate during the drop weight impact test as shown in the following formula.

$$E_{Absorbed} = E_{Impact} - E_{Released}$$

3.4.1.3.1 Force-Time Plots Observations

In order to do the observations on the Energy-Time Plot a conventional way is to see the damage caused by the impactor on the laminates. Absorbed energy can also give a quick idea for each laminate but a parameter called the Damage Degree can tell quickly how much damage has been caused to the laminate.

Damage Degrees:

Energy time graph gives the energy of the impactor at the time of the impact at t=0 seconds. The value of the damage degree is given by the following formula

$$Damage\ Degree = \frac{E_{Absorbed.}}{E_{impact}}$$

The ratio of the absorbed energy to the impact energy is introduced here as done in many other studies et al. [55]-[57] to examine how much damage is caused to the laminate. Mostly increase or decrease in the damage degree is checked with changing the structure as was done by Sarasini F et al. [54].

The theoretical value of the damage degree must be equal to 1 for 8 m/s tests because all the laminates are perforated and theoretically all energy is wasted on the laminate

breaking and the impactor does not return. The material which shows the lowest damage degree is least effected by the drop weight test. In order to understand the behavior of each structure each structure's Energy-Time Plot is examined separately. The incident energy of the impactor is lower than the ½ mv² theoretical value attributed to the apparatus error or unspecified reason. However, it does not affect the collective results as same numerical value of the error should be present for all three energies. The values of the incident energies are seen in Table-3.10 under the impact energy's tab. Before the impact the impactor comes with a uniform energy and this value decreases to a value of the zero and then it starts increasing when it bounces back.

Table-3.10 values of the impact, absorbed energy and damage degree for each laminate

Impact Speeds	Specimens	Impact energy (J)	Absorbed energy (J)	Damage Degree
4 m/s	**1B1C**	41.03	27.05	0.659
	2B2C	41.25	28.08	0.681
	3B3C	41.01	27.76	0.677
	HYB	39.88	24.48	0.662
6 m/s	**1B1C**	79.05	61.46	0.778
	2B2C	80.01	71.51	0.844
	3B3C	81.09	65.26	0.805
	HYB	79.76	64.73	0.782
8 m/s	**1B1C**	105.20	103.06	0.980
	2B2C	106.43	106.42	1.000
	3B3C	109.05	108.59	0.996
	HYB	98.61	97.89	0.993

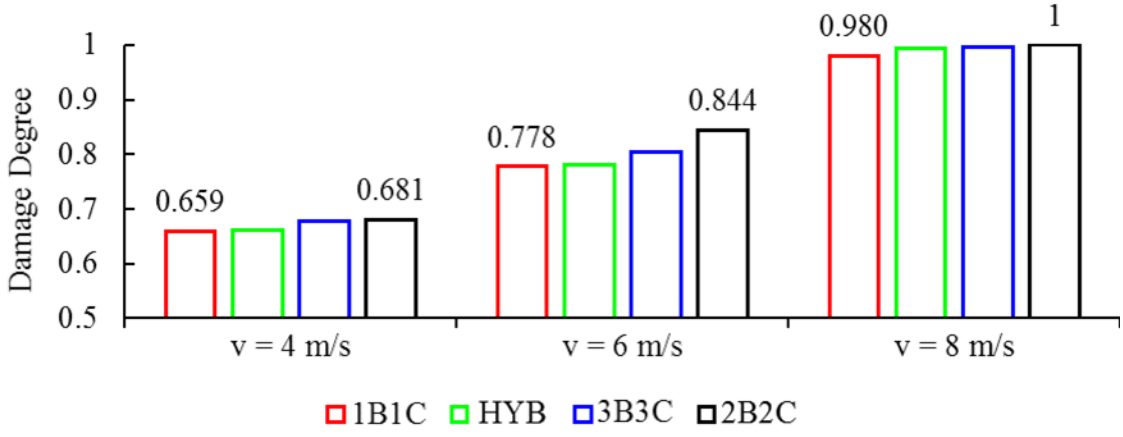


Fig-3.16 Damage Degree for 4 m/s, 6 m/s and 8 m/s

In order to better understand this, this data too is evaluated on the graph as shown in Fig-3.16 to have a quick recognition of the damage degrees for each laminate.

This data shows that the value of the damage degree is always least for 1B1C and the maximum for 2B2C. In-plane hybrid composite shows the similar damage degree values to the 1B1C structure.

3.4.2 Discussion of Impact Test Results

After detailed observations from the plots and the macroscopic view of the impacted samples this section serves the discussion of these observations and about the probable reasons behind a particular behavior from these particular samples is witnessed.

Drop weight impact test of the metals, such as low speed drop weight impact and charpy impact test, helps understand the failures caused and the energy absorptions are taken into account to characterize the mechanical behavior of the samples. However, the failure phenomenon of the composite materials is complex and all three failure modes like compression, tension and shear can be seen at the same time. This makes the characterization limited. That's why the low speed drop weight impact test is considered to be the more general and widely used impact characterization test for composite materials.

$$Normalized\ P.F\ = \frac{Peak\ Force}{Displacement}$$

1B1C hybrid composite shows the maximum Peak-Force values for all impact speeds. This is the value a laminate can bear before seeing major damage. This means this structure can bear the maximum load. But what about deformation? If the laminates have same width, then only peak forces can determine the capacity of maximum load. But composite laminates also involve the epoxy in the structure which might not distribute itself uniformly. This means my four laminates, indeed hybrid composite laminates, have different widths despite the amount of the material used is same in quantity and type. An easier way to take care of this problem is dividing the maximum load with the deformation for each test using following formula.

Normalized peak loads also showed the same results as it did for only peak force values. 1B1C composite showed the maximum peak load and 3B3C showed the minimum peak load value. 3B3C showed the minimum peak load values. This means that 1B1C is the stiffest of all laminates. This could be possible because 1B1C structure has epoxy between two different types of fabrics because it propagates in the order of one basalt fabric and next carbon fabric. It interchanges the type of fabric at every step and between them is epoxy composite. However, 3B3C changes the type of fabric after three steps because it is constructed as three basalt fabrics and 3 carbon fabrics joined together. This is shown in Fig-3.17

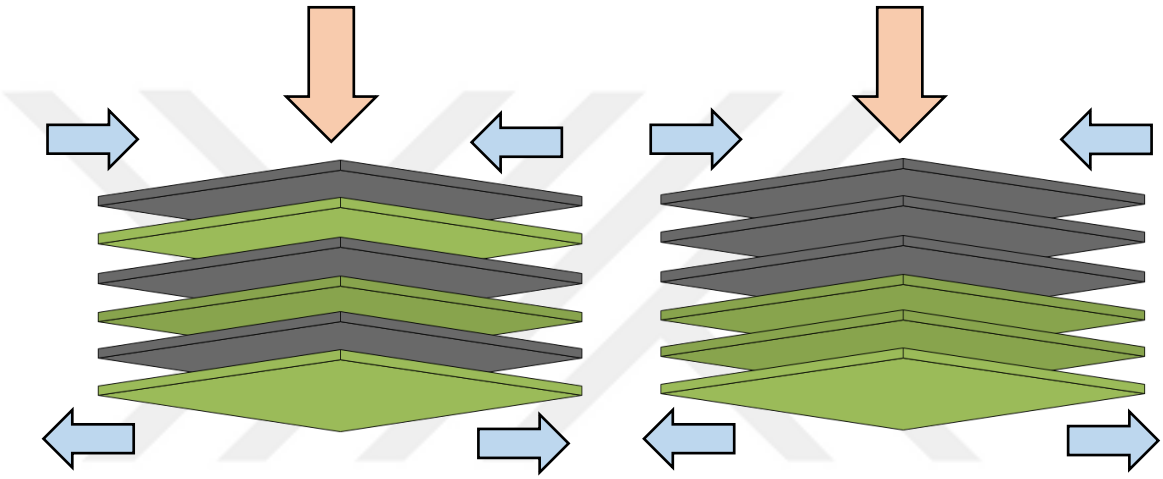


Fig-3.17 Alternating layers of 1B1C (left) and 3B3C (right) for the lowest 6 fabrics of the laminates

The least peak load and normalized peak load is seen for 3B3C. Probably this is the most flexible structure from all the four laminates. The in-plane hybrid composite laminate has the maximum load value between the 1B1C and 3B3C. This is as expected because the in-plane hybrid composite has the yarns made of carbon and basalt fibers in both directions and the properties are intermediate of upper and lower limit (upper limit being 1B1C showing maximum peak force value and lower being 3B3C showing minimum peak force value)

Area under the Force-Displacement curves has the maximum value for 3B3C which means it has maximum damage absorption capacity. Probably reason behind this is that it has three consecutive same types of fibers of basalt on the impact face. Basalt has better damage absorbing properties and has longer load-to-deformation values as compared carbon fibers. When the impactor touches the surface of the structure 1B1C,

it faces the only *one* layer of basalt and the next to this ballast layer is carbon which is not very good at absorption energies because it is brittle in nature. When the impactor touches the surface of the 2B2C and 3B3C it discharges its energy on the *three* consecutive layers of basalt. On the lower limit, in-plane HYB hybrid composite laminate has the least area under the F-d Curve, lowest damage absorption in this sense, which can also be cross checked by the absorbed energy values from the energy-time plots. This is because in in-plane HYB composite laminate there are *no* 100% basalt layers and it does not show good damage absorption values. Table-3.10 shows the amount of the absorbed energy to be lowest for in plane hybrid laminate HYB. It also shows that 1B1C has the lowest damage absorbing capacity. The damage absorption capacity for 2B2C and 3B3C is similar.

Force-Time plots gave an idea about the ductility index of the laminates. As told in the last paragraph, 3B3C is expected to be most flexible and 1B1C is stiffest in the structure. The ductility index for 1B1C is lowest and 3B3C has the highest ductility index. The reason behind this could be the way how layers of the carbon and basalt fabrics are arranged in the structure. Fig-3.17 shows how the laminates are arranged. The tension side, which is the lower part of the laminate opposite to the impact side, has three ductile lower young's-modulus value possessing basalt fabrics which under tension elongate more than carbon fibers. This makes the 3B3C material most flexible and this is confirmed by the data as 3B3C has the highest ductility index. The opposite of the 3B3C situation is the case for 1B1C. In the structure for 1B1C there are *one basalt* fabric; which is ductile in nature and has higher load-to-elongation values as compared to carbon, and *one carbon* fabric; which has lower load-to-elongation values. This makes the tension of the lower layers stiffer in 1B1C. As far as the in-plane hybrid HYB composite laminates are concerned, the elongated vertical and horizontal yarns made of carbon and basalt bear the tension of the impact opposite the impact face of the laminate. HYB in-plane laminate has the ductility index value either similar to 1B1C or is between the values of 1B1C and 2B2C.

The values of the damage degree were gained from the Energy-Time plots. If we see the damage degree values of all the structures, already established stiffest 1B1C is least damaged. Other than the reason explained in the last paragraph, this is because 1B1C has the epoxy attached with carbon from one side and basalt on the other side. The effect of the shearing forces between the laminates and the between the particular laminate and epoxy also plays an important role on the damage absorbing properties of the laminates. From the academic review done until now, a study by Sarasini F. et al. [54] gives an index which shows the adhesiveness of carbon fabrics and the basalt fabrics by providing their shear values. It is defined ILSS (interlaminar shear stress) in

the units of MPa as shown in Fig-3.18. Carbon shows better ILSS values which means it has better bonding capacities as compared to that of Basalt. Sarasini F. et al. [54] says in the article that interlaminar shear strength actually affects the mechanical properties of the material collectively. This value is affected by the nature of the consecutive materials on the both sides of the epoxy which changes according to the stacking sequence. The laminate fails when the load value is higher than the ILSS.

The cross shape on the impact area shows the matrix cracking on the front side which is caused by the brittle behavior of the carbon fibers and ductile behavior of the basalt fibers. This cross shape is prominent on the 1B1C and 2B2C which disappears while reaching towards 3B3C and Hybrid laminates. Possible reason for that is as we move from 1B1C towards 3B3C laminates, the distance of the impactor increases from the first carbon layer and the ductile nature of the basalt absorbs much of the energy

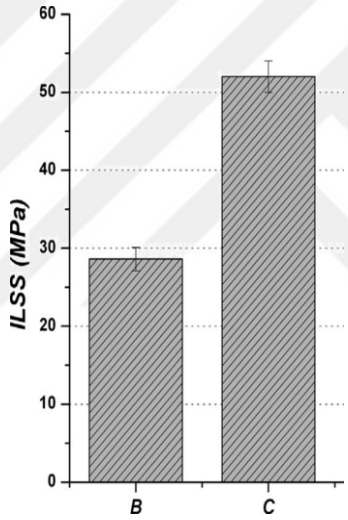


Fig-3.18 Interlaminar shear stress values for basalt and carbon fabrics (taken from the study by F. Sarasini et al. [54]

resisting the cross shaped cracking. Fig-3.17 shows the distance of the impactor from the first carbon layer. Same was confirmed by a study by Sarasini F. et al. [54] where it showed basalt has better impact resistance as compared to carbon. Here too, it is seen from the energy plots values that structures with two and three impact face layers of basalt show much better energy absorption properties. A cross shape on the surface of the Hybrid laminate is also evident if looked carefully which upon microscopic inspection revealed the filament leaving basalt fibers.

If the microscopic view (60x) of HYB in-plane hybrid composite laminate of the sample after the impact test is examined as shown in Fig-3.10, it can be seen that the basalt fibers leave small filaments when they crack while the carbon fibers break in a brittle way. Microscopic view of the damage pattern on the back side of HYB laminate reveals

the pulled fiber filaments from the basalt fibers and the brittle clear cuts on the carbon fibers. This again is because basalt has poor interlaminar shear stress behavior as shown in Fig-3.18 and the ductile behavior of the basalt laminates. The clear and brittle cuts for the carbon yarns are also evident in the cracked side of the in-plane HYB composite laminate.

3.4.3 Results of Tensile Test

The results of the tensile test for all the composite laminates are given in the previous chapter where the stress-percent elongation graph of each laminate is provided along with Table containing the numerical values of the peak stress values of each laminate. The composite materials do not show the failure phenomenon like metals or alloys in the tensile test because of their inner structure. There is no plastic region and the structure breaks at the elastic limit of the laminate. The shape of the laminate *after* the failure is important because it gives clues of about the type of the tension a particular material had to face before it failed.

3.4.3.1 Discussion of Low Speed Drop Weight Impact Test Results

It can be seen from Table-3.8 and graph in Fig-3.11 that 1B1C shows the lowest stress values among all the hybrid composite laminates. The core of carbon layers increases in 1B1C, 2B2C and 3B3C being 2, 4 and 6 consecutive layers of the carbon fabrics. This core of the carbon fabrics resists more upon tension and causes the stress value to increase being largest for 3B3C and lowest for 1B1C *only* for the hybrid through thickness composite laminates. What about in-plane hybrid composite laminate HYB? There is no core of carbon fabrics present in this structure because this structure is made of the in-plane hybrid fabrics of carbon and basalt fibers present at 0^o and 90^o in the laminate which reduced the thickness of the laminate samples. This reduces the area of the HYB laminate too. That's why the stress value, which is calculated from the division of Force to Area (definition of stress) is higher as compared to other samples in the group. The failures of the laminates under tensile test can be seen in Fig-3.19. HYB hybrid composite fails or breaks at a quite higher stress value as compared to other hybrid through thickness composite laminates.



Fig-3.19 Failures of the Laminates Under Tensile test

3B3C hybrid through thickness laminate is not failed from the grip as compared to the other hybrid laminates it has failed rather at the edge of the grip. The closer inspection of the broken pieces of the 3B3C shows that the core of the laminate by the thicker layer of the carbon fabrics has not broken totally as shown in Fig-3.6.

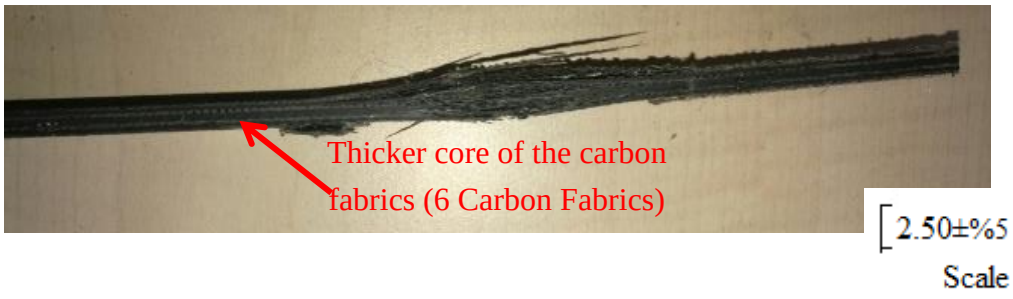


Fig-3.20 Failure pattern of the 3B3C Hybrid through thickness Composite Laminate

In Fig-3.20 it can be seen that the core of the carbon fabrics is not broken during the tensile test. The fabrics which are present on top and bottom of the laminate break because there are the most pulled fabrics clamped by the grip of the tensile machine.

According to these observations, the same type fabrics joined together resist most to the tension and show higher stress values. 1B1C as the most number of different types of fabrics joined together. It means that it has basalt fabrics on one side of the epoxy and

carbon fabrics on the other side of the epoxy except the core where two carbon fabrics are joined. 2B2C has the lower number of the alternating fabric types around the epoxy and the 3B3C has the lowest number of alternating fabric types around the epoxy. HYB in-plane hybrid composite has the same fabric types all around the laminate. The structural changes in the laminates cause the stress values for these laminates to be different.

In the next chapter, the conclusion and suggestions are given based on the results, observations and the discussions on these results.

,

CHAPTER 4

CONCLUSIONS AND SUGGESTIONS

After the evaluation and discussion on the results gained from the tensile and drop weight impact test are completed, now we are in position of giving a conclusion and suggestions for future studies.

4.1 Flexibility

- During the drop weight impact test, it is observed that the stacking sequence has effects on flexure properties of the composites. The tension side of the laminates having fabrics with higher young's modulus and lower elongation to break distances, for example carbon fibers in this study, increases the amount of force needed to break the material. If the higher young's modulus possessing fibers like carbon are put in the core of the material, they do not alter the results as effectively because they are neither under the direct effect of compression nor under the effect of tension.

- The tension side of the composite having ductile fibers with lower young's modulus and longer elongation to break distances show lower values force to break the laminates. In this study the laminates in which basalt fibers, which have longer elongation to break distances under tension, show more flexibility under the drop weight impact test.

4.2 Tensile Strength

- The values of the maximum stress are calculated by using the tensile test on all the laminates to compare this parameter. The results gained from this showed a particular pattern depending on the inner structure of the composite laminates. The hybrid composites having same type of fabrics stacked together showed the maximum stress value till the fibers broke. The inner core made of carbon fibers played an important role to the maximum stress value of the composites. The thickest core in the laminates I

used was composed of 6 carbon fabrics for 3B3C laminate which showed the maximum stress value in the group of hybrid through thickness composites. In-plane hybrid shows the maximum value of stress outperforming all the composites with 2 times higher maximum stress values because it has the 24 same fabrics (in-plane hybrid) stacked together. 1B1C composite had maximum bending stiffness but lowest maximum stress value.

4.3 Damage Absorption

- The damage absorption is calculated by the capacity of the material to absorb damage during the drop weight test. A parameter defined as the damage degree calculated from the energy-time plots shows that 3B3C has the maximum capacity of absorbing damage because it has 3 same type basalt fibers on top and bottom of the composite. 1B1C however has the lowest capacity to absorb energy because it has only 1 same type basalt fiber on top and bottom of the composite. These observations tell that damage absorption can be altered by changing the number of same type ductile fabrics (basalt in this study).

4.4 General Conclusion

A general conclusion about the percentage change in the evaluating factors for all the laminates is given as follows

1. Pattern of Damage Absorption values show a mean value of increase in the damage absorption capacity of the 5.5% in 2B2C as compared to that of 1B1C arrangement.

2. No value of damage absorption can be seen for 8 m/s drop weight impact test due to penetration as all the energy is used to break the laminate while it is minimum for 4 m/s.

3. Peak force values show an average decrease of 14% in 3B3C as compared to 1B1C arrangement of hybrid composites.

4. The stiffness of the material is increased by an average value of 14% if the carbon fabric in the laminate is moved towards the tension side of the through thickness hybrid composite by one step symmetrically.

5. Ductility index is calculated using force-time plot of the hybrid composites which showed an average increase of 80% value in 3B3C as compared to 1B1C.

6. The number of the basalt fabrics on compression and tension faces increases overall ductility of the hybrid through thickness composites.

7. Approximately 80% increase in maximum tensile stress before the breakage of laminate during the tensile loading is seen for HYB hybrid in plane composite as compared to 1B1C arrangement of the hybrid through thickness composite.

8. The alternating basalt and carbon fabrics inside hybrid through thickness laminates contribute to the overall stiffness showing an increase of 16% in 1B1C as compared to 3B3C for 4 m/s impact speed.

4.5. Suggestions

Like every academic study, this work also needs continuity. There are some of the topics which need a little more detail until an ultimate review about their properties could be given. Though each aspect of the possible variations during the tests was thought before starting the experiment, some things still needed little different approach.

In order to give an ultimate conclusion about the properties of the laminates, we first need to know that mechanical properties of the materials are inter-related. We always have to sacrifice on some property in order to enhance another.

1. The drop weight impact test and tensile test give different sets of parameters which can be reviewed later to understand the mechanism of failure and comment about the mechanical behavior related to the inner structure, external conditions and composition of the constituents of the material. However only optical observations on the failed materials had been made which of course is not enough to comment about the failure pattern. A quasi-static loading on the residual samples after the drop weight impact test would give a better view of the failure pattern. This way it will be possible to see which layers of the composite faced the maximum damage. Virgin samples can directly be used to start the quasi-static loading test which can later be checked under Scanning Electron Microscope to see the failure pattern.

2. The symmetry of the laminates was kept to have the tests independent from direction. The only difference between the hybrid through thickness was their sequence. Same material was used but only with different arrangements and the purpose of the whole study was to see the difference between the mechanical properties of *hybrid-through thickness* and *in-plane hybrid composite laminates.* In order to see deviation of

the mechanical properties from total carbon and total basalt fibers and comparing the results for evaluation, two hybrid composite made from totally carbon and totally basalt would be better. This way we can compare the mechanical properties of each hybrid composite with the total carbon composite and total basalt composite.

3. There is a range of mechanical tests which are applied on the composite materials to test their mechanical properties. Tensile test, drop weight impact test and bending test are some of them. Other than that after these mechanical tests, acoustic emission and ultrasonic phased array type non-destructive tests are used to further understand the extent and the nature of the failure mechanism.

4. There is a scope of introducing metal as the initial fabrics (in the tension or compression side of the laminate) which ensures that electrical conductivity *and/or* if needed the thermal conductivity. The reason to introduce a metal in the laminate separately is to provide the opportunity of controlled flow of electricity or heat. In the academic studies it is shown that the carbon fibers have high flexure modulus, tensile and flexure strength and resistance to the crack propagation but it is very brittle and has short elongation to break distances. Aluminum on the other hand is ductile and flexible but its crack propagation properties are not as good. The introduction of the aluminum and basalt in the full carbon fiber reinforced laminates will provide not only ductility and flexibility but also make it better for damage absorption.

5. Most of helmets used in the industry are made of plastic or metals. Plastics do not promise highest mechanical properties while the metals are heavy. Composite materials are used in the helmets because of their light weight and better mechanical properties. Some modern heavy machinery produces *shock waves.* The composite materials have proven to be resistant to the shock waves. The future production of these type of materials containing fibers resistant to the shock weaves can provide the availability of operation in the environment vulnerable to shockwaves.

REFERENCES

1. Fiore V., Di Bella G., Valenza A., 2011. Glass-basalt/epoxy hybrid composites for marine applications. **Mat Des, 32**: 2091-9.
2. Lopresto V., Leone C., De Iorio I., 2011. Mechanical characterization of basalt fiber reinforced plastic. **Compos Part B-Eng, 42**(4):717–23.
3. Wei B., Cao H., Song S., 2011. Degradation of basalt fibre and glass fibre/epoxy resin composites in seawater. **Corros Sci, 53**(1):426–31.
4. Wang X., Wu Z., Wu G., Zhu H., Zen F., 2013. Enhancement of basalt FRP by hybridization for long-span cable-stayed bridge. **Compos Part B Eng, 44**(1): 184–192.
5. Liu Q., Shaw M., Parnas R., McDonnell A., 2006. Investigation of basalt fiber composites mechanical properties for applications in transportation. **Polym Compos, 27**(1):41–8.
6. Szabo J., Czigany T., 2003. Static fracture and failure behavior of aligned discontinuous mineral fiber reinforced polypropylene composites. **Polymer Testing, 22**(6): 711–719
7. Wei B., Cao H., Song S., 2010. Tensile behavior contrast of basalt and glass fibers after chemical treatment. **Mater Des, 31**:4244-50.
8. Czigany T., 2006. Special manufacturing and characteristics of basalt fiber reinforced hybrid polypropylene composites: mechanical properties and acoustic emission study. **Compos Sci Technol, 66**:3210-20.
9. Chikhradze N., Marquis F., Japaridze L., Abashidze G., Okujava L., 2010. Polymer-based composite and hybrid materials for wind power generation. **Mater Sci Forum, 654-6**:2612-5.
10. Park R., Jang J., 1999. Performance improvement of carbon fiber polyethylene fiber hybrid composites. **J Mater Sci, 34**(12):2903–10.
11. Scheffler C., Forster T., Mader E., Heinrich G., Hempel S., 2009. Mechtcherine V. Aging of alkali-resistant glass and basalt fibres in alkaline solutions: evaluation of the failure stress by Weibull distribution function. **J Non-Cryst Solids, 355**:2588-95.
12. Zhu L., Sun B., Gu B., 2012. Frequency features of basalt filament tows under quasistatic and high strain rate tension. **J Compos Mater, 46**:1285-93.

13. Hao L., Yu W., 2011. Comparison of the thermal protective performance of aluminized fabrics of basalt fiber and glass fiber. Fire Mater, 35:553-60.
14. Ary Subagia I., Kim Y, Beijing L., Kim C., Shon H., 2014. Effect of stacking sequence on the flexural properties of hybrid composites reinforced with carbon and basalt fibers. **Compos B Eng, 58**:251-8.
15. Schwartz M., 1997. Composite Materials: Properties, Nondestructive Testing, and Repair. Prentice-Hall Inc. New Jersey, USA.
16. Militky J, Kova V., Rubnerov J., 2002. Influence of thermal treatment on the tensile failure of basalt. **Eng Fract Mech, 69**:1025-33.
17. Militky J, Kovacic V., 1996. Ultimate mechanical properties of basalt filaments. **Text Res, 66**:225-9
18. Deak T, Czigany T., 2009. Chemical composition and mechanical properties of basalt and glass fibers comparison. **Text Res J, 79**:645-51.
19. Wei B, Cao H, Song S., 2010. Environmental resistance and mechanical performance of basalt and glass fibers. **Mat Sci Eng A Struct, 527**:4708-15.
20. Morova N., 2013. Investigation of usability of basalt fibers in hot mix asphalt concrete. **Constr Build Mater, 47**:175-80.
21. Novitskii A., 2004. High temperature heat insulating materials based on fibers from basalt type rock materials. **Refract Ind Ceram, 45**:144-6.
22. Sim J., Park C., Moon D.,2005. Characteristics of basalt fiber as a strengthening material for concrete structures. **Compos Part B, 36**:504-12.
23. Kim J., Lim J., Huh Y., 2013. Melt-spinning basalt fibers based on dielectric heating and steady-state process characteristics. **Fibres Polym, 14**:1148-56.
24. Kogan F, Nikitina O., 1992. The solubility of chrysotile asbestos and basalt fibers in relation to their fibro genic and carcinogenic action, workshop on persistence of respirable synthetic fibres and minerals. **Environ Health Perspect, 102**(5): 205–206.
25. Quagliarini E., Monni F., Lenci S., Bondioli F., 2012. Tensile characterization of basalt fibre rods and ropes: a first contribution. **Constr Build Mater, 34**: 372-80.
26. Kogan F., Nikitina O., 1994. Solubility of chrysotile asbestos and basalt fibres in relation to their fibrogenic and carcinogenic action. **Environ Health Perspect, 102**:205-6.

27. MConnell E., Kamstrup O., Musselman R., Hesterberg T., Chevalier J., Miller W., 1994. Chronic inhalation study of size-separated rock and slag wool insulation fibres in Fischer 344/N rats. **Inhal Toxicol, 6**:571-614.

28. Fiore V., Di Bella G., Valenza A., 2011. Glass-basalt/epoxy hybrid composites for marine applications. **Mat Des, 32**:2091-9.

29. Wei B., Cao H., Song S., 2010 Tensile behavior contrast of basalt and glass fibres after chemical treatment. **Mater Des, 31**:4244-50.

30. Scheffler C., Forster T., Mader E., Heinrich G., Hempel S., Mechtcherine V., 2009. Aging of alkali-resistant glass and basalt fibres in alkaline solutions: evaluation of the failure stress by Weibull distribution function. **J Non-Cryst Solids, 355**:2588-95.

31. Zhu L., Sun B., Gu B., 2012. Frequency features of basalt filament tows under quasistatic and high strain rate tension. **J Compos Mater, 46**:1285-93.

32. Morozov N., Bakunov V., Morozov E., 2001. Materials based on basalt from the European North of Russia. **Glass Ceram, 58**:100-4.

33. Hao L., Yu W., 2011. Comparison of thermal protective performance of aluminized fabrics of basalt fibre and glass fibre. **Fire Mater, 35**:553-60.

34. Hao L., Yu W., 2009. Evaluation of thermal protective performance of basalt fiber nonwoven fabrics. **Journal of Thermal Analysis and Calorimetry, 100**: 551-55.

35. Ramachandran B., Velpari V., Balasubramanian N., 1981. Chemical durability studies on basalt fibres. **J Mater Sci, 16**:3393-7.

36. Nasir V., Karimipour H., Taheri-Behrooz F., Shokrieh M., 2012 Corrosion behavior and crack formation mechanism of basalt fibre in sulphuric acid. **Corros Sci, 64**:1-7.

37. Rabinovich F., Zueva V., Makeeva L., 2001 Stability of basalt fibres in a medium of hydrating cement. **Glass Ceram,58**:431-4.

38. Oztürk B., Arslan F., Oztürk S., 2007. Hot wear properties of ceramic and basalt fibre reinforced hybrid friction materials. **Tribol Int,40**:37-48.

39. Wang X., Hu B., Feng Y., Liang F., Mo J., Xiong J., 2008. 3D woven basalt/aramid hybrid composites. **Compos Sci Technol,68**:444-50.

40. Militky J., Kovacic V., Rubnerova J., 2002. Influence of thermal treatment on tensile failure of basalt fibres. **Eng Fract Mech, 69**:1025-33.

41. LanduCi G., Rossi F., Nicolella C., Zanelli S., 2009. Design and testing of innovative materials for passive fire protection. **Fire Saf J**, 44:1103-9.

42. Novitskii A., Sudakov V., 2004. An unwoven basalt-fibre material for the encasing of fibrous insulation: an alternative to glass cloth. **Refract Ind Ceram, 45**:239-41.

43. Shindo A., 1961. Report 317. Studies on graphite fibers. Government Industrial Research Institute, Osaka, Japan.

44. Bradley A., 2016. Processing, structure, and properties of carbon fibers. **Composites: Part A, 91**:262–282

45. Das S., Warren J., West D., Schexnayder S., 2016. Global carbon fiber composites supply chain competitiveness analysis. **Golden, CO (United States)**: National

Renewable Energy Lab.

46. Edie D., 1998. The effect of processing on the structure and properties of carbon fibers. **Carbon, 36**:345–62.

47. Qiu L., Zheng X., Zhu J, Su G., Tang D., 2013. The effect of grain size on the lattice thermal conductivity of an individual polyacrylonitrile-based carbon fiber. **Carbon, 51**:265–73.

48. Oya N., Johnson D., 2001. Longitudinal compressive behaviour and microstructure of PAN-based carbon fibres. **Carbon, 39**:635–45.

49. Morgan P., 2005. Precursors for carbon fiber manufacture. Carbon fibers and their composites. **Taylor & Francis Group**: 121–84.

50. Reynoldss W., Sharp J., 1974. Crystal shear limit to carbon fibre strength. **Carbon, 12**:103–10.

51. Honjo K., 2003. Fracture toughness of PAN-based carbon fibers estimated from strength–mirror size relation. **Carbon, 41**:979–84.

52. Kumar S., Helminiak T., 1988. Compressive strength of high performance fibers. **Symp J - Mater Sci Eng Rigid-Rod Polym**:134.

53. D'Almeida J., Monteiro S., 1997. The Role of the Resin Matrix/Hardener Ratio on the Mechanical Properties of Low Volume Fraction Epoxy Composites. **Advanced Performance Materials, 4**: 285–295.

54. Sarasini F., Tirillo J., Ferrante L., Valente M., Valente T., 2014. Drop-weight impact behavior of woven hybrid basalt–carbon/epoxy Composites. **Composites: Part B, 59**: 204–220.

55. Benevolenski O., Karger-Kocsis J., Mieck K., Reubmann T., 2000. Instrumented perforation impact response of polypropylene composites with hybrid reinforcement flax/glass and flax/cellulose fibers. **J Thermoplast Compos Mater, 13**:481–96.

56. Belingardi G., Cavatorta M., Salvatore Paolino D., 2008. Repeated impact response of hand lay-up and vacuum infusion thick glass reinforced laminates. **Int J Impact Eng, 35**:609–19.

57. Bledzki A., Mamun A., Faruk O., 2007. Abaca fibre reinforced PP composites and comparison with jute and flax fibre PP composites. **eXPRESS. Polym Lett, 1**:755–62.

58. Reis P., Ferreira J., Santos P., Richardson M., Santos J, 2012. **Composite Structures, 94**(12): 3520–3528

CURRICULUM VITAE

PERSONAL DATA

Name and Surname:	:	Hafız Muhammad Numan ZAFAR
Nationality	:	Pakistani (PK)
Birth Date and Place	:	June 1, 1989.
Marital Status	:	Single
Tel:	:	+90 553 498 1482
Fax	:	+90 553 498 1482
email	:	numan.zafar@live.com
Address		Cemilbaba Caddesi Mevlana Mah. Şahin Apt. 6/24 Talas/KAYSERİ

Degree	Institute	Date of Graduation
MSc	EÜ Fen Bilimler Enstitüsü	2017
Bachelor's	EÜ Fen Fakültesi, Fizik	2013
High School	GOVT High School Khewra	2006

PROFESSIONAL EXPERIENCE

Year	Institute	Mission
2013- Currently	Turkish Wushu Federation	Foreign Relations
2011–2013	BİSOM Madencilik	Foreign Relations

Language

English, Urdu, Hindi, Punjabi, Turkish.